LEHRSTUHL FÜR EXPERIMENTELLE GENETIK DER TECHNISCHEN UNIVERSITÄT MÜNCHEN

Development of the ”chemokine flow cytometry” assay and its application to the characterization of pathogen-specific T cells.

JENS EBERLEIN

Vollständiger Abdruck der von der Fakultät Wissenschaftszentrum Weihenstephan für Ernährung, Landnutzung und Umwelt der Technischen Universität zur Erlangung des akademischen Grades eines

Doktors der Naturwissenschaften

genehmigten Dissertation.

VORSITZENDER: UNIV.-PROF. DR. M. KLINGENSPOR

PRÜFER DER DISSERTATION:

1. UNIV.-PROF. DR. M. HABRÉ DE ANGELIS
2. UNIV.-PROF. DR. D. BUSCH

Die Dissertation wurde am 05.11.2010 bei der Technischen Universität München eingereicht und durch die Fakultät Wissenschaftszentrum Weihenstephan für Ernährung, Landnutzung und Umwelt am 21.04.2011 angenommen.

This thesis is dedicated to my children, Ford and Stella, my wife Lisa, my mother Christa and in loving memory to my father, Bernd Eberlein.

Contents

List of Figures

List of Tables

1 Introduction

1.1 The innate and adaptive immune response

A multicellular organism's protection from infectious agents such as bacteria, viruses and parasites is carried out by the immune system. The vertebrate immune system can be divided into two distinct, yet intertwined, components: The adaptive and innate immune system. Innate immunity provides a first line of defense against pathogens characterized by a relatively short response time (measured in hours) whereas the adaptive immune response takes days to develop in response to a pathogen that was not encountered before. The major cellular constituent of the innate immune system are phagocytes of the myeloid lineage termed monocytes/macrophages (Mo/MΦ), granulocytes (neutrophils, eosinophils, basophils) as well as dendritic cells (DCs) named after their distinct morphology [1]. DCs are commonly distinguished as conventional (cDC) or interferon-producing plasmacytoid (pDC) dendritic cells based on their surface marker expression, morphology and function, although significant plasticity in these characteristics are observed [2].

The innate immune system responds to re-infection with the same pathogen with identical kinetics as its specificity is limited to recognizing general evolutionary conserved molecule patterns. Examples of damage-associated molecular patterns (DAMPs) are histones and DNA released by necrotic cells [3]. Another class of patterns are pathogen-associated molecular patterns (PAMPs) such as lypopolysaccharides expressed by gram$^-$ bacteria or viral double-stranded RNA (dsRNA) [3]. Some pattern recognition receptor (PRRs) are expressed by most nucleated cells which may respond to viral dsRNA by secreting small proteins called interferons to induce an anti-viral state in neighboring cells. Secreted molecules, like interferons, cytokines and chemotactic cytokines, so called chemokines, can direct the immune response by shaping the maturation of DCs [3].

The complement system consists of a group of proteins found in high concentrations in the serum. It is activated by PAMPs as well as antibodies generated by B cells of the adaptive immune response resulting in the direct destruction of pathogen by opsonization, tagging for clearance by phagocytic cells or inhibition by neutralization [1]. Innate immune cells constantly survey their environment for pathogens by phagocytosing and processing particles. Activation of innate immune cells occurs

by binding of PAMPs and DAMPs to PRRs, most notably members of the Toll-like receptor family (TLR), resulting in increased phagocytosis, production of effector molecules and interferons. Chemokines can contribute to a pro-inflammatory environment and attract other immune cells to the site of infection. Intracellular pathogens can downregulate the expression of certain cell surface molecules in an attempt to escape immunosurveillance. This abnormal expression of cell surface molecules can be recognized by a small lymphoid subpopulation called natural killer cells (NK) which have the ability to directly and immediately kill infected host cells via cytolytic molecules (granzymes, perforin) [4].

While MΦ and neutrophils are mainly responsible for the clearance of pathogens by phagocytosis, dendritic cells mature upon activation into specialized antigen-presenting cells (APCs) capable of activating the adaptive immune response upon migration into the draining lymph node [3]. B cells and MΦs are also able to act as APCs, but the DC is considered the principal APC responsible for inducing the adaptive immune response. Although the innate immune system is able to mount an immediate immune response to pathogens that trigger PRRs and/or cytokine/chemokine release, it does not protect from pathogens that do not elicit these mechanisms. Furthermore, the response kinetics to reinfections remain the same.

1.2 Cellular constituents of the adaptive immune response.

In contrast, the adaptive immune response, a hallmark of jawed vertebrates, has evolved to specifically distinguish between self and non-self by employing so called 'antigen receptors' [1]. Furthermore, the adaptive immune response is able to mount an accelerated response to subsequent infections with the same pathogen, a property known as 'immunological memory'. The two principal cellular components of the adaptive immune system are antigen receptor-bearing bone marrow-derived lymphocytes (B cells) and thymus-derived lymphocytes (T cells). B cells are instrumental in the humoral immune response due to their ability to produce highly specific soluble antigen receptors, so called antibodies, whereas T cells are critically involved in the cellular immunity towards intracellular-replicating pathogens [1].

In order to be able to recognize a vast range of antigenic determinants, immature B and T cells

assemble their B cell antigen receptor (BCR) or T cell antigen receptor (TCR) genes from different alternative elements. Random somatic mutations are introduced during the receptor gene splicing which greatly enhances receptor diversity resulting in a pool of B and T cells where each cell expresses monogenic antigen receptors of random specificity. B cells that successfully rearranged their BCR and do not react with self-antigens survive the maturation process and circulate in the body as 'naive', antigen-inexperienced B cells until encountering antigen [1].

The vast majority of mature T cells express a heterodimeric TCR consisting of an α and a β chain (α:β T cells) and express either the co-receptor CD4 or CD8. Productive signaling by the TCR requires the presence of one of these two co-receptors in order to stabilize TCR:MHC interactions. A minor thymus-derived T cell population (1-2%) expresses an alternative, less variable γ:δ TCR of less understood specificities [5]. As the main focus of this thesis is on α:β T cells, these γ:δ T cells will not discussed in further detail. Unlike B cells, which can bind their antigen directly, recognition of antigen by α:β T cell activation requires the cognate antigen to be presented as small peptides (antigenic peptides) by members of one of the dichotomous classes of highly polymorphic molecules encoded in the major histocompatibility complex region of the genome, the so called 'MHC class I or class II molecules' (MHC-I, MHC-II) [6, 7].

Due to the random specificity of their T cell receptor, immature T cells require a selection process to eliminate potentially auto-reactive and non-reactive cells. To this end, immature T cells expressing a functional α:β TCR of random specificity undergo a stringent selection process in the thymus where only those cells survive that recognize specific MHC molecules (positive selection) but do not bind peptide-loaded or empty MHC molecules with high affinity (negative selection). This selection process results in so called naive $CD4^+$ or $CD8^+$T cells (T_N) that can recognize their antigenic peptide only in the context of a specific type of MHC molecule, a concept termed MHC restriction [6, 7]. The type of antigenic peptide determines the class of MHC molecules by which it is presented and therefore the type of T cell it can activate: Peptides derived from proteins synthesized in the cytoplasm of a cell, *e.g.* viral antigens, are presented by all nucleated cells via members of the MHC class I to α:β T cells expressing the co-receptor CD8 ($CD8^+$T cells). In the mouse, MHC-II molecules are exclusively expressed by APCs and present peptides derived from exogenous and endogenous peptides on MHC class II molecules as part of the endocytic pathway. Ingested particles,

e.g. bacteria, and proteins (via pinocytosis and endocytosis) are presented to $CD4^+$T cells via this pathway. However, while this division is generally valid, cross-presentation of exogenous peptides (MHC-II peptides) by MHC-I occurs in APCs and facilitates the presentation of peptides derived from certain viruses and bacteria that do not infect APCs directly [8] and from tumor-associated peptides [9].

The induction of the adaptive immune response occurs in the secondary lymphoid organs, such as the lymph nodes, spleen and gut-associated lymphoid tissue including Peyer's patches [1]. Naive T cells exit the thymus and circulate through the secondary lymphoid system via the blood and lymph until encountering their antigen. The initial activation of naive T cells in response to antigenic-peptide is referred to as 'priming'. Upon proper priming, naive $CD4^+$ and $CD8^+$ T cells proliferate and differentiate into effector T cells (T_E) and acquire new functions. $CD4^+T_E$ cells are often called 'helper T cells' (T_H) for their role in guiding the adaptive immune response towards certain classes of pathogens. T_H cells can in turn activate B cells, induce their antibody production, isotype switching and affinity maturation. T_H cells are also able to recruit and help prime $CD8^+$T cells, macrophages, neutrophils, eosinophils, basophils and other effector cells. Four T_H cell 'lineages' have been identified so far: T_H1, T_H2, T_H17 and T_{reg}, although significant plasticity and heterogeneity exists within and among these populations [10].

The cytokine environment during the priming event influences T_H cell differentiation and the ensuing type of immune response. The two major helper cell populations T_H1 and T_H2 generally skew the system by secreting different sets of cytokines and interferons towards a cellular immune response (T_H1 response) against intracellular pathogens or towards a humoral immune response (T_H2 response) important for IgE production, eosinophil recruitment and clearance of extracellular parasites. IFNγ is the characteristic effector molecule produced by T_H1 cells whereas IL-4, IL-5 and IL-13 are major cytokines produces by T_H2 cells [10]. The recently discovered of T_H17 cells [11], named after their ability to produce IL-17, are implicated in the pathogenesis of various autoimmune diseases and play a role during immune responses against extracellular bacteria and fungi whereas T_{reg} cells recognize self-antigen and are involved in immunological tolerance [10].

$CD8^+T_E$ cells are able to kill infected host cells via targeted release of cytolytic proteins, mainly

perforin and granzymes, and also secrete other effector molecules such as interferon γ (IFNγ) and tumor necrosis factor α (TNFα). Another effector mechanism is the employment of T cell-expressed CD178 (FasL) to induce apoptosis of CD95 (Fas)-expressing target cells (FasL:Fas) [12]. T cells capable of killing cells are termed 'cytotoxic T cells' (CTLs, T_C) and consist mostly of $CD8^+$T cells, however, cytotoxic $CD4^+$T cells also exist, albeit at much smaller frequencies [13].

Generation of immunological memory

The ability of the adaptive immune system to specifically recognize previously encountered pathogens is referred to as 'immunological memory'. Routinely, this recognition results in an accelerated pathogen clearance and reduced pathogenesis when compared to a primary infection. Antibody-mediated immunity is the principal mechanism of humoral immunological memory exercised by plasma cells derived from long-lived memory B cells [1]. While the significance of $CD4^+$T cell memory in immune protection remains unclear [14], the role of $CD8^+$ memory T cells ($CD8^+T_M$) in heightened immune protection has been well established [15].

Figure 1 depicts the timecourse of a typical $CD8^+$T cell response to an acute primary and secondary infection with the same viral pathogen. During the expansion phase (**Fig.1**), properly primed pathogen-specific $CD8^+$T cells proliferate and differentiate into effector cells. The overall population size of antigen-specifc $CD8^+T_E$ increases approximately 1000-fold when compared to the naive precursor population [15]. After pathogen clearance, $\sim$90-95% of the $CD8^+T_E$ cells die during the contraction phase by a regulated process resulting in a stable population of long-lived memory cells ($CD8^+T_M$, **Fig.1**) [16]. Re-infection with the same pathogen triggers a secondary response characterized by a lower activation threshold, faster acquisition of effector functions and increased proliferative potential when compared to naive T cells of the same specificity [17]. A combination of increased cell frequency compared to their naive precursors, lower activation thresholds, reduced lag phase and rapid reacquisition of effector functions are key mechanisms of enhanced immune protection afforded by $CD8^+T_M$ [18].

Two subpopulations of $CD8^+T_M$ have been described based on a combination of phenotypic markers, tissue distribution and functional properties: So called $CD8^+$ effector memory T cells ($CD8^+T_{EM}$) preferentially home to peripheral non-lymphatic tissues and display immediate effec-

tor functions upon restimulation whereas central memory T cells ($CD8^+T_{CM}$) are mainly localized to lymphatic tissues and display high proliferative potential associated with increased IL-2 production and delayed acquisition of effector functions [19]. Phenotypically, $CD8^+T_M$ populations are frequently distinguished from each other and from $CD8^+T_E$ by differential expression of CD62L (L-selectin) and CD44: $CD8^+T_{CM}$ are $CD62L^{hi}/CD44^{hi}$, whereas $CD8^+T_{EM}$ and T_E are $CD62L^{lo}/CD44^{hi}$ distinguishing them from naive $CD62L^{hi}/CD44^{lo}CD8^+$T cells.

Additionally, the lymph node-homing chemokine receptor CCR7 is frequently utilized as a marker to distinguish $CCR7^{lo}$ T_{EM} from $CCR7^{hi}$-expressing T_E and T_{EM} [20, 21]. However, stratification according to CD62L and CCR7 expression revealed significant heterogeneity of marker expression and phenotypes among T_M populations [22]. Furthermore the clear distinction between T_{CM} and T_{EM} has been questioned by several observations indicating that, depending on the experimental design, $CD8^+T_{EM}$ and $CD8^+T_{CM}$ are able to proliferate with similar kinetics [23, 24] and $CD8^+T_{CM}$ may, on a per cell basis, exhibit a higher cytolytic capacity than $CD8^+T_{EM}$ [25].

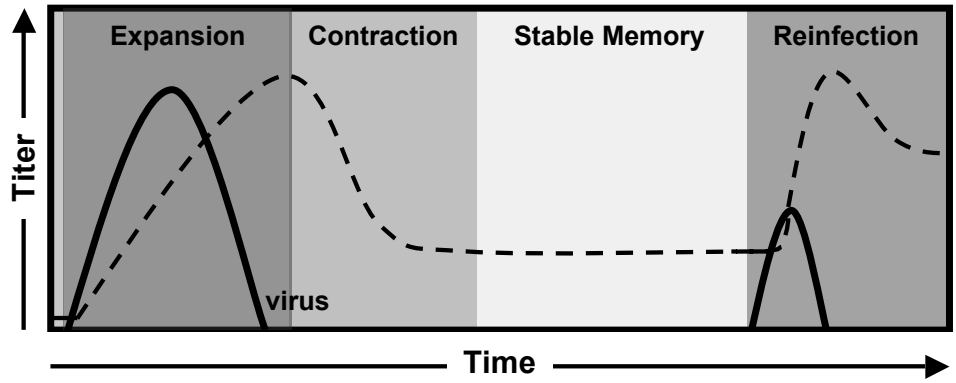

Figure 1: ***Timecourse of an acute viral infection with stable $CD8^+$T cell memory generation in the absence of an antibody response.*** *The Y-axis depicts relative virus titers (solid line) and virus-specific $CD8^+$ T cell titers (dashed line). After a lag period, pathogen-specific T cells proliferate and differentiate into effector T cells (expansion phase) resulting in clearance of the virus. During the ensuing contraction phase 90-95% of the T cells die giving rise to a stable population of memory T cells. Upon re-infection with the same pathogen, the antigen-specific memory T cell pool rapidly expands and clears the virus with accelerated kinetics. Graph adapted from [26].*

1.3 Chemokines as regulators of cell trafficking and activation

Mobility is a key aspect of the immune system exemplified by the constant circulation of T and B cells through the lymphatic system and the requirement of immune cells to traffic to sites of inflammation. The spatio-temporal positioning of these cells is regulated by adhesion molecules such as integrins and selectins as well as chemokines and their receptors.

Chemokines are small, mainly secreted proteins of 8-11 kDa size that transduce their biological signals through receptor binding, whereas binding to glycosaminoglycans (GAGs) is important for the formation of chemotactic gradients, along which cells travel across endothelia and into tissues [27–29]. The chemokine receptors, expressed by the migrating cells, belong to the superfamily of seven transmembrane receptors (7TMR) and are thought to bind chemokines in their monomeric form, although higher order homo- or oligomeric chemokine aggregates have previously been reported for several chemokines [30].

The activities of chemokines are not restricted to chemotaxis, but are rather diverse. For example, chemokines are known to control lymphopoiesis and lymphoid organogenesis, alterations of leukocyte adhesive properties by modulation of integrins as well as regulation of lymphocyte differentiation, proliferation, survival, cytokine release and degranulation [31–35]. Furthermore, chemokines have been implicated in a wide variety of pathological states such as infectious disease and cancer, autoimmunity, allergy and transplant rejection [32, 36–40]. Interestingly, molecular mimicry of chemokines and chemokine receptors by pathogens, such as viruses, have been reported and the selective pressure of co-evolution of host-pathogen interactions might be in part reflected by the divergent sequence composition of chemokines across species [41] and by independent gene duplication events in mouse and man [42]. To date, 40 murine and more than 50 human chemokines (**Table 1**) have been identified and might in fact comprise one of the few superfamilies known in their entirety. Chemokine biology is inherently complicated due to the promiscuity of receptor:ligand interaction: Multiple chemokines can bind to one of the 18 (human) receptors and one receptor can bind multiple chemokines giving rise to more than 50 different combinations of receptor:chemokine interactions (**Table 1**, [42]).

Table 1: Murine chemokine superfamily nomenclature and their receptors

Name	Other name(s)	Gene symbol	Chr.	Fct.	Cluster	Receptor(s)
CC family						
CCL1	TCA-3/I-309	Ccl1	11qB5	I	MCP	CCR8
CCL2	JE/MCP-1	Ccl2	11qB5	I	MCP	CCR2
CCL3	MIP-1α	Ccl3	11qB5	I	MIP	CCR1, CCR5
CCL4	MIP-1β	Ccl4	11qB5	I	MIP	CCR5
CCL5	RANTES	Ccl5	11qB5	I		CCR1, CCR3, CCR5
CCL6	C10	Ccl6	11qB5	I	MIP	CCR1, FPR3
CCL7	MARC/MCP-3	Ccl7	11qB5		MCP	CCR1, CCR2, CCR3
CCL8	MCP-2	Ccl8	11qB5	I	MCP	CCR1, CCR2, CCR3, CCR5
CCL9/10	MIP-1γ	Ccl9	11qB5	H	MIP	CCR1, CCR3
CCL11	Eotaxin	Ccl11	11qB5	I	MCP	CCR3
CCL12	MCP-5	Ccl12	11qB5	I	MCP	CCR1, CCR2, CCR3, CCR5
CCL17	TARC	Ccl17	8qC5	D	none	CCR4
CCL19	ELC/exodus-3	Ccl19	4qB1	H	none	CCR7
CCL20	MIP-3α, LARC	Ccl20	1qC5	D	none	CCR6
CCL21a*	SLC/6Ckine/CCL21ser	Ccl21a	4qB1	D	none	CCR7
CCL21b/c*	CCL21leu	Ccl21b/c	4qB1	D	none	CCR7
CCL22	MDC	Ccl22	8qC5	D	none	CCR4
CCL24	Eotaxin-2	Ccl24	5qG1	I	none	CCR3
CCL25	TECK	Ccl25	5qG1	I	none	CCR9
CCL26	CCL26L/Eotaxin-3	Ccl26	5qG1	I	none	CCR3
CCL27	CTACK	Ccl27a	4qB1	H	none	CCR10
CCL28	MEC	Ccl28	13	U	none	CCR10, CCR3
CXC family						
CXCL1	KC	Cxcl1	5qE2	I	GRO	CXCR2, CXCR1
CXCL2	MIP-2	Cxcl2	5qE2	I	GRO	CXCR2
CXCL3	DCIP1/GM1960	Cxcl3	5qE2	I	GRO	CXCR2
CXCL4	PF4	Pf4	5qE2	U	GRO	CXCR3
CXCL5	LIX	Cxcl5	5qE2	I	GRO	CXCR2
CXCL7	NAP-2/β-TG/TCK-1	Ppbp	5qE2	I	GRO	unknown
CXCL9	MIG/CRG-10	Cxcl9	5qE3	I	IP10	CXCR3
CXCL10	IP-10/CRG-2	Cxcl10	5qE3	I	IP10	CXCR3
CXCL11	I-TAC	Cxcl11	5qE3	I	IP10	CXCR3, CXCR7
CXCL12	SDF-1/PBSF	Cxcl12	6qF1	H	none	CXCR4, CXCR7
CXCL13	BLC	Cxcl13	5qE3	H	IP10	CXCR5
CXCL14	BRAK/MIP-2γ	Cxcl14	13q82	I	none	unknown
CXCL15	Lungkine/WECHE	Cxcl15	5qE2	U	none	unknown
CXCL16	SR-PSOX	Cxcl16	11qB4	I	none	CXCR6
CXCL17	DMC/VCC1	Cxcl17	7qA3	U	none	unknown
CX3C family						
CX_3CL1	fractalkine/neurotactin	Cx_3cl1	8qC5		none	CX3CR1
C family						
XCL1	lymphotactin/ATAC	Xcl1	1qH2	D	none	XCR1

Table 1: ***The murine chemokine superfamily nomenclature and their receptors.*** *(*) Three distinct CCL21 genes (a/b/c) give rise to only two unique proteins (CCL21a [Ser65] and the identical gene products CCL21b and CCL21c [Leu65]). Chromosomal location (Chr.), function (Fct.), genomic clusters (Cluster) and receptor binding were adapted and modified from Zlotnik et al. [42]. Function: H = homeostatic, I = inflammatory, U = unknown, D = dual function (inflammatory and homeostatic).*

Furthermore, 'decoy' or 'scavenger' receptors exist (DARC and D6 in mice, possibly CXCR7 [43]) which are not able to signal upon chemokine binding but are thought to fine tune the immune response [44] through sequestration of chemokines [43]. DARC expression on the surface of red blood cells has been proposed to function as a 'sink' removing circulating chemokines [45]. Another putative function of DARC is the transcytosis of chemokines from the abluminal side of endothelial cells and subsequent presentation and/or release at the luminal surface [45].

Unlike cytokines, which were predominantly identified as such due to their biological properties, the chemokines family members were chiefly identified by cloning efforts after discovery of an evolutionary conserved N-terminal motif [42]. This tetracysteine motif is responsible for the proper folding of the chemokines. Based on the spacing of the first two cysteine residues of this motif, chemokines can be divided into four subfamilies (CC, CXC, C, CX_3C). The human CC and CXC families comprise of 27 (23 in mice) and 17 (15 in mice) members, respectively. The C family contains only one member in mice and two in humans, whereas the CX_3C contains a single gene in both species. Although CXCL4 (PF4) was the first chemokine discovered in 1961, it was not until 1988 that the long postulated existence of chemotatic proteins was proven by functional studies of CXCL8 (IL-8) [46, 47]. The term 'chemokine' and the definition of the superfamily of chemokines was endorsed in 1992 [48] in order to help unify the field of chemokine biology.

Besides grouping according to the tetracystein motif, chemokines can also be grouped by their genomic location and functional activity as summarized in Table 1 [42]. Genomic clusters of chemokines, probably arisen from gene-duplication events, allow their grouping into four major groups: The CC chemokines-containing monocyte chemotactic protein (MCP) group and macrophage inflammatory protein (MIP) group. The GRO group, named after the alternative name for CXCL1, and the IP-10 (CXCL10) group both consist of CXC chemokines (**Fig.2A/B**). Additionally, several non-cluster chemokines exist as described in [42]. Alternative categorization according to functional activity divides chemokines into inflammatory, homeostatic or dual-function chemokines (**Table 1** and **Fig.2**) based on their expression profiles during steady state and inflammation [42]. Homeostatic chemokines are constitutively expressed under non-inflammatory conditions and facilitate functions such as circulation of T cells into and out of lymphatic tissues (*e.g.*, CCL19:CCR7 [50]) and migration of naive T cells within lymphoid tissues.

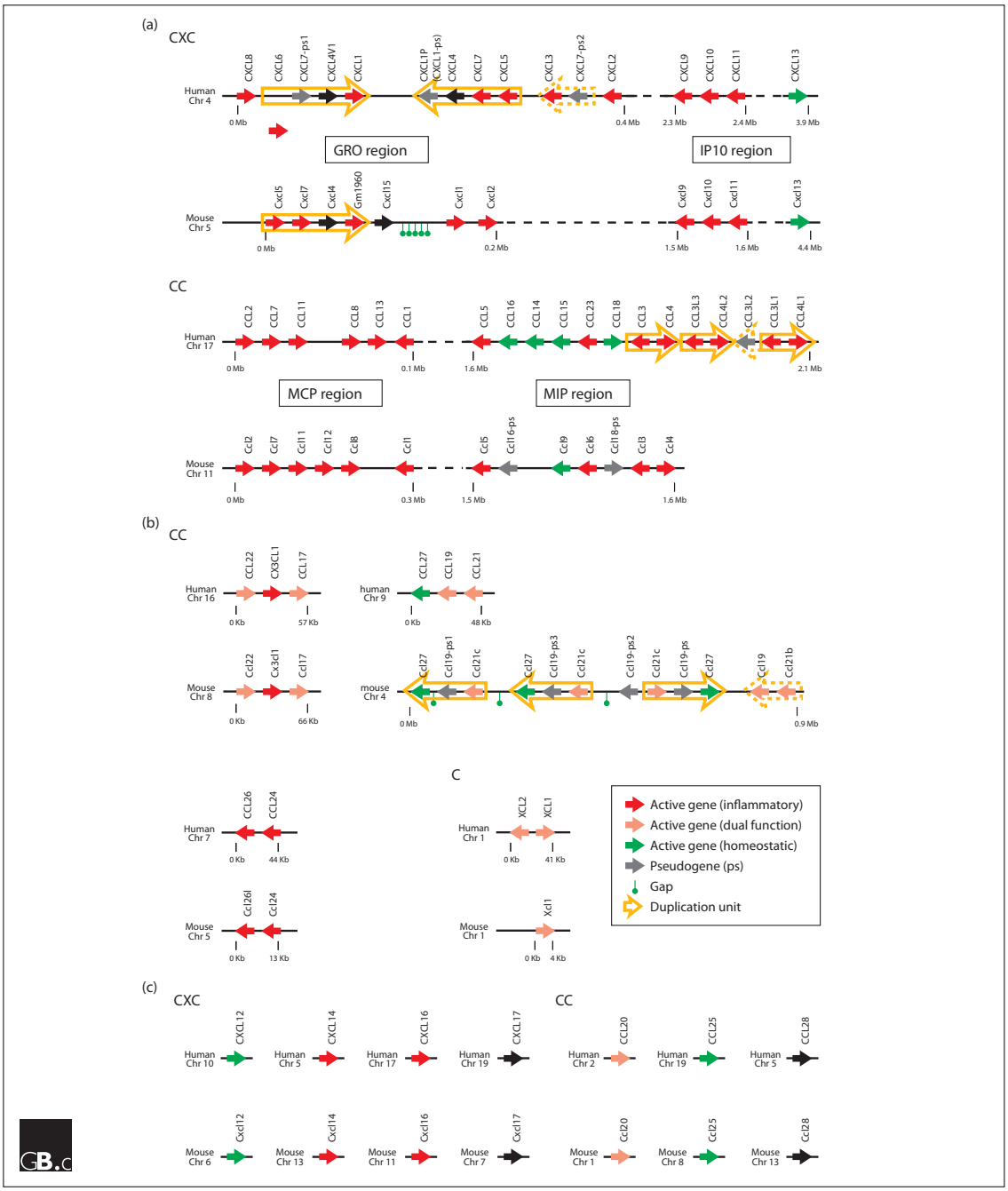

Figure 2: *Schematic genomic organization of the human and mouse chemokine superfamily. (a) Major-cluster chemokines; (b) mini-cluster chemokines; (c) non- cluster chemokines. Solid arrows indicate chemokine genes and their transcriptional orientation; red, green and pink arrows indicate inflammatory, homeostatic and dual function chemokine genes, respectively, and gray arrows indicate pseudogenes. Duplication units in the major clusters are indicated by open yellow arrows. This figure is based on the NCBI 36 and 35 assemblies of the human and mouse genomes [49]. A gap indicates a region not yet covered by the genome sequencing consortiums, while a dashed line denotes a similar region of more than 1 Mb. Note: The figure and legend were reproduced from a review article by Zlotnik et al. [42] with friendly permission from the Editors of Genome Biology.*

Inflammatory chemokines are only expressed during inflammation and are involved in directing immune cells to sites of infection and implicated in shaping the local immune response. For example, CCL5 expression in inflammed tissue prolongs macrophage survival resulting in reduced spread of virus by effective clearance of infected cells [51]. Dual-function chemokines are expressed under non-inflammatory conditions and are further upregulated upon inflammation. While this pragmatic categorization has useful applications it also bears the risk of chemokines being incompletely defined in regards to their functions during homeostasis and inflammation potentially necessitating reclassification of some chemokines as more insights into their roles are established.

1.4 Induction and trafficking of the CD8$^+$ T cell response.

During the initial stages of a typical acute viral infection, peripheral DC capture antigen and can be activated through two different types of stimuli: direct recognition of pathogens (through PRRs) and indirect sensing of infection, *e.g.* via inflammatory cytokines, chemokines and DAMPs [52]. Activated DCs upregulate CCR7 and home via afferent lymphatic vessels to the draining lymph in a CCR7-dependent process [20, 52]. Differentiation from poor antigen presenters to immunogenic APCs is marked by upregulation of MHC-I and -II and the co-stimulatory molecules CD40, CD80 / CD86 as well as adhesion molecules such as ICAM-1/2 and LFA-1 [3].

The principal port of entry of blood-borne lymphocytes to secondary lymphoid organs (but not spleen) are specialized postcapillary venules, the so-called high endothelial venules (HEV) [53]. HEV constitutively express members of the addressin family of adhesion molecules, which support the homing of lymphocytes to secondary lymphoid organs [53]. In contrast, endothelial cells not associated with secondary lymphatic tissue permit little or no leukocyte binding unless they are exposed to inflammatory mediators [53]. Binding of constitutively expressed CCL21, and to a lesser extend CCL19, on the surface of HEV by naive T cells induces conformational changes in their adhesion molecules leading to diapedesis across the HEV and into the T cell area of the lymph node [53]. Although a role of chemokines in guiding T cells to specific immunogenic DCs is beginning to emerge [54], models of random traffic patterns for screening APCs still retain their validity. Effective priming by immunogenic DCs presenting cognate antigen to naive CD8$^+$T cells requires

two additional signals: CD80/86 provides co-stimulatory signals to the TCR co-receptor CD28 and soluble factors such as IL-12 provide the third signal. Help provided to $CD8^+$T cells by T_H cells is dispensable for some pathogens inducing strong T_H1 responses, but critical for efficient recall responses [55–57]. After a lag period marked by proliferation and differentiation, $CD8^+T_E$ exit the secondary lymphatic organs via the efferent vessels and home to sites of infection via cell adhesion molecules, cytokines and inflammatory chemokines [53]. Once in the tissue, further signals generated from inflammatory chemokine gradients can guide T cells to specific areas of inflammation and these in turn are able to attract other lymphocytes via chemokine release [53].

Lastly, homeostatic CCL1-expression in the human skin has been associated with trafficking of T_M cells expressing the CCL1 receptor CCR8 under non-inflammatory conditions which might facilitate the strategic positioning of T_M for enhanced immuneprotection [58, 59].

1.5 T cell-produced chemokines.

The main focus of the second part of this thesis is to determine the spectrum, expression and release kinetics of chemokines produced by pathogen-specific T cells. Although T cells have been identified as a relevant source of chemokines more than a decade ago [60], a systematic and coherent analysis of the complete spectrum of chemokines produced by pathogen-specific T cells at the single cell level has not been established which is most likely due to the scarcity of suitable antibody reagents. Probably the most prolific research into T cell-produced chemokines has been in the area of HIV biology. The observation that the T cell-produced chemokines CCL3/4/5 can competitively inhibit HIV entry *in vitro* [61] led to the discovery of CCR5 as the co-receptor for HIV and to the identification of CCR5-mutant individuals with high resistance to the virus [62]. The regulation of T cell chemokine expression has shown conflicting results in regards to CCL3, 4 and 5 expression. Murine memory-phenotype $CD8^+$T cells of undefined specificity (MP$CD8^+$T) also contain abundant *Ccl3, Ccl4* and in particular *Ccl5* mRNA transcripts but apparently no corresponding proteins, the synthesis of which requires TCR stimulation [63, 64]. In contrast, Catalfamo et al., working mostly with in vitro generated human T cell blasts, reported high levels of CCL5 protein expression confined to a unique subcellular compartment and rapidly released upon TCR engagement [65]. However,

this observation is challenged by other studies that demonstrate a preferential association of constitutively expressed CCL5 with cytolytic granules in human MPCD8$^+$T cells and an HIV-specific CD8$^+$T cell clone [66, 67].

To this date, only one T cell-produced chemokine has been shown to display a critical role in immune protection: CCL3-production by adoptively transferred T_E into naive mice was shown to be critical for protection from lethal doses in the experimental *L. monocytogenes* model (LM model) [68] and another study established that protection conferred by CD8$^+$$T_M$ cells depends on their ability to secrete CCL3. [69]. In the LM model, Dorner *et al.* established the notion that the NK-produced chemokines CCL3/4/5 and XCL1 act together with IFNγ as a unit of 'type 1 cytokines' in the innate immune response which is subsequently 'handed over' to CD8$^+$$T_E$, but not CD4$^+$$T_E$, after initiation of the adaptive immune response [70]. A recent publication by the same group provides new insight into the role of XCL1 and its only receptor XCR1. The latter was found to be exclusively expressed by murine CD8$^+$DCs [71]. Furthermore it was demonstrated that the development of cytotoxicity to antigens cross-presented by CD8$^+$DCs was significantly impaired [71]. Lastly, a role for CCL3 and CCL4 in the trafficking of CD8$^+$T cells within draining lymphnodes to sites of DC:CD4$^+$T cell interaction was reported using intra-vital microscopy [54].

The majority of experiments in this thesis will employ lymphocytic choriomeningitis virus (LCMV) system for investigations into the range and role of pathogen-specific T cell-produced chemokines. However, to assess the generality of our principal findings, we will also conduct complementary experiments in the vesicular stomatitis virus (VSV) and Listeria monocytogenes (LM) models. Although these model systems share certain features, the nature of the pathogens (viral *vs.* bacterial), the pathology they cause (non-cytopathic *vs.* cytopathic) and the immunological determinants leading to their effective control are fundamentally different.

LCMV is a non-cytopathic RNA virus and natural murine pathogen. Since its first description $\sim$75 years ago, the LCMV system has become one of the best-characterized models for the study of infectious disease. Depending on viral isolate, dosage, route of infection and host immune status, multiple aspects of viral disease can be studied [72]. Two principal experimental protocols can be employed:

(1) Acute infection: intraperitoneal (i.p.) infection of adult mice with LCMV Armstrong (Arm) at 1.5x10^5 pfu leads to transient disease in the absence of overt clinical symptoms. Effective virus control is primarily dependent on a powerful $CD8^+T_E$ response and established $CD8^+T_M$ can be maintained for life in the absence of persisting virus, viral proteins or nucleic acids [16, 73–75]. Specific $CD4^+T_E$ contribute to the effective generation and possibly also maintenance of $CD8^+T_M$ [76–79]. While the regulation of LCMV-specific $CD4^+$T cell immunity is generally similar to that of $CD8^+$T cells, expansions of specific $CD4^+$T cells are significantly smaller at all stages of the immune response and $CD4^+T_M$ are subject to a slow and progressive decline [16, 80]. $CD8^+T_M$-mediated protection is commonly demonstrated by efficient virus control following a re-challenge with the immunosuppressive LCMV isolate clone13 (cl13).

(2) Persistent infection: intravenous infection of adult mice with high dose LCMV cl13 (2-4x10^6 pfu) generates an abortive $CD8^+$ cytotoxic T lymphocyte (CTL) response incapable of virus control. Nevertheless, over a period of 3-4 months, infectious virus is cleared in a T cell-dependent fashion from many but not all organs. Key features of this model are a generalized immunosuppression [81, 82] and the progressive, epitope-dependent functional impairment of antiviral T cells [83–85]. Interestingly, improved virus control over time is associated with a reacquisition of diverse T cell functions [86,87]. As this 'rescue' of virus-specific T cells also occurs in thymectomized mice [88], 'exhausted' peripheral T cells are amenable to therapeutic interventions that accelerate the regain of effector functions [89].

In addition to studying the endogenous response to LCMV-infection in wild type mice, we will employ an adaptive transfer model in which $CD8^+$T cells from a T cell receptor transgenic (TCRtg) mouse specific for the immunodominant LCMV epitope GP_{33-41} are transferred into B6.wt mice (p14 mice [90], for details see methods section).

VSV is an abortively replicating cytopathic virus that causes a polio- or rabies-like neurotropic infection in immunodeficient mice [91, 92]. Virus control is dependent on neutralizing antibodies (Abs) [93], but the contribution of specific T cell immunity is apparently more complex than previously appreciated. VSV induces a pronounced expansion of specific $CD8^+T_E$ that is independent of CD4 help [94, 95], yet in the absence of $CD4^+$T cells, $CD8^+$T cell function, ab production and

long-term survival can be compromised [96–99]. Furthermore, efficient protection relies on B cell help, direct T_H1 effector activities and associated migratory capabilities [100]. Immunocompetent mice establish long-term $CD8^+T_M$ with kinetics comparable to the LCMV system [95] and the analysis of chemokine production by VSV-specific $CD8^+$T cells will serve to validate or modify central concepts developed in our studies of LCMV-specific T cell immunity.

LM is a Gram-positive, facultative intracellular bacterium that causes severe disease in immunocompromised patients [101]. Mouse models for listeriosis have demonstrated that infections with live bacteria are primarily controlled by specific $CD8^+$T cell populations [102–104] that expand, contract and enter into memory in a highly coordinated fashion [105]. In spite of the dominant role exerted by the $CD8^+$T cell response, MHC class II-deficient mice are susceptible to a markedly reduced LD_{50} and show an exacerbated disease course as well as delayed clearance after low-dose LM infection [106]. In fact, the identification of MHC II-restricted LM epitopes has revealed that the dominant T cell epitope in B6 mice (LLO190) is MHC-II-restricted [107] and LM-specific $CD4^+$T responses follow expansion/contraction kinetics that are commensurate to those of specific $CD8^+$T cell responses [108]. Similar to acute LCMV infection, stable maintenance of $CD8^+$T cell memory contrasts with a slow decline of specific $CD4^+T_M$ [109]. To identify LM-specific $CD8^+$T cell responses in infected B6 mice, a recombinant strain is employed that expresses the entire coding sequence of ovalbumin including the dominant K^b-restricted OVA257 epitope (rLM-OVA) [110, 111].

Altogether, the employed model systems offer a comprehensive and flexible set of experimental tools to evaluate the role of T cell-produced chemokines in infectious disease.

1.6 Flow cytometry as a tool for chemokine detection

Experimental detection of chemokines has largely been restricted to measuring mRNA expression (PCR, Northern, microarrays) or immunological methods (Western blotting, ELISA, in situ histochemistry [ISH]). Furthermore, with the exception of ISH and single cell PCR, important information regarding the populations dynamics might be lost due to the fact that these methods often require pooling of cells into one sample thus averaging out the signal. Furthermore, mRNA expression often does not correlate with protein expression due to several layers of translational regulation.

On the other hand, flow cytometry is a tool to simultaneously measure and analyze physical parameters of a particle, usually a single cell, such as size, granularity and relative fluorescence. The ability to detect fluorescence at different light spectra of thousands of cells per seconds makes flow cytometry a powerful tool to visualize the relative expression of several different proteins within a single cell using fluorchrome-conjugated antibodies. Fluorochrome-conjugated monoclonal antibodies are the preferred staining reagents as they are their cross-reactivity with other proteins is generally low and direct conjugation to fluorochromes reduces background staining while allowing the simultaneous usage of different antibodies raised within the same species. Although some FC-approved monoclonal antibodies against chemokines exist, no such reagents are currently available for the clear majority of murine chemokines **(Table 9, pg.65)**.

Polyclonal antibodies (pAbs) are an appropriate alternative and indeed have been used for the flow cytometric detection of selected murine chemokines in a variety of immune cell subsets such as T cells, NK cells, NKT cells, dendritic cells, monocyte/macrophages (Mo/MΦ), granulocytes and others [70, 112–120]. However, these studies have not rigorously excluded potential cross-reactivities of these reagents and for most murine chemokines a direct visualization by means of flow cytometry has not been reported.

1.7 Aim of this Ph.D. thesis

Chemokines and their receptors are involved in many diverse biological processes ranging from tissue development, tissue and cell homeostasis, innate and adaptive immune responses. The ability to detect chemokines using intracellular flow cytometry has several advantages over more traditional methods as it allows to detect chemokine content of single cells at the protein level either directly *ex vivo* or after a brief stimulation culture. However, only five murine chemokine-specific antibodies are currently approved for flow cytometry therefore greatly limiting the ability to detect chemokines using flow cytometry. Only recently, polyclonal antibodies against the full spectrum of murine chemokines became commercially available thus allowing the possibility of using flow cytometry as a comprehensive screening tool.

The first aim of this thesis is to test the suitability of commercially available polyclonal antibodies

for intracellular flow cytometry and to subsequently apply the methodology to the visualization of chemokine expression by hematopoietic cells in general. The second aim of this thesis work is to define the complete spectrum of chemokines produced by T cells in response to intracellular-replicating pathogens using flow cytometry, to determine their co-expression profiles, kinetics and activation thresholds.

2 Abbreviations

Table 2: Abbreviations.

Abbreviation	Term
Ab	antibody
ActD	actinomycin D
ActD	actinomycin D
APC	antigen presenting cell
APC	allophycocyanin
BCR	B cell receptor
BFA	Brefeldin A
BHK	Baby hamster kidney cell line
BM	bone marrow
BMDC	bone marroe-derived DC
cds	coding sequence
CFSE	carboxyfluorescein succinimidyl ester
cfu	colony-forming units
CHX	cycloheximide
CHX	cycloheximide
CTL	cytotoxic T lymphocyte
DC	dendritic cell
dpi	days post infection
ER	endoplasmatic reticulum
EST	expressed sequence tag
FACS	fluorescent-activated cell sorting
FC	flow cytometry
Fc-block	Fc receptor-blocking reagent
FCS	fetal calf serum
FITC	Fluorescein isothiocyanate
FSC	forward scatter
GAG	glycosamino glycans
GFP	green fluorescent protein
GP	glycoprotein

Continued on next page

Table 2 – continued from previous page

Abbreviation	Term
GP_{33-41}	peptide 33-44 of the LCMV glycoprotein
HCV	hepatitis C virus
HIV	human immunodeficiency virus
iDC	immature dendritic cell
IFNγ	interferon gamma
IgG	immunoglobulin G
IHC	immunohistochemistry
IR	immune response
IRES	internal ribosomal entry site
KDEL	amino acid sequence 'KDEL'
LCMV	lymphocytic choriomenengitis virus
LCMV Arm	LCMV clone Armstrong
LCMV cl13	LCMV clone 13
LM	*Listeria monocytogenes*
rLM-OVA	recombinant LM expressing ovalbumin
LN	lymph node
LPS	lipopolysaccharides
Mϕ	macrophage
mAb	monoclonal antibody
MHC	major immunohistocompatibility complex
MHC tetramer	fluorescently labeled tetrameric MHC:peptide complexes
Mo	monocyte
Mon	Monensin
MPCD8$^+$T cells	CD8$^+$memory phenotype T cell
mRNA	messenger RNA
NK cell	natural killer cell
NKT	natural killer T cells
NP_{396}	fluorescently labeled tetrameric MHC:NP_{396} complexes
OVA	ovalbumin
p14 cells	p14 CD8$^+$ GP_{33-41}-specific T-cell receptor invariant T cells

Continued on next page

Table 2 – continued from previous page

Abbreviation	Term
pAb	polyclonal antibody
PAMP	pathogen-associated molecular pattern
PE	phycoerythrin
PerCP	Peridinin-chlorophyll-protein complex
PFA	paraformaldehyde
pfu	plaque forming units
PMA	phorbol-12-myristate-13-acetate
PRR	pattern recognition receptor
RBC	red blood cell
SSC	side scatter
T_{CM}	central memory T cell
T_H17	T helper 17 cell
TCR	T cell receptor
T_E	effector T cell
T_{EM}	effector memory T cell
T_H	T helper cell
TLR	Toll-like receptor
T_M	memory T cell
T_N	naive T cell
TNFα	tumor necrosis factor alpha
TPA	see PMA
T_{reg}	regulatory T cell
VSV	vesicular stomatitis virus

Table 2: ***Abbreviations.***

3 Materials and Methods

3.1 Materials and Equipment

Type	Model	Manufacturer
Flow cytometers	FACSCalibur	Becton-Dickinson, Franklin Lakes, USA
	LSRII	Becton-Dickinson, Franklin Lakes, USA
	FACS Canto	Becton-Dickinson, Franklin Lakes, USA
Cell sorter	FACSAria	Becton-Dickinson, Franklin Lakes, USA
Centrifuges	Marathon 16 KM	Fisher Scientific, Fair Lawn, NJ, USA
	Thermo Forma Microcentrifuge	Forma Scientific, Marietta, OH, USA
	Centrifuge Model 100/120	Forma Scientific, Marietta, OH, USA
	Cytospin 3	Shandon, UK
FPLC		GE Healthcare, WI, USA
Heating blocks	Standard Heatblock	VWR, West Chester, USA
	TropiCooler 260014	Boekel Scientific, Feasterville, PA, USA
Incubators	Isotemp	Fisher Scientific, Fair Lawn, NJ, USA
Laminar flow hood	Class II Type A2	Nuaire, Plymouth, MN, USA
Microscopes	Olympus BH-2	Olympus, San Diego, USA
	Leica DMI 6000 (confocal)	Leica Microsystems, Bannockburn, USA
Cell counter	Neubauer counting chamber	Hausser Scientific, Horsham, PA, USA
Spectrometer	Nanodrop	Thermo Scientific, Waltham, MA, USA
Photometer	BioPhotometer, Eppendorf	Eppendorf, Hamburg, Germany
PCR machines	Genius	Techne, Burlington, NJ, USA
	GeneAmp PCR System 9700	Applied Biosystems, Foster City, CA, USA
Shaker	Multitron,Version 2	INFORS AG, Bottmingen Switzerland
Waterbath	Isotemp 215	Fisher Scientific, Fair Lawn, NJ, USA
pH meter	SevenEasy	Mettler Toledo, Columbus, OH, USA
Scales	XS104	Mettler Toledo, Columbus, OH, USA
	PJ400	Mettler Toledo, Columbus, OH, USA

Table 3: ***Equipment used.***

Table 4: Materials and Reagents used (excluding antibodies).

Reagent	Supplier
3,3'-dihexyloxacarbocyanine iodide	Invitrogen, Molecular Probes
5x loading dye	Biorad, Philadelphia, PA
Acrylamide/Bis 40%	Biorad, Philadelphia, PA
Actinomycin D	Fluka biochemika, Buchs, Switzerland
Agar	Fisher Scientific, Fair Lawn, NJ, USA
Annexin V-PE Apoptosis Detection Kit	BD Pharmingen, San Diego, CA, USA
β-Mercaptoethanol	Sigma, St. Louis, MO, USA
Bovine Serum Albumin	Fisher Scientific, Fair Lawn, NJ, USA
Bir A enzyme kit	Avidity, 2349 Eudora St, Denver, CO, USA
Brefeldin A	Sigma, St. Louis, MO, USA
Carboxyfluorescein succinimidyl ester (CFSE)	Fisher Scientific, Fair Lawn, NJ, USA
αCD40, clone FGK45.5	gifted by Dr. R. Torres, NJMRC, CO, USA
Cellular preparation tubes	Becton-Dickinson
Chemokine oligo array OMM-022	SABiosciences, Frederick, MD, USA
Crystal Violet	Sigma, St. Louis, MO, USA
Cycloheximide	Sigma, St. Louis, MO, USA
Cyclosporin A	Sigma, St. Louis, MO, USA
DAPI	Invitrogen, Molecular Probes
DMEM	Gibco Life Technologies, MD, USA
DMSO	Sigma, St. Louis, MO, USA
DNA ladder	Biorad, Philadelphia, PA
DNA primers (see Table 8)	IDT, IA, USA
Dulbecco's PBS, pH 7.2	Gibco Life Technologies, MD, USA
EasySep Mouse $CD8^+$ T cell enrichment kit	StemCell Technologies Inc., Canada
EasySep anti-PE kit	StemCell Technologies Inc., Canada
EDTA	Fisher Scientific, Fair Lawn, NJ, USA
Ethanol, 200 Proof	AAPER Alcohol, KY, USA
Ethidium bromide solution 10mg/ml	Promega, Madison, WI, USA
F68	Sigma, St. Louis, MO, USA
Fetal Bovine Serum	Atlanta Biologicals, GA, USA
FuGENE 6	Roche Diagnostics, Indianapolis, IN, USA
Graces Insect Medium plain	Biosource P167-500
Gel extraction kit	Qiagen Sciences, MD, USA

Continued on next page

Table 4 – continued from previous page

Reagent	Supplier
Hoechst 33342	Invitrogen, Molecular Probes
IFNγ, recombinant, murine	Peprotech, NJ, USA
αIgM, donkey αIgM F(ab)2	Jackson Immunoresearch, PA, USA
IL-15, recombinant, murine	Peprotech, NJ, USA
Ionomycin	Sigma, St. Louis, MO, USA
Isopropanol	Fisher Scientific, Fair Lawn, NJ, USA
Laemmli buffer	Biorad, Philadelphia, PA
LB broth	Becton Dickinson, Sparks, MD, USA
Leupeptin	Sigma, St. Louis, MO, USA
MEM	Gibco, Gaithersburg MD, USA
Methanol	Fisher Scientific, Fair Lawn, NJ, USA
MG-132, proteasome inhibitor	Fisher Scientific, Fair Lawn, NJ, USA
MHC peptides	see Table 7
Micro slides (Cat. No. 3039)	Becton Dickinson, Sparks, MD, USA
Mouse CD8$^+$T cell enrichment kit	StemCell Technologies Inc., Canada
Ovation Biotin RNA Amplification & Labeling System	NuGen, USA
Penicillin-Streptomycin	Gibco Life Technologies, MD, USA
Percoll	Amersham, Piscataway, NJ, USA
Pepstatin	Sigma, St. Louis, MO, USA
paraformaldehyde (PFA)	Sigma, St. Louis, MO, USA
phorbol 12-myristate 13-acetate (PMA / TPA)	Sigma, St. Louis, MO, USA
ProLong Gold antifade reagent with DAPI	Invitrogen, Molecular Probes
Propidium iodide (1.0 mg/ml)	Invitrogen, Molecular Probes
Protein ladder	Biorad, Philadelphia, PA
Quantikine MIP-1α Immunoassay (MMA00)	R&D Systems, MN, USA
Quantikine MIP-1β Immunoassay (MMB00)	R&D Systems, MN, USA
Quantikine Rantes Immunoassay (MMR00)	R&D Systems, MN, USA
Rapid Ligation Kit	Roche, Indianapolis, IN, USA
RNeasy Micro Kit	Qiagen Sciences, MD, USA
RNeasy Mini Kit	Qiagen Sciences, MD, USA
RPMI 1640	Gibco Life Technologies, MD, USA
Saponin	Sigma, St. Louis, MO, USA
Sodium dodecyl sulfate (SDS)	Fisher Scientific, Fair Lawn, NJ, USA

Continued on next page

Table 4 – continued from previous page

Reagent	Supplier
Sodium azide	Fisher Scientific, Fair Lawn, NJ, USA
Streptavidin-PE	Invitrogen
T4 DNA ligase and ligation buffer	New England Biolabs, MA, USA
Taq-Polymerase	Fisher Scientific, Fair Lawn, NJ, USA
Temed	Biorad, Philadelphia, PA
TRI reagent BD	Sigma, St. Louis, MO, USA
Tris	Fisher Scientific, Fair Lawn, NJ, USA
Triton X-100	Fisher Scientific, Fair Lawn, NJ, USA
Trypan Blue Solution	MP Biomedicals Inc, Solon, OH, USA
Tryptic soy broth	Becton, Dickinson and Company, NJ, USA
Tween 20	Fisher Scientific, Fair Lawn, NJ, USA
Zenon antibody labeling kits (α-goat, α-mouse)	Invitrogen

Table 4: ***Materials and Reagents used (excluding antibodies).***

Name	Ingredients
autoMACS sort buffer	PBS (pH 7.2), 0.5% BSA and 2 mM EDTA, degassed
Brefeldin A (BFA)	10 mg/ml in methanol, stored at -20°C
22% BSA (w/v)	22% BSA (w/v) in PBS (ph 7.2)
Complete RPMI	RPMI-1640/GIBCO, supplemented with 7% FCS, 1% L-glutamine, 1% Pen/Strep
Duncan 'tail buffer' for genotyping	500 μl 1M NaOH, 100 μl 0.5M EDTA, 49.4 ml H_2O
EasySep sort buffer	2% FCS in PBS (pH 7.2)
FACS buffer (PBS staining buffer)	500 ml PBS (GIBCO), 5 ml FCS, 0.5g sodium azide
Dulbecco's phosphate-buffered saline (PBS), pH 7.2	GIBCO (cat.-#D8537)
HEPES, 1M	GIBCO (cat.-#15630)
90% Methanol fixing solution for flow cytometry (v/v)	90% Methanol + 10% PBS
PBS/saponin buffer	99 ml FACS buffer + 1 ml saponin stock
PFA/saponin solution	58 ml HBSS, 40 ml PFA Stock, 1ml saponin stock, 1 ml HEPES
RBC lysis buffer	200 ml H_2O, 200 μl 1M HEPES, 1.66g NH_4Cl
RPMI Medium 1640	GIBCO (cat.-#11875)
Saponin stock	1g saponin in 10 ml HBSS
Trypsin-EDTA, 0.25%	GIBCO (cat.-#25200)

Table 5: ***Commonly used media and buffers.***

Table 6: Antibodies used in flow cytometry other than chemokine antibodies

Antigen	Other name(s)	Antibody clone	Ab species/ isotype	Format	Supplier
Surface & intracellular					
CD3ϵ		145-2C11	hamster	FITC/PE/PerCP	BD/ebio
		17A2	rIgG2b	eFluor450	ebio
CD4		GK1.5	rIgG2b	FITC/PE/APC	ebio
		RM4-5	rIgG2a	FITC/PE/PerCP	BD
CD8α		53-6.7	rIgG2a	FITC/PE/PerCP/APC/ PE-Cy7/APC-Cy7/PB	BD/ebio
CD11b	integrin aM	M1/70	rIgG2b	FITC/PE/APC/PerCP-Cy5.5	BD/ebio
CD11c	integrin aX	HL3	hamster	FITC/PE/APC	BD
CD16/32	'Fc block'	2.4G2	rIgG2b	purified	BD
CD19		1D3	rIgG2a	PE/PerCP-Cy5.5	ebio
CD44		IM7	rIgG2b	PE	BD
CD45		30-F11	rIgG2b	FITC/PerCP	BD
CD45.1				FITC/PE/PerCP	BD
CD45.2		104	mIgG2a	FITC	BD
CD45R	B220	RA3-6B2	rIgG2a	FITC/PE/APC	ebio
CD49b	integrin a2	DX5	rIgM	FITC/PE	ebio
CD90.1	Thy1.1	HIS51	mIgG2a	PE, PerCP, A647	ebio
CD90.2	Thy1.2	53-2.1	rIgG2a		ebio
CD122				PE	ebio
CD154	CD40L	MR1	hamster	PE	BD
CD161c	NK1.1	PK136	mIgG2a	FITC/PE/PerCP-Cy5.5	BD/ebio
CD197	CCR7	4B12	rIgG2a	PE	BioL
F4/80		BM8	rIgG2a	PE	Inv/Cal
Gr-1	Ly6C/G	RB6-8C5	rIgG2b	FITC/Alx488/PE	ebio
GzmA			rabbit	unconjugated	*)
GzmB		GB12	mIgG1	PE/APC	Cal
IFNγ		XMG1.2	rIgG1	PE/APC/PE-Cy7	BD/ebio
IL-2		JES6-5H4	rIgG2b	PE/APC/PB	BD/ebio
TNFα		MP6-XT22	rIgG1	PE	
hCD3		SK7	mIgG1	PerCP	BD
hCD56		B159	mIgG1	PE/APC	BD
hIFNγ		4S.B3	mIgG1	Pacific Blue	ebio
Isotype controls					
unkown		R35-95	rIgG2a	FITC/PE	BD
secondary Abs					
goat IgG			donkey F(ab')2	FITC/PE/Cy5	Jackson
sheep IgG			donkey F(ab')2	FITC/PE/Cy5	Jackson

Table 6: ***Antibodies used other than chemokine antibodies.*** *BD = BDBiosciences, BioL = Biolegend, RnD = RnD Biosystems, ebio = ebiosystems, SB = Southern Biotech, Cal = Caltech, Inv = Invitrogen, *) gifted by Dr. Simon, MPI Freiburg.*

Table 8: Subcloning of chemokine cDNA into the pIRES-AcGFP1 expression vector.

Gene	Vendor	Clone ID	Accession No.	Insert 3' RE or primer (5'→3')	Insert 5' RE or or primer	Target 3' RE	Target 5' RE
Ccl1	OBS	40129729	BC120806	EcoRI	EcoRI	EcoRI	EcoRI
Ccl2	OBS	40131170	BC145867	CCG CTC GAG CGG ACC ATG CAG GTC CCT G	CCG GAA TTC CGC TAG TTC ACT GTC ACA CTG GTC	XhoI	EcoRI
Ccl3	OBS	40041119	BC111443	CCC CCT CGA GAT CAT GAA GGT CTC CAC CAC	CCC CGA ATT CTC AGG CAT TCA GTT CCA G	XhoI	EcoRI
Ccl4	OBS	8734006	BC119257	CCC CTC GAG ACC ATG AAG CTC TGC GTG TCT GC	CCC CCC GGG TCA GTT CAA CTC CAA GTC ACT C	XhoI	EcoRI
Ccl5	OBS	4925413	BC033508	CCG CTC GAG ACC ATG AAG ATC TCT GCA G	CCG GAA TTC TAG CTC ATC TCC AAA TAG TTG ATG	XhoI	EcoRI
Ccl6	OBS	3492808	BC002073	EcoRI	DraI	EcoRI	SmaI
Ccl7	OBS	30276350	BC061126	SalI	RsaI	XhoI	SmaI
Ccl8	OBS	40126422	BC117101	GTG CTC GAG AAC ATG TAC GCA GTG C	CGG AAT TCT CAA GGC TGC AGA ATT TGA GAC TTC	XhoI	EcoRI
Ccl9/10	OBS	40131265	BC145962	EcoRI	EcoRI	EcoRI	EcoRI
Ccl11	OBS	1527856	BC027521	EcoRI	EcoRV	EcoRI	SmaI
Ccl12	OBS	1548072	BC027520	XhoI	EcoRV	XhoI	SmaI
Ccl17	ATCC	3328278	BC028505	CCG AGA TCT CCC ATG AAG ACC TTC ACC	GCG AAT TCG GGA AGG TCA TGG CCT TGG G	BglII	EcoRI
Ccl19	OBS	1349213	BC051472	GTG CTC GAG GCC ATG GCC CCC CGT G	CGG AAT TCT CAA AC ACA GGG CTC CTT CTG GTG C	XhoI	EcoRI
Ccl20	OBS	1380543	BC028504	EcoRI	PvuII	EcoRI	SmaI
Ccl21b	OBS	3372243	BC038120	GTG CTC GAG ACC ATG GCT CAG ATG ACT CTG	GGG AAT TCT ATC CTC TTG AGG GCT GTG TCT	XhoI	EcoRI
Ccl22	OBS	4192393	BC012658	EcoRI	HpaI	EcoRI	SmaI
Ccl24	OBS	3472002	BC065389	EcoRI	XmnI	EcoRI	SmaI
Ccl25	OBS	40126352	BC117033	BglII	EcoRI	BglII	EcoRI
Ccl27	OBS	3471454	BC028511	GTG CTC GAG ACC ATG ATG GAG GGG CTC	CCG GAA TTC CGG TTA GTT TTG CTG TTG GGG G	XhoI	EcoRI
Ccl28	OBS	4240191	BC055864	EcoRI	PstI	EcoRI	PstI
Cxcl1	OBS	40130779	BC132502	EcoRI	EcoRI	EcoRI	EcoRI
Cxcl2	OBS	40055368	BC119511	SacI	XmaI	SacI	XmaI
Cxcl3	OBS	40126333	BC117014	EcoRI	EcoRI	EcoRI	EcoRI
Cxcl4	OBS	30280161	BC061111	SalI	PstI	XhoI	PstI
Cxcl5	OBS	4976854	BC024392	EcoRI	EcoRI	EcoRI	EcoRI
Cxcl7	OBS	40053104	BC127043	XhoI	BamHI	XhoI	BamHI
Cxcl9	OBS	3257716	BC003343	EcoRI	RsaI	EcoRI	SmaI
Cxcl10	OBS	1446589	BC030067	CCG CTC GAG CGG ACC ATG AAC CCA AGT GCT G	CCG GAA TTC CGG TTA AGG AGC CCT TTT AGA CC	XhoI	EcoRI
Cxcl11	OBS	5035983	BC025903	GTG CTC GAG ACC ATG AAC AGG AAG GTC AC	GCC GGA ATT CTC ACA TGT TTT GAC GCC	XhoI	EcoRI
Cxcl12	OBS	6406409	BC046827	CCG CTC GAG ACC ATG GAC GCC AAG GTC	CGC TTC TTT TTT CCT ATC TTT TCT TTT TTC CCC AC	XhoI	1)
Cxcl12	OBS	6406409	BC046827	GTG GGG AAA AAA GAA AAG ATA GGA AAA AAG AAG CG	GGA ATT CCC TAG TTT TTC CTT TTC TGG GC	1)	EcoRI
Cxcl13	OBS	4217539	BC012965	CCG CTC GAG CCG ACC ATG AGG CTC AGC ACA GC	CCG GAA TTC CGG TCA GGC AGC TCT TCT CTT AC	XhoI	EcoRI
Cxcl14	OBS	9056321	BC147274	CCC CTC GAG ACC ATG AGG CTC CTG GCG	GGG AAT TCT TAA AGT TCG TCC TTT TCT TCG TAG ACC CTG CG	XhoI	EcoRI
Cxcl15	OBS	30298837	BC061138	CCG CTC GAG CGG ATC CAG ACC AGA GTC AGG C	CCC CCC GGG TTA AAG TTC GTC CTT GGC ATC ACT GCC TGT	XhoI	EcoRI
Cxcl16	OBS	3988542	BC019961	CCG CTC GAG ACC ATG AGG CGG GGC TTT G	GGG AAT TCG GCG CTA GGG TCT TGG TTC	XhoI	EcoRI
Cxcl17	OBS	1547987	BE197231	CCC CTC GAG ACC ATG AAG CTT CTA GCC TCT CC	CCC GAA TTC CTA TAA GGG CAG CGC AAA GCT	XhoI	EcoRI
Xcl1	OBS	3974601	BC062249	CCG CTC GAG CCA TGA GAC TTC TCC TCC	CGG GAA TTC CTT ACC CAG TCA GGG TTA TCG C	XhoI	EcoRI
Cx3Cl1	OBS	6490082	BC054838	CCG CTC GAG CGG CCA TGG CTC CCT CG	CGG AAT TCC GTC ACA CTG GCA CCA GGA CG	XhoI	EcoRI
mIL15	2)			GCT GCT CGA GCT CGG CCA CCA TGT ACA GCA TG	CTG CAG AAT TCC GAG TCA GGA CGT GTT GAT G	XhoI	EcoRI
pIRES2-AcGFP1	CL			AGC AGA GCT GGT TTA GTG AAC CGT *3)	TAT TCC AAG CGG CTT CGG CCA GTA A *3)		

Table 8: ***Clones, primers and restriction enzymes (RE) used for subcloning of chemokine cDNA into the pIRES-AcGFP1 expression vector.*** *For subcloning details see Methods section.* [1] *Primers for PCR-driven overlap extension to correct frame-shift [122].* [2] *Gift from Tomasz Sosinowski, National Jewish Hospital, Denver, CO.* [3] *Sequencing primers for target vector to verify proper insert sequence and orientation. ATCC = American Tissue Culture Consortium, CL = Clontech, OBS = OpenBiosystems.*

Epitopes & tetramers	Sequence	MHC restriction	MHC class
LCMV			
GP_{33-41}	KAVYNFATC	D^b	I
$GP_{276-286}$	SGVENPGGYCL	D^b	I
$NP_{396-404}$	FQPQNGQFI	D^b	I
GP_{64-80}	GPDIYKGVYQFKSVEFD	IA^b	II
GP_{66-77}	DIYKGVYQFKSV	IA^b	II
$NP_{118-126}$	RPQASGVYM	L^d	II
VSV			
N_{52-59}	RGYVYQGL	K^b	I
$GP_{415-433}$	SSKAQVFEHPHIQDAASQL	IA^b	II
rLM-OVA			
$LLO_{190-201}$	NEKYAQAYPNVS	IA^b	II
$OVA_{257-264}$	SIINFEKL	K^b	I
MHC Tetramers			
D^bNP_{396}			I
D^bNP_{276}			I
L^dNP_{118}			I
IA^bGP_{66}			II
$IA^bhuCLIP_{87}$			I
K^bOVA_{257}			I
CD1/αGalCer			

Table 7: ***Peptides and MHC tetramers utilized.*** *Peptides corresponding to the indicated pathogen or ovalbumin epitopes were obtained from Peptidogenic or the NJMRC Molecular Core Facility at purities of >95% (GP: glycoprotein; NP or N: nucleoprotein); their MHC-restriction and amino acid sequences are indicated. NIH tetramer core facility as APC or Alx488 conjugates. Biotinylated D^bGP_{33} monomers were a gift from Dr. U. Christen and tetramerized as described [16]; K^bOVA_{257} tetramers and CD1/αGalCer tetramers were provided by Drs. R. Kedl and L. Gapin (NJMRC), respectively. Note that the shorter sequences (GP_{64-80} and GP_{66-77}) within the dominant IA^b-restricted LCMV GP_{61-80} epitope are recognized by the same population of LCMV-specific $CD4^+$T cells [121]. Tetramer staining was performed as described, i.e. for 45 min at 4°C for MHC-I tetramers and for 90 min at 37°C in the presence of sodium azide for MHC-II tetramers [16]. In addition, similar results were obtained using IA^bGP_{61-80} tetramers prepared in the laboratory (not shown).*

3.2 Methods

3.2.1 Mouse strains and human blood samples

C57BL6 (B6) mice, congenic B6.CD90.1 (CD45.2/CD90.1), congenic B6.CD45.1 (CD45.1/ CD-90.2) and B6.Ccl3$^{-/-}$ mice on a B6 background (B6.129P2-Ccl3$^{tm1Unc/J}$), *Ccl2*$^{-/-}$ (B6.129S4--Ccl2$^{tm1Rol/J}$) and *Cxcl10*$^{-/-}$ (B6.129S4-Cxcl10$^{tm1Adl/J}$), as well as Balb/c mice were purchased from the Jackson Laboratory. B6.*Ccl5*$^{-/-}$ mice (Makino et al., 2002) were obtained from Dr. M. von Herrath (these mice are identical to the commercially available B6.129P2-Ccl5$^{tm1Hso/J}$ strain), backcrossed to B6 mice and F1 mice intercrossed to yield B6.*Ccl5*$^{-/-}$, B6.*Ccl5*$^{+/-}$ and B6.*Ccl5*$^{+/+}$ littermates. The following mice or tissues are not commercially available and were gifted by the originating labs: B6.*Ccl7*$^{-/-}$ and B6.*Cxcl16*$^{-/-}$ (Dr. I. Charo, [123, 124]), B6.*Cxcl4*$^{-/-}$ (Dr. A. Kowalska, [125]) and B6.*Cxcl9*$^{-/-}$ mouse (Dr. J. Farber [126]).

P14 TCRtg mice recognize the immunodominant LCMV-GP$_{33-41}$ epitope restricted by H2-D^b [90] and were obtained on a B6.CD90.1 background from Dr. M. Oldstone. P14, OT-I and *Ccl5*$^{-/-}$ mice were housed and bred at the animal facility of the University of Colorado Health Sciences Center according to approved animal protocols under specific pathogen-free conditions. Mice infected with pathogens (LCMV, VSV, LM) were housed in micro-isolator cages in the infectious quarters of the University of Colorado Health Sciences Center animal facility. All animals were evaluated at 8-12 weeks of age and all procedures were performed in accordance with regulations as set forth by the University of Colorado IACUC. Human PBMCs were obtained from healthy subjects and isolated from whole blood using cellular preparation tubes (Becton-Dickinson). Informed consent was obtained in all cases and the study protocol approved by the University of Colorados Institutional Review Board.

3.2.2 Pathogens and their infection protocols

Lymphocytic choriomeningitis virus (LCMV) Armstrong (clone 53b) and clone13, as well as vesicular stomatitis virus (VSV) Indiana, were obtained from Dr. M. Oldstone and stocks prepared by a single passage in BHK-21 cells; plaque assays for determination of virus titers were performed

as described [127]. Recombinant L. *monocytogenes* (LM) expressing full-length ovalbumin (rLM-OVA) [110] was grown and titered as described [128]. Briefly, aliquots of 10^8 mouse-passaged rLM-OVA were frozen at -80°C. To estimate titers prior to *in vivo* challenge, thawed aliquots were used to inoculate 5-10ml fresh TSB media, grown at 37^{o}C in a shaker for 2-3h to log phase followed by determination of OD_{600} values.

8-10 week old mice were infected with a single intraperitoneal (i.p.) dose of 1.5x10^5 plaque-forming units (pfu) LCMV Armstrong, 1x10^6 pfu VSV i.v. or 5x10^3 cfu LM-OVA i.v.. Analyses of concurrent primary and secondary T cell responses were conducted using B6 recipients of LCMV-immune B6.CD45.1$^+$ donor cells challenged i.v. with 2x10^6 pfu of the more virulent LCMV strain clone13. All procedures employed were in accordance with the NIH and University of Colorado Institutional Animal Care and Use Committee (IACUC) guidelines.

3.2.3 Generation of clonotypic, antiviral CD8$^+$ memory T cell populations for gene array analyses (p14 chimera system)

To study clonotypic T cell responses to LCMV the P14 peripheral chimera mouse model has been used throughout this thesis where indicated. This system allows to trace specific T cell populations of known specificity throughout all stages of LCMV infection and memory maturation. CD8$^+$ T cells of the transgenic mouse strain P14 bear an invariant T cell receptor alpha and beta chain specifically recognizing the LCMV glycoprotein peptide GP_{33-44}, which is a major epitope during primary responses to LCMV. To generate peripheral chimera, splenocytes of six week-old P14 mice on a CD90.1 background are purified to $\sim$95% purity using negative enrichment (StemCell Technologies) and transferred either into 6 week-old C57/BL6 wildtype recipient mice (CD90.2$^+$) or OT-I mice which are not able to mount a CD8$^+$T cell response to LCMV. For most of the studies, $5x10^5$ P14 CD8$^+$ T cells were transferred into recipient mice via injection into the retro-orbital plexus and the mice were infected 24 hrs later with either $5x10^5$ pfu Armstrong i.p. or $2x10^6$ pfu clone 13. For the microarray time-course, peripheral chimera were generated and infected in a staggered fashion to allow for sample collection and processing at the same time.

3.2.4 Blood, Tissue and organ preparation

For the isolation of PBMCs, mice were sedated and blood was collected from the retro-orbital plexus using heparinized capillaries and Eppendorf tubes containing 50 μl of heparin. Erythrocytes were lysed by addition of 1 ml of RBC buffer and incubated at RT until the suspension turned from cloudy red to clear red (approx. 2 min). The lysis reaction was stopped by addition of 12 mls of complete RPMI and the cells spun down for 7 minutes at 300g and resuspended in the appropriate volume of complete RPMI or FACS staining buffer for downstream analysis. Spleens and lymph nodes were gently passed through a 70 μm nylon mesh suspended in complete RPMI using a sterile glass plunger to yield a single cell suspension. Cells were spun down for 7 minutes at 300g and splenocyte samples resuspended in 1 ml of RBC lysis buffer for 2 minutes to remove erythrocytes. The lysis reaction was stopped by addition of 12 mls of complete RPMI and the cells spun down for 7 minutes at 300g and resuspended in 10 mls of complete RPMI or FACS staining buffer and counted using a Neubauer chamber.

3.2.5 Cell counts

An aliquot of cells to be counted was diluted 1:1 - 1:20 in Trypan blue and 10 μl loaded into a Neubauer chamber. All 16 fields of all 4 quadrants were counted, averaged and the number of cells per ml determined using the following formula: average cell count x dilution factor x 10^4. In cases were a more exact cell count was required, at least 3 different aliquots were counted as described above and averaged.

3.2.6 Stimulation and cultivation of primary cells

Primary murine cells were cultured for 0.5-5.0h in complete RPMI (RPMI1640/GIBCO, supplemented with 7% FCS, 1% L-glutamine, 1% Pen/Strep) and, where indicated, T cells were stimulated with specific peptides (1 μg/ml for MHC-I- and 5 μg/ml for MHC-II-restricted peptides), plate-bound αCD3 (10 μg/ml) and soluble αCD28 (2 μg/ml), LPS (500ng/ml), recombinant IFNγ(1000U/ml, Peprotech) or PMA/ionomycin (5ng/ml and 500ng/ml, respectively) in the presence or absence

of 1μg/ml Brefeldin A (BFA). For transcriptional and/or translational blockade, cells were pre-incubated for 30min at 37°C with 5μg/ml actinomycin D (ActD, Sigma) and/or 10μg/ml cycloheximide (CHX) prior to addition of peptide and/or BFA.

3.2.7 Generation and infection of bone marrow derived dendritic cells

Femurs and tibias were obtained from C57/BL6 mice sacrificed by lethal exposure to CO_2 and subsequent cervical vertebrae dislocation according to approved IACUC protocol. Muscle tissue was removed and bones were wiped with 70% alcohol and then washed two times in sterile PBS prior to cutting the epiphyses using scissors. The marrow was flushed from the dyaphysis and the epiphyses by fluid pressure using a 25G needle attached to a 5ml syringe containing complete RPMI (RPMI 1640 (Gibco/Invitrogen) +L-Glutamine, 10% FCS, 5% Penicillin/Streptomycin (Gibco/Invitrogen)). BM cells were pooled and red blood cells were lysed by incubation for 2 minutes in 1 ml of RBC lysis buffer, washed once with complete RPMI and resuspended in BM media (complete RPMI supplemented with 50 μM2-Mercaptoethanol and 10 ng/ml GM-CSF) at a concentration of 10^6 cells/ml. 10^6 cells were plated per well of a 24-well plate and cultured at 37°C and 5% CO_2. On day 2 and 4, media was refreshed and floating cells removed by spinning down 2/3 of the media for 5 minutes at 300g. The supernatant was mixed at a ratio of 1:3 with fresh BM media and added back onto the cells. Cells were left undisturbed until day 6. The general morphology of the culture was observed using light microscopy and the loosely adhering dendritic cells were harvested by gently pipetting up and down. Typically, the harvested cells consisted of $>$90% CD11c$^+$ cells that for the most part expressed low levels of CD40 and CD86 characteristic of immature DCs as determined by flow cytometry (not shown).

A single colony of recombinant L. *monocytogenes* (LM) expressing full-length ovalbumin (rLM-OVA) [125] was used to inoculate 2-3 ml of tryptic soy broth (TSB) and cultured at 37°Covernight along with an un-inoculated control. The next day, a 1:50 dilution of the overnight culture was used to inoculated 5 ml of TSB and grown until an OD_{600} of $\sim$0.1. The colony-forming units (cfu) were determined assuming an OD_{600} of 0.1 equals 2x10^8 cfu/ml. Bacteria were washed twice in PBS and used at a multiplicity of infection (MOI) of one for *in vitro* BM-DC infection. Infection was

allowed to proceed for 9h with 1 μg/ml BFA added for the final 5h. Analyzed by FC, infected DCs exhibited slightly increased CD11c expression and elevated SSC properties, likely resulting from the presence of intracellular bacteria.

3.2.8 Subcloning of full-length chemokine coding sequences

All chemokine clones were purchased from OpenBiosystems with the exception of the *CCL17* clone, which was purchased from ATCC, and murine *IL15*, which was gifted by Tomasz Sosinowski (National Jewish Hospital and Research Center, Denver, USA) and subcloned into the bicistronic expression vector pIRES-Ac1GFP2 (Clontech). Subcloning was performed by either digesting plasmids using restriction enzymes or by PCR amplification with primers introducing restriction sites up and downstream of the cds. Generally, primers were designed with an approximate annealing temperature of 65°C and PCRs optimized where necessary and standard PCR performed (5 min at 94°C followed by 35 amplification cycles [30°C at 94°C, 30 sec. at 60°C and 72°C] and 5 min of final extension at 72°C). For the restriction digest of plasmids and PCR products, 1-2μg of plasmid or 0.2-1μg of PCR product were digested using restriction enzymes and buffers according to the manufacturer's published standard protocols (New England Biolabs, NEB). Digests were gel-purified and extracted from the gel using Qiagen's gel extraction kit. pIRES-Ac1GFP2 target plasmid and chemokine insert were ligated at a molar ratio of 1:3 using either a rapid ligation kit (Roche) or a standard 4h - overnight T4 DNA ligase protocol (NEB). Table 8 provides a comprehensive overview of the clones, primers and restriction enzymes used during the subcloning process. All primers were designed using a combination of the 'A plasmid Editor' software [129] and the primer vendor's online 'oligo analyzer' software (Integrated DNA Technologies, Coralville, IA 5224, USA). To increase the weak *Cxcl15* expression observed in the initially generated clones, an endoplasmatic reticulum retaining sequence ('KDEL', [130]) was introduced in-frame via PCR at the 5'-end of the cds. Competent *E. coli* was transfected with the chemokine constructs and plated onto Kan^+ agar plates. Single colonies were picked and cultured in 3ml of Kan^+ LB broth overnight and plasmids isolated using a MiniPrep Kit (Qiagen). Clones were screened for proper size and orientation of the insert using restriction digest and positive clones sequenced.

3.2.9 Transient transfections of cell lines

Vero cells, Cos7 and HEK293T cells were gifts from Drs. M. Oldstone, J. Hutton and G. Eisenbarth, respectively. HEK293T cell were tranfected using a modification of a $CaPO_4$ protocol by Nolan et al [131]. Briefly, 12 μg plasmid DNA and 91.5 μl 2M $CaCl_2$ were diluted into H_2O to yield 750 μl of a 240 mM $CaCl_2$ solution. 750 μl 2x HBS, pH 7.05, was added and the solution bubbled by expelling air through a 2 ml pipette for 10 seconds using an automatic pipettor. 500 μl of the solution was added to the well of a freshly seeded six-well plate containing 2 x 10^6 HEK293T cells in 1.5 ml complete DMEM (10% FCS, 1% Pen/Strep) supplemented with 25 μM f.c. chloroquine 5 minutes prior to transfection. Cells were manually rocked for a few seconds to disperse the transfectant and incubated at 37C / 5% CO_2. The media was replaced 4 hours later with 2 ml complete DMEM supplemented with 1 μg/ml BFA and the cells were incubated until the indicated timepoints, washed once in ice-cold PBS containing 1 μg/ml BFA and immediately fixed in 1.6% PFA for 10 minutes at room temperature. Where indicated, 5 x 10^5 HEK293T or Cos7 cells were transfected using 3 μl Fugene6 reagent (Roche) for every 1 μg DNA according to the manufacturer's instructions. For some control stains, Cos7 cells were transfected with chemokine vectors or empty vectors using FuGENE according to the manufacturers protocol, harvested 24-48 hrs later and stained according to our standard intracellular staining protocol with polyclonal goat abs.

3.2.10 Microarray analysis of gene expression

Total RNA was extracted either directly from purified p14 T_E (8 dpi) and T_M (46, 156, 286 and 400 dpi) or after a 3h stimulation with αCD8 / αCD28 as described above and DNA digested using the MinElute kit (Qiagen) according to the manufacturers instructions. RNA integrity was confirmed using PicoChip RNA gels (Agilent) according to the manufacturer's instructions. Amplification of mRNA (Ovation Biotin RNA Amplification and Labeling System, NuGen), hybridization to Affymetrix M430.2 arrays and quality control were performed by the Affymetrix Core Facility of the University of Colorado Cancer Center according to standard protocols. The GC-RMA algorithm was chosen for the data analyses. MAS5 and RMA normalization were performed as well producing similar results (data not shown). In addition, *ex vivo* purified and TCR-stimulated p14 T_E

were analyzed by 'macroarrays' (OMM022 chemokine array, SuperArray) according to protocols provided by the manufacturer and yielded results comparable to Affymetrix analyses (not shown).

3.2.11 Confocal microscopy

Suspensions of splenocytes and PBMC prepared on d8 after LCMV infection of B6 mice were stained directly ex vivo or after 5h peptide stimulation for surface and intracellular markers, and $NP_{396}B220^{-}CD4^{-}$ (*ex vivo*) or IFN$\gamma^{+}B220^{-}CD4^{-}$ (NP_{396}-stimulated) cells were sorted on a FACS Aria (BD), spun onto glass slides for 5 minutes at 800 rpm using a cytospin (Cytospin3, Shandon) and mounted using the 'ProLong Gold reagent' (Invitrogen) containing DAPI. Slides were analyzed with a Leica TCS SP5 confocal laser scanning microscope equipped with an inverted Leica DMI 6000 microscope, a high performance PC TCS workstation, a 488/543/633 excitation beam splitter, a UV laser (405 nm, diode 50 mW), an argon laser (458/476/488/496/514 nm, 100 mW, attenuated to 20%), a green helium/neon laser (543 nm, 1 mW) and a red helium/neon laser (633 nm, 10 mW) for excitation of DAPI, Alexa-488, PE, and Cy5, respectively. 2048x2048 pixel images were acquired sequentially with a 63x/N.A. 1.4 oil immersion lens at 1.9x zoom (effective pixel size 63.2nm), and prism spectral detectors manually tuned to separate labels (DAPI, 415-487nm; Alexa-488, 497-579nm; PE, 585-699nm; Cy5, 640-778nm). The pinhole size was set at 1 airy unit to give an effective optical section thickness of approximately 0.51.0μm. Gray-scale images were digitized at 8 bits per channel, and exported as TIFF files for processing in Adobe Photoshop CS (version 8.0). For optimal visualization of the relationship between fluorescence-labeled components, images from all channels were pseudocolored blue (for DAPI), green (for Alexa-488), and red (for Cy5). DAPI-labeling was omitted from superimposed (merged) images due to the large size of the nucleus relative to cell size. Splenocytes or PBMC were stained as as described in the flow cytometry staining protocol, fixed with 1% PFA and sorted on a FACS Aria cell sorter (BD) to enrich for IFNγ $^{+}B220^{-}CD4^{-}$ cells. Cells were then spun down and resuspended in 22% BSA and spun onto glass slides (Gold Seal Micro Slides, Ultra StickTM, Cat No. 3039) using a cytospin (Cytospin3, Shandon) for 5 minutes at 800 rpm . One drop of Gold Seal containing DAPI was placed on the slide and a 1.5 mm cover slip was placed on top (No. 1 1/2, Corning). After drying over night, slides were sealed with nail polish. Slides were stored in the dark at 4°C until acquisition.

3.2.12 Flow cytometry, fluorescent activated cell sorting and magnetic bead sorting

Flow cytometric analyses was performed either on a FACS Calibur (BD) for up to four colors or on a LSRII (BD) for up to 7 colors. Fluorescence activated cell sorting was performed on a FACS Aria (BD) by the staff of the University's flow cytometry facility. To yield highly purified cell populations for RNA extraction a two-step enrichment was performed. The first step was to quickly enrichment protocol of the desired population using a magnetic sorter (RoboSep, StemCell technologies) and the second step consisted of sorting on a FacsAria (BD) to increase the purity of the desired cell population to $> 98\%$. Spleens were processed as described above, but without red blood cell lysis. The cell suspension was adjusted to 10^7 nucleated cells/ml and incubated with Fc-block and PE-conjugated primary antibody (i.e. 0.6 μl/ml CD90.1-PE) for 10 minutes at RT, according to the StemCell Technologies standard protocol and sorted on the RoboSep sorter using anti-PE magnetic antibodies. The presorted cells were resuspended in 10% FCS/PBS and enriched to $\sim$99% purity on a FacsAria cell sorter and collected into tubes containing ice-cold FCS. For experiments requiring B-cell depletion, paramagnetic αB220-beads were used (Milteny) or cells were stained with α-B220-PE and sorted using α-PE paramagnetic beads (StemCell Technologies) according to the manufacturer's instructions.

3.2.13 MHC class II tetramer production

The IA^b-LCMV GP_{61-80} baculovirus stock was obtained from Drs J. Kappler and P. Marrack and originally constructed by Dr. M. Jordan. The tetramer production was performed under guidance of Ms. Francis Crawford in the lab of Prof. P. Marrack. The first step was the preparation of sufficient virus stock in order to infect the tetramer-producing Hi-5 host cells. A total of 3 x 10^7 SF-9 cells were resuspended in 20 ml of TMN/FH and incubated in a T225 flask for one hour at 27°C. The media was aspirated and replaced with 20 ml Graces Insect Medium plain (Biosource P167-500) containing Glutamine and 200 μl of virus stock is added. After an additional incubation of one to two hours at 27°C, 50 ml of TMN/FH was added to each flask and the virus containing supernatant is harvested 10 days later by centrifugation. 25x10^8 cells are resuspended in 1.5 l of Graces Plain + F68 and distributed to five 1L spinner flasks. 10 ml of the virus stock is added to

each flask and the cells are incubated for 1-2 hours at 27^{o}C und slow spinning conditions. The volume in each spinner flask was adjusted to 1000 ml with TMN/FH + F68 and incubated for another 24h at 27°C and then incubated at 19^{o}C for additional five days. Cells and debris were removed by centrifugation and the supernatant containing the protein was sterile-filtered through a 21 micron filter. The MHC II protein was antibody-affinity purified and protease inhibitors were added (0.1 mM Pepstatin f.c.). The protein was subjected to buffer exchange into 10 mM Tris, p.H. 8.0 containing Pepstatin, Leupeptin and PMSF (at the above concentrations) while aiming for a concentration of 38 μMas measured by OD_{280}. The protein was subsequently labeled using the Bir A enzyme kit (Avidity, 2349 Eudora St, Denver, CO 80207, called biotin ligase). Briefly, the volume of the protein solution was set as eight parts and one part of Bio Mix A and one part of Bio Mix B are added (both mixes are contained in the Avidity kit). The Bir A enzyme was added at a f.c. of 5 μg/ml and the reaction mix incubated at RT overnight. The reaction was stopped by incubating at RT for 30 minutes under the addition of 1/100th volume of 1 M lodoacetamide. The tagged protein was filtered after addition of 1/10th volume of PBS. The extend of biotinylation was determined by capture ELISA using avidin-agarose beads (2 mg avidin/ml of gel, Vectra Labs) and measuring the amount of precipitated protein vs. unprecipitated protein. The preparation of tetravalent biotinylated protein complex occurs by incubation of 8 moles of biotinylated protein with one mole of dye-linked streptavidin, e.g. streptavidin-PE (BioSource Intl, cat-# 6966). Unbound biotinylated protein was separated from tetravalent complexes using a sephadex sizing column (Superdex200 Prep Grade). The tetramer was contained in the excluded peak at an appropriate MW of 600 kDa. To assess the quality of the tetramer, T-cell hybridomas or T-cells were stained with the tetramer as follows: 1 x 10^5 hybridomas or 1x10^6 T-cells were stained in 30 μl of medium using 20 μl of 50 μg/ml for a f.c. of 20 μg/ml and 5 mM sodium azide. Incubation at 37C for two hours was followed by three washes in FACS buffer and resuspension in 1% FCS/1%PFA.

3.2.14 Antibody and MHC multimer staining

Information about the antibodies used throughout this thesis are listed in table 6 (non-chemokine abs) and table 6 (chemokine abs).

Surface staining: For antibody and tetramer staining, about 10^6 cells were stained in 96 well V-bottom plates. To block binding of antibody to Fcγ receptors, cells were at first incubated for 10 minutes in 100μl of Fc block (4μg/ml in FACS buffer). Cells were then spun down (4 min at 350g) and incubated in 50μl of antibody mix on ice for 30 min (or 45 minutes for staining with MHC class I multimers). Optimal antibody and MHC tetramer concentrations were determined by titration for each new batch. The samples were then washed two times with FACS buffer (4 minutes at 350g). If a two-step or three-step surface stain was required, samples were incubated sequentially with the secondary and tertiary antibodies for 30 minutes each on ice and washed twice as described above. Cells were then resuspended and fixed in 1% PFA/ 1% FCS. **Intracellular staining:** Cells were fixed and permeabilized with 1%PFA/saponin for 10 min at RT, washed twice (6 min at 350g) with PBS/saponin buffer and resuspended in 50 μlPBS/saponin buffer containing the intracellular staining antibodies. After 45 min. incubation at RT, cells were washed twice (6 min at 350g) with PBS/saponin buffer and, if required, incubated for 30 min at RT with 50 ul of secondary antibody in PBS/saponin (typical dilution of secondary antibodies was 1:300 f.c.), washed twice and resuspended in FACS buffer. Staining with the MHC II tetramer required a 2h incubation at 37°C in RPMI followed by two washes with FACS buffer.

Alternatively, transfected cells were fixed with 2% PFA (10min at RT), permeabilized with 90% methanol and stored at -20°C in 90% methanol prior to chemokine staining and analysis. Cells were washed twice (6 minutes at 350g) with FACS buffer to remove the methanol. All stains are performed as described for the PBS/saponin method, but FACS buffer was used instead of PBS/saponin as methanol irreversibly permeabilizes cells.

Chemokine flow cytometry: Intracellular chemokine stains were performed using affinity-purified pabs (CXCL17 pAb: sheep, all other pabs: goat) as well as goat and sheep IgG controls obtained from RnD Systems 1. Chemokine expression was visualized by staining of cells with $\leq$0.1μg pab for 45min at RT in a volume of 50μl followed by detection of primary pab with FITC- or Cy5-conjugated donkey anti-goat or-sheep F(ab)2 fragments (Jackson Immunoresearch) (30min at RT) as outlined in the above staining protocols. Where available, chemokine-specific mabs were used in addition (αCCL2-PE [2H5], Biolegend; αCCL3-PE [39624], αCCL6-APC [262016], αCXCL12 [79018] and αhCXCL14 [131120], RnD Systems). Pre-conjugation of mabs and corresponding iso-

type controls to Alexa-647 was performed using Zenon technology (Invitrogen). For detection of human chemokines we employed fluorochrome-conjugated mabs (αCCL3-APC [93342], αCCL4-FITC [24006], αCCL5-FITC [21445], αCCL22-PE [57203], αCXCL8-FITC [6217]) and affinity-purified goat pabs specific for CCL1 (AF272), CCL5 (AF278-NA) and XCL1 (AF695) (RnD Systems). Although not formally tested, the XCL1-specific AF695 pab likely recognizes both XCL1 and XCL2 since these chemokines differ by only 2 amino acids in positions 7/873. All samples were acquired on FACSCalibur, FACSCanto or LSR II flow cytometers (BDBiosciences) and analyzed with CellQuest, DIVA (BDBiosciences) and/or FlowJo (TreeStar) software. Unless stated otherwise, the PFA/saponin method was used to perform intracellular chemokine staining.

3.2.15 Genotyping of mice

DNA was extracted from 1-2 mm mouse tail snips by boiling for 20 min in 300 μl Duncan Lysis buffer using a heating block heated to 110°C. 4 μl of DNA was used for subsequent PCR analysis using the PCR primers and protocols published by the Jackson Laboratory. In addition, CCL3 and CCL5 deficiency of mice was determined using flow cytometry. For CCL3 analysis, PBMCs were stimulated for 5 hrs in complete RPMI supplemented with TPA (20ng/ml) / Ionomycin (500 ng/ml) in the presence of 1 μg BFA and CCL3 and stained for CD8 followed by αCCL3 staining. CCL5 screening was performed on *ex vivo* PBMCs stained with αNK1.1 followed by intracellular αCCL5 staining as per our intracellular flow cytometry protocol. Blood from P14 mice and OT-I mice were screened for a high frequency (>95%) of $CD8^+$ T cells expressing either the T cell receptor chains TCRα-V2, TCRβ-V8.1 (P14) or TCRα-V2 and TCRβ-V5 (OT-I) using flow cytometry.

3.2.16 Enzyme-Linked Immunosorbent Assays (ELISA)

Quantitation of CCL3, CCL4 and CCL5 in sera and tissue culture supernatants was performed using respective Quantikine ELISA kits according to the protocols provided by the manufacturer (RnD Systems). For evaluation of CCL3/4/5 chemokine complex formation, supernatants of NP_{396}peptide-stimulated effector spleen cells (d8 after LCMV, 5h stimulation, no BFA) were diluted and incubated for 2.5h at RT in plates pre-coated with 5.0 μg/ml polyclonal goat IgG, αCCL3, αCCL4, or αCCL5.

Absorbed supernatants were immediately analyzed for CCL3/4/5 content by standard ELISA. To determine chemokine production on a per cell basis, FACS analyses were performed in parallel to calculate the exact numbers of NP_{396}-specific $CD8^+$T cells in the stimulation culture.

3.2.17 Statistics

Data handling, analysis and graphic representation was performed using Prism 4.0 (GraphPad Software, San Diego, CA). All data summarized in bar and line diagrams are expressed as mean $\pm$ 1 SE. Asterisks indicate statistical differences calculated by unpaired or paired Students t-test and adopt the following convention: *: $p<0.05$, **: $p<0.01$ and ***: $p<0.001$. ET_{50} values (response kinetics) and EC_{50} values (activation thresholds) were calculated by plotting the fraction of specific T cells demonstrating detectable chemokine/cytokine staining (flow cytometry) or the amount of secreted chemokines (ELISA) as a function of stimulation time (0-5h, 10^{-6}M peptide) or peptide concentration (5h, 10^{-6}-10^{-11}M peptide) followed by non-linear regression analysis using appropriate data format and analysis functions in the Prism software. Note that ET_{50} and EC_{50} values are independent of the fact that not all effector functions are induced in all T cells of a given specificity.

4 Results

The results section is subdivided into two main parts. The first part describes the establishment of the chemokine flow cytometry methodology and its application to visualize chemokine protein expression by T cells, B cells, NK cells and dendritic cells. The second part specifically determines the chemokine repertoire of pathogen-specific T cells in response to different intracellular pathogens and identifies chemokines as the major effector gene family expressed by these cells during acute infections.

4.1 Development and validation of a flow cytometric method to measure chemokine expression at the protein level

4.1.1 Subcloning and flow-cytometric validation of constructs

Intracellular flow cytometry requires fixation of the cells prior to permeabilization in order to prevent cytolysis and leakage of soluble intracellular proteins. Commonly used crosslinkers such as paraformaldehyde can mask some epitopes unrecognizable to the cognate antibodies. This results in the limited repertoire, when compared to Western blotting or ELISA, of monoclonal and polyclonal antibodies available for intracellular flow cytometry and the suitability of a given antibody has to be determined experimentally. Only recently did the complete spectrum of chemokine antibodies become commercially available to potentially allow the visualization of the complete spectrum of CCL, CXCL, XCL and CX_3CL chemokines, but most of these antibodies have not been tested for flow cytometry. As seen in table 9 on page 65, only seven mAbs antibodies have been approved for flow cytometry. Since the goal of this thesis project was the exhaustive delineation of the chemokine profile of pathogen-specific T cells at the protein level, it was of critical importance to develop a reliable assay system. While monoclonal antibodies for some of the chemokines were available, the majority of the available chemokine-specific antibodies are of polyclonal origin. We obtained all 35 available polyclonal antibodies from one vendor (generously gifted by Dr. F. Mortari, R&D Systems) as we had previously good experience with the quality of the antibodies obtained from this vendor. The advantage of polyclonal antibodies over monoclonal antibodies is the increased likelihood that at least one epitope is recognized by one of the subclones. If deemed necessary,

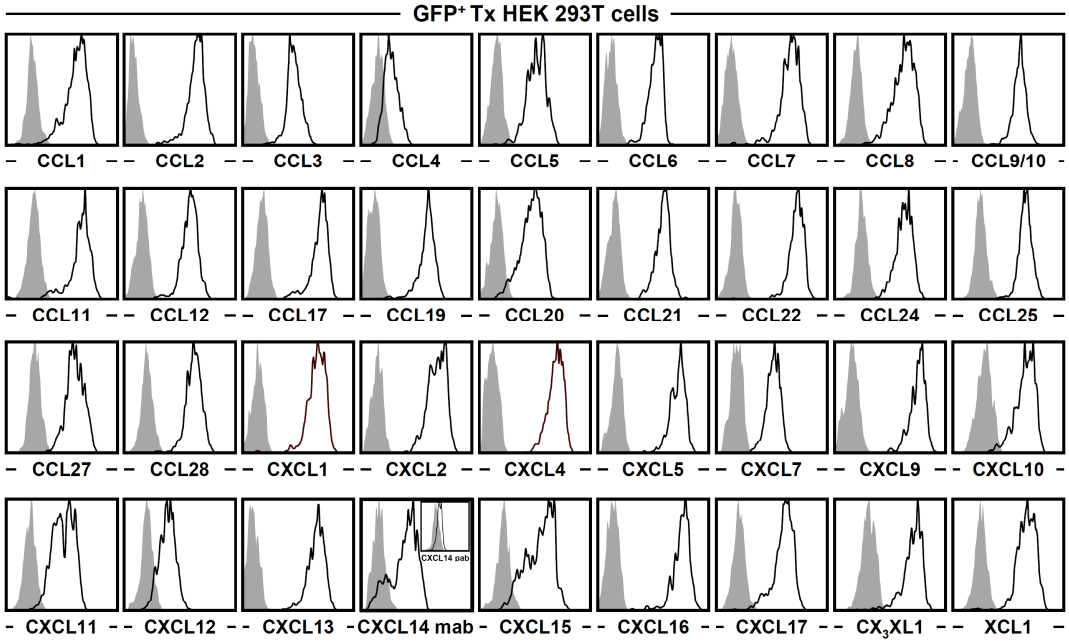

Figure 3: ***Validation of polyclonal chemokine-specific antibody usage for flow cytometry.*** *HEK 293T cells were transfected with individual pIRES2-AcGFP1 vectors containing Il15 (negative control) or 36 distinct murine chemokines and cultured for 18h. BFA was added for the final 14h to limit chemokine secretion and cells were analyzed for expression of corresponding chemokine proteins by FC as detailed in Methods. All histograms are gated on GFP$^+$ HEK cells comparing Il15 transfectants (gray solid) and respective chemokine transfectants (black tracing) stained with the same chemokine-specific pab. To reduce proteasomal degradation, Cxcl14-transfected HEK cells were cultured in the presence of 10μM of the protease inhibitor MG-132 and stained with an αhuman CXCL14 pAb (insert) or αhuman CXCL14 mAb (large panel).*

testing of antibodies from other vendors would be included in order to obtain as complete of a panel as possible. In order to test if these antibodies work under conditions of cell fixation, expression vectors were created by subcloning chemokine clones obtained from Openbioscience or ATCC into the bicistronic pIRES2-AcGFP1 plasmid (Clontech) as described in the Materials & Methods section. The chemokine expression is driven by the CMV promotor and an internal ribosomal entry site (IRES) sequence facilitates the translation of the downstream green fluorescent protein (GFP) allowing identification of transfected cells. The successful detection of all 35 chemokines after an 18 hour transfection of HEK293T cells with addition of 1 μg / ml Brefeldin A (BFA) for the last 14 hours of incubation is described in detail in figure 3. The addition of BFA inhibits the anterograde transport of proteins from the endoplasmatic reticulum (ER) to the Golgi apparatus therefore

reducing chemokine release from the cell.

Problems were encountered detecting CXCL14 using an antibody specific for murine CXCL14 (AF730) which did not yield any positive staining despite high expression of GFP. Due to the high homology (95%) between murine and human CXCL14, I further tested the suitability of an antibody against human CXCL14 (AF866) which initially did not stain CXCL14-transfected cells either. Upon closer investigation of the current CXCL14 literature, I found a recent article describing a unique proteosomal degradation sequence within the human *Cxcl14* gene [132] which efficiently facilitates the degradation of human CXCL14 in cells expressing the 26S proteasome. The human and mouse sequences were aligned in order to determine if the same mechanism is responsible for the lack of murine CXCL14 detection in our transfected cells. Indeed, the so called 'destruction box' is highly conserved between human and mouse *Cxcl14* (**Fig.4A**). Peterson *et al.* were able to prevent degradation of human CXCL14 in cell lines expressing the 26S proteasome using the protease inhibitor MG-132. Culturing the CXCL14-transfected HEK293T cells in the presence of the protease inhibitor MG-132 suppressed the degradation of our murine construct and allowed the detection of CXCL14 protein expression by flow cytometry using a monoclonal α-human antibody (**Fig.4B**), but not by any of the tested mouse-specific CXCL14 antibodies (not shown). This observation confirms that targeting of CXCL14 for proteosomal degradation is conserved between mouse and human, which has not been experimentally shown before, and establishes the flow-cytometric use of an α-human monoclonal antibody against murine CXCL14.

The initially weak CXCL15 expression was enhanced by fusing the ER-retaining sequence 'KDEL' [130] to the C-terminus of the CXCL15 protein thus effectively enhancing the staining intensity. Suitable antibodies for CCL26 and CXCL3 were not available and therefore further analysis of these chemokines was not performed.

4.1.2 Determination of the cross-reactivity of chemokine antibodies

One putative problem of polyclonal, and to some respect monoclonal, antibodies is the potential of cross-reactivity with other proteins. Although the R&D polyclonal antibodies are affinity-purified to exclude unspecific antibodies, some cross-reactivity with other chemokines (and unrelated proteins)

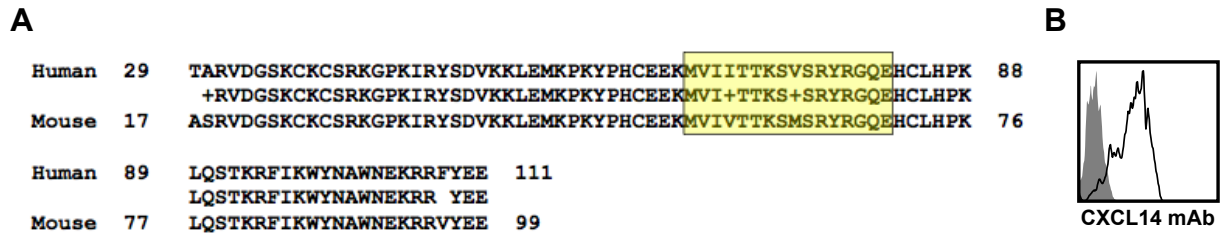

Figure 4: ***Murine CXCL14 can be targeted for proteosomal degradation by the 26S ribosome via a conserved targeting sequence.*** *(**A**) Sequence alignment of human and murine CXCL14 demonstrates strong conservation (13/15 AA) of a proteosomal targeting sequence. (**B**) To inhibit proteasomal degradation, HEK 293T cells transfected with the pIRES2-AcGFP1-Cxcl14 vector were cultured for 18 hours in the absence (grey) or presence (black line) of 10μM of the protease inhibitor MG-132 and stained with the mouse α-human CXCL14 mAb clone 131120. BFA was added for the last 14 h of culture.*

can not be ruled out as some members of the chemokine family show a high degree of sequence similarity and overall 3D structure. Many chemokine antibodies were tested for cross-reactivity by the manufacturer using ELISA and Western blotting, but none have been systematically tested using flow cytometry (see Table 9, pg.65). Since cross-reactivity can only be determined experimentally, a "library" of single chemokine-transfected HEK293T cells was created to allow testing of every antibody against every chemokine. To this end, HEK293T cells were transfected as described in the materials and methods in the presence of 1 μg/ml BFA for 18 hours, harvested, fixed in 1% PFA for 10 minutes and subsequently stored in 90% methanol at -20^{o}C until further processing. Prolonged storage in methanol reduced GFP fluorescence minimally and had no impact on chemokine antibody binding thus allowed testing of the antibodies in three batches (data not shown).

While all of the 36 tested antibodies detected their cognate antigen, 14 antibodies displayed partial cross-reactivity with other chemokines (**Fig.5)** as summarized in the "partial x-reactivity" column of Table 9 on page 65. The observed cross-reactivities are mainly restricted to the "CC-MCP" (CCL2/7/8/11/12) and "CXC-GRO" (CXCL1-7) clusters [42] thus emphasizing the role of structural homology in the generation of cross-reactive antibodies. The application of these antibodies in flow cytometry is not negated as the staining intensity of most cross-reactive antibodies is often more than ten-fold lower than the positive signal. Utilizing complementary approaches, *e.g.* mRNA expression analysis and the use of knockout mice, can further aid in the discrimination between specific and cross-reactive binding.

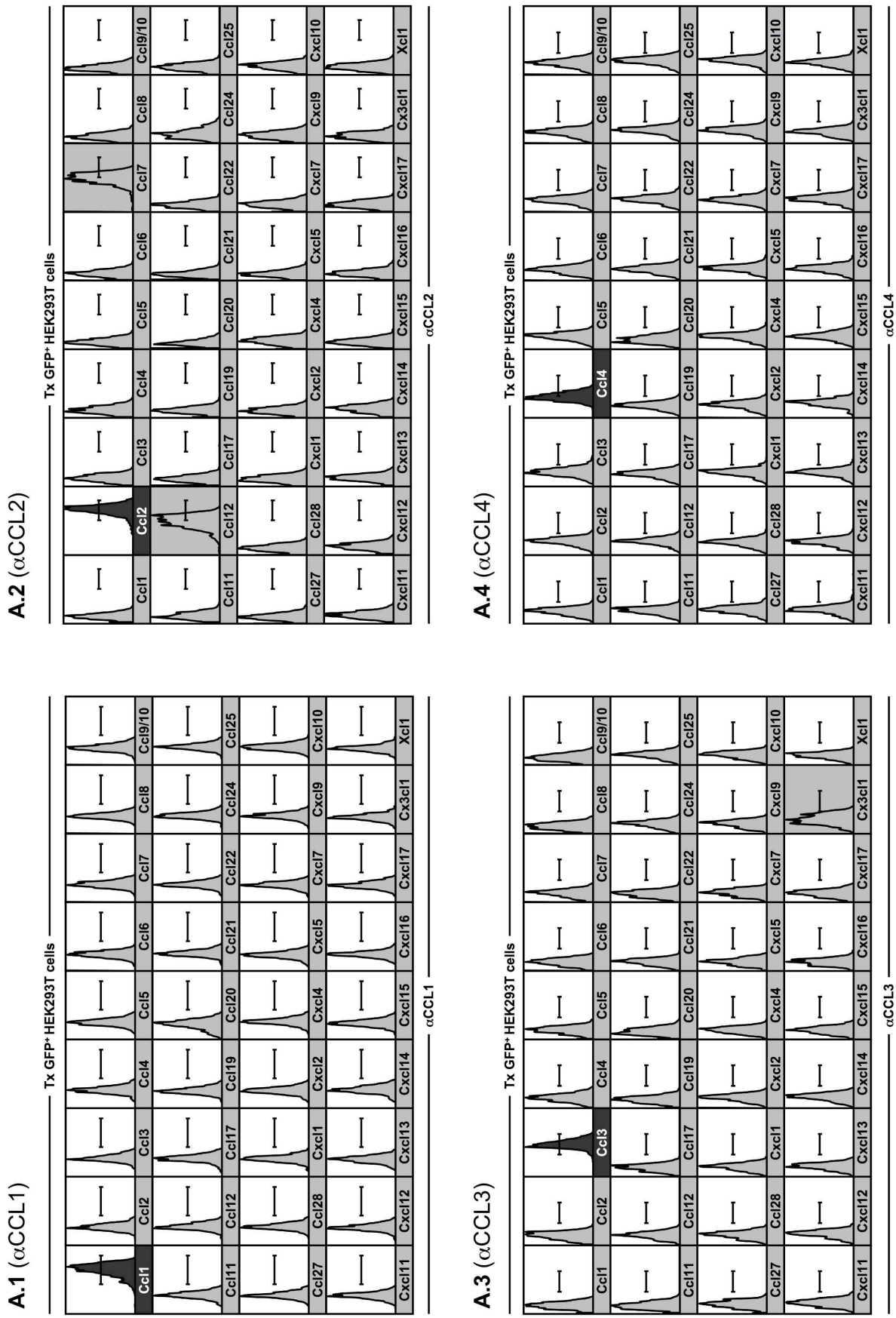

Figure 5 - continued on next page

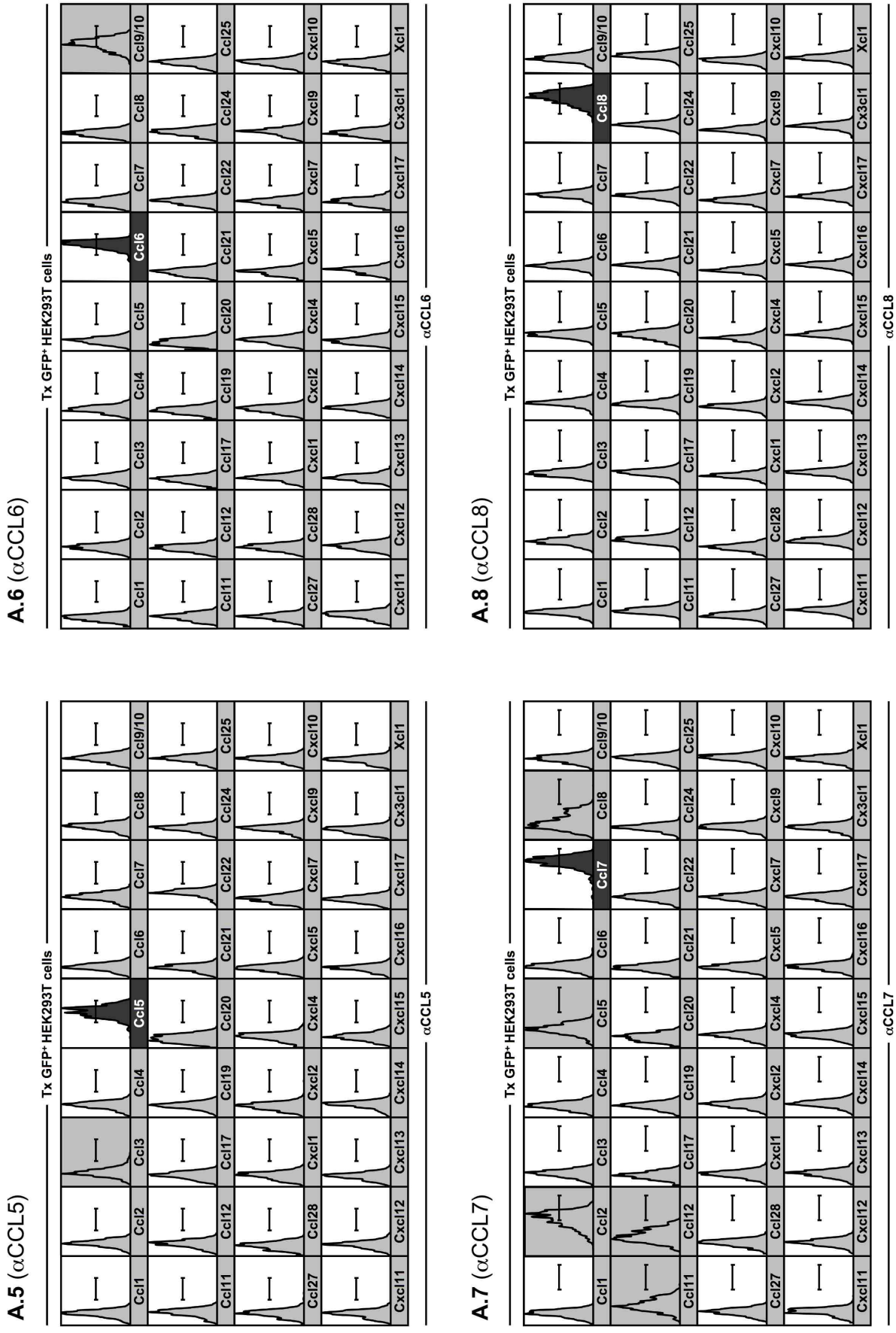

Figure 5 - continued on next page

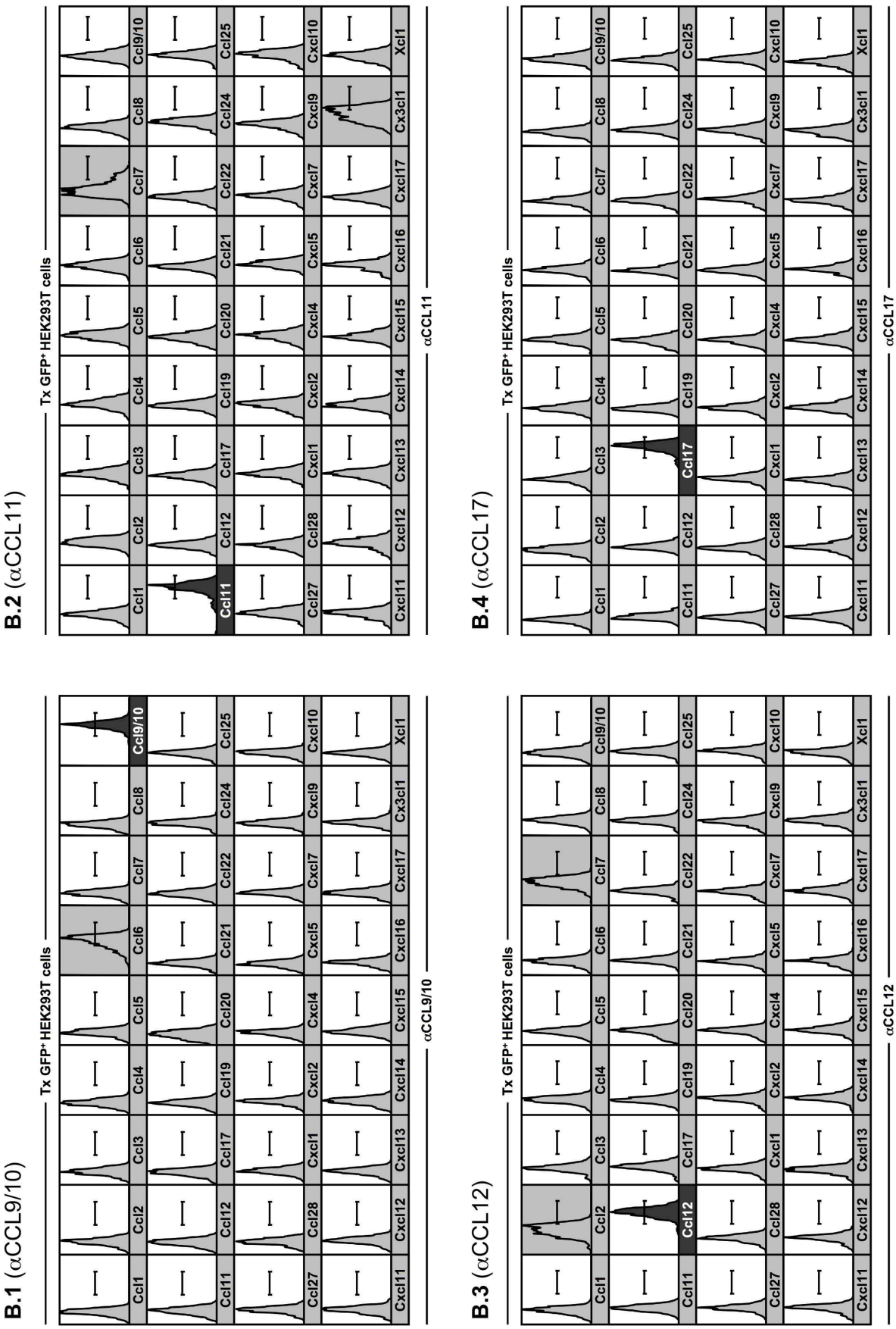

Figure 5 - continued on next page

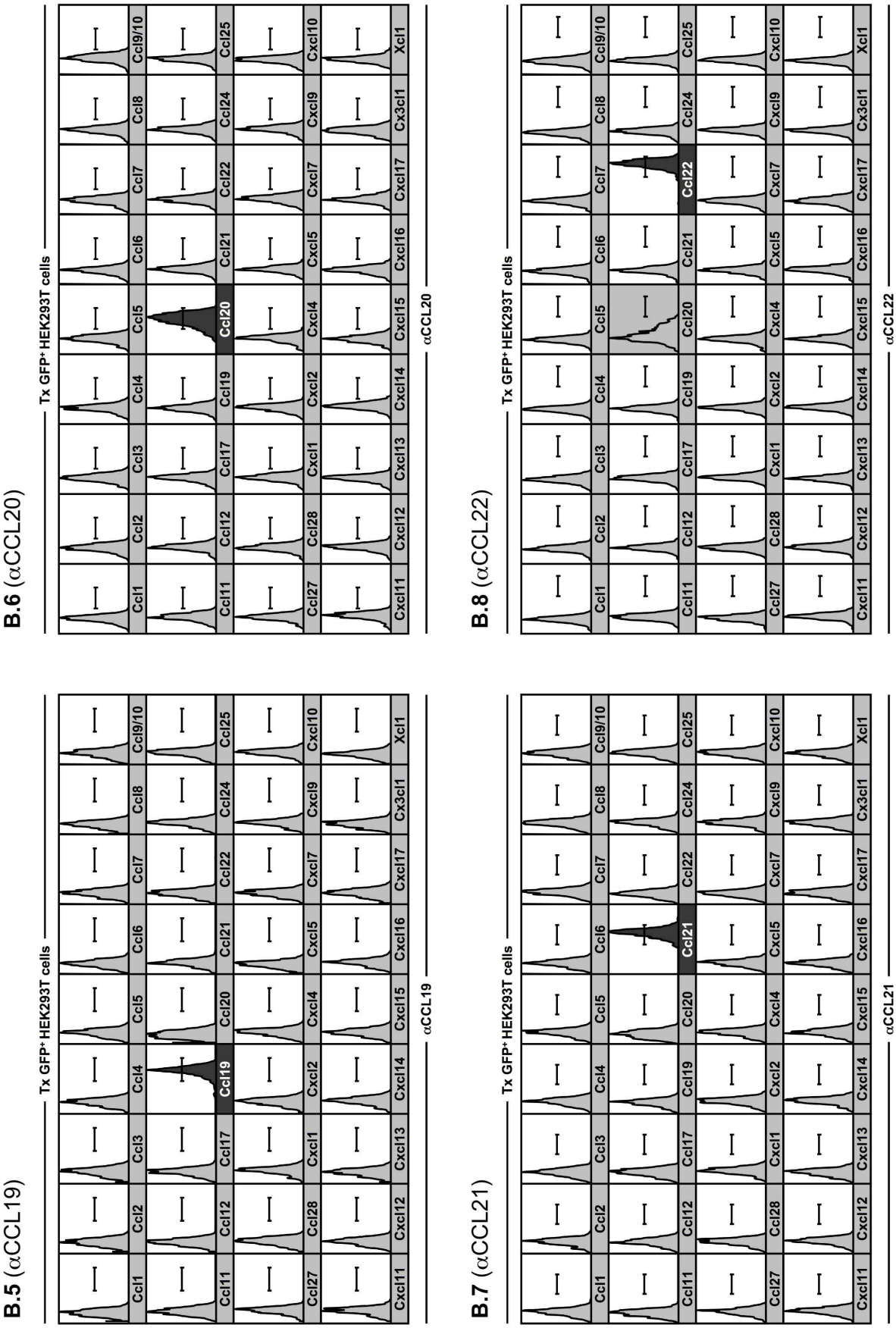

Figure 5 - continued on next page

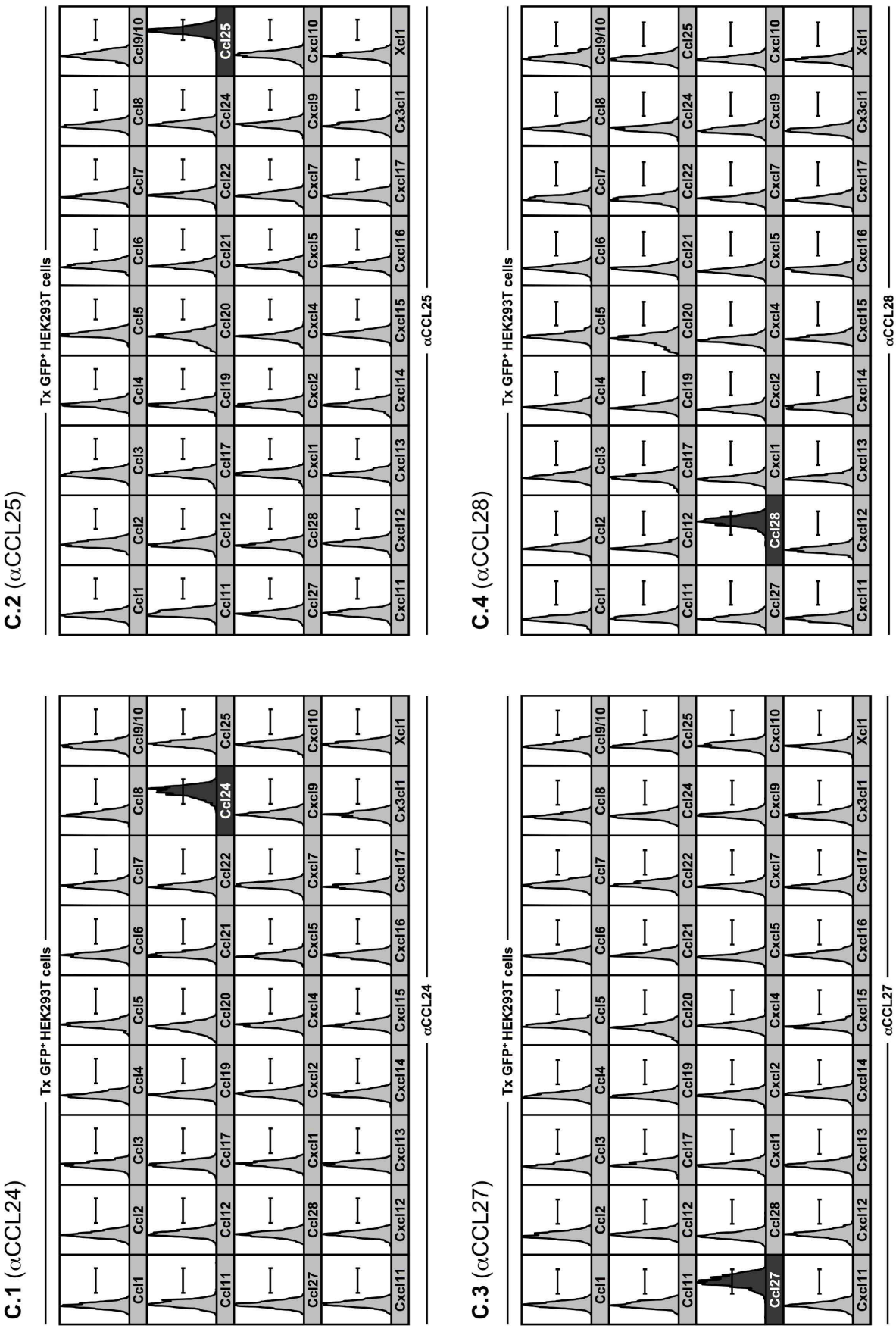

Figure 5 - continued on next page

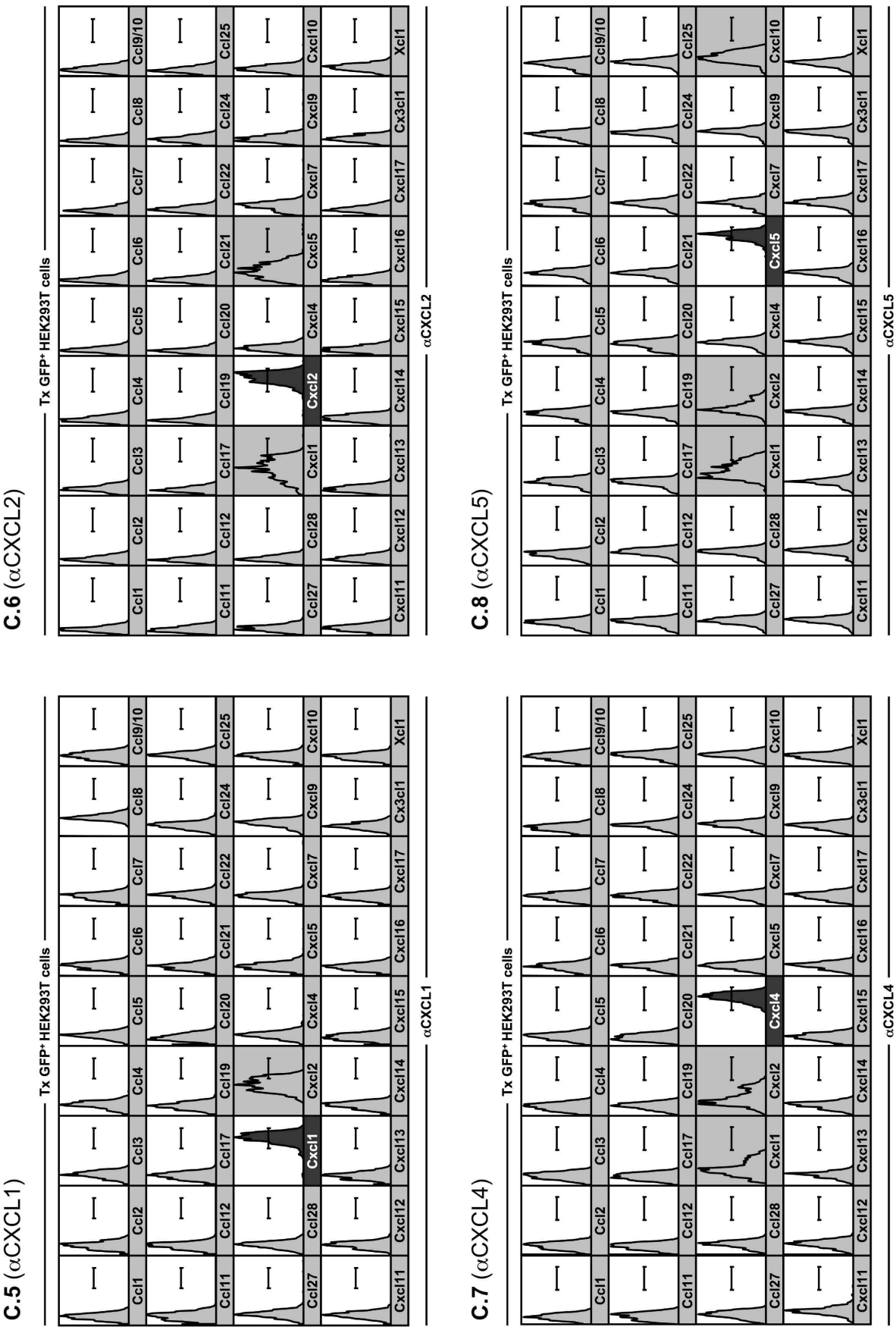

Figure 5 - continued on next page

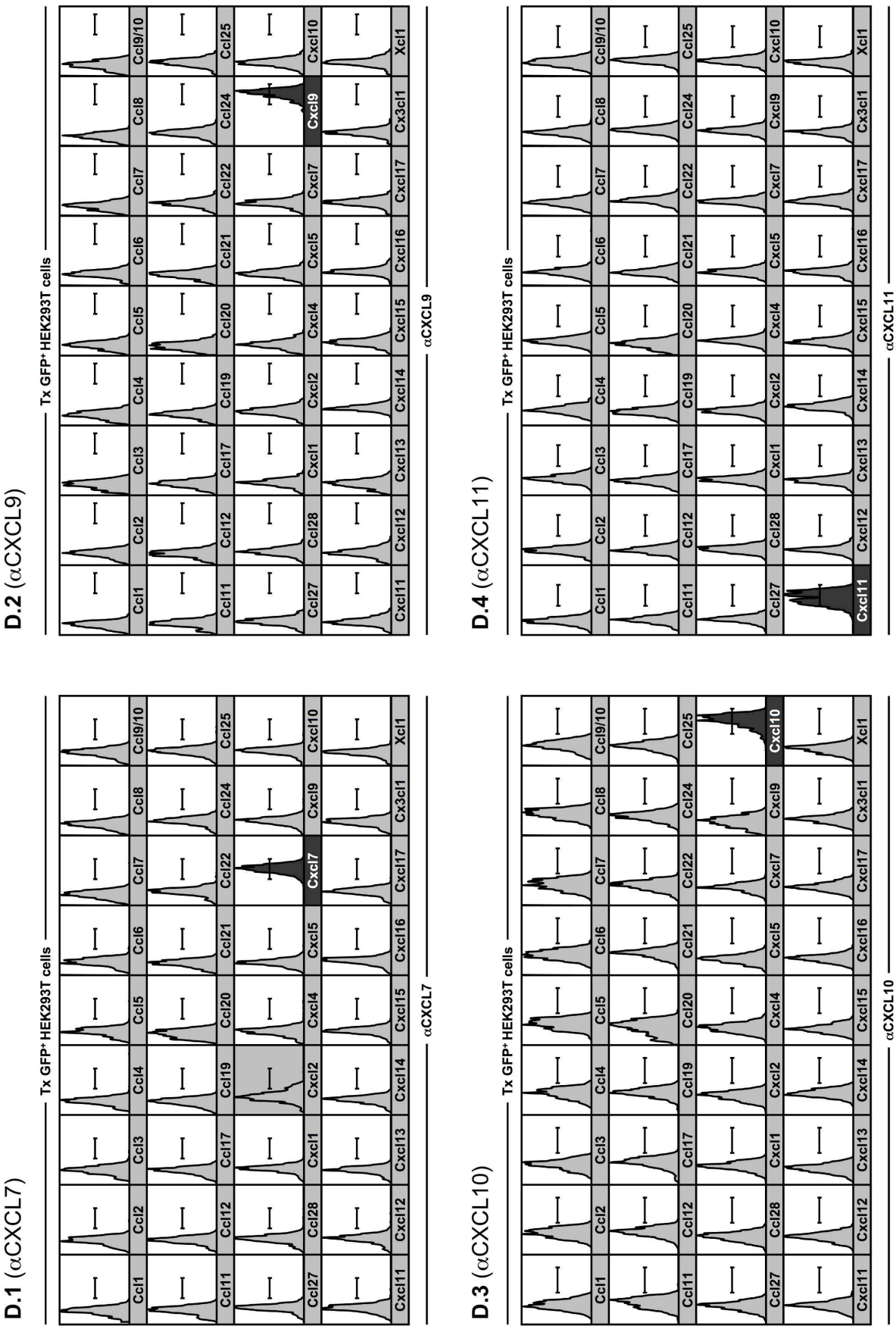

Figure 5 - continued on next page

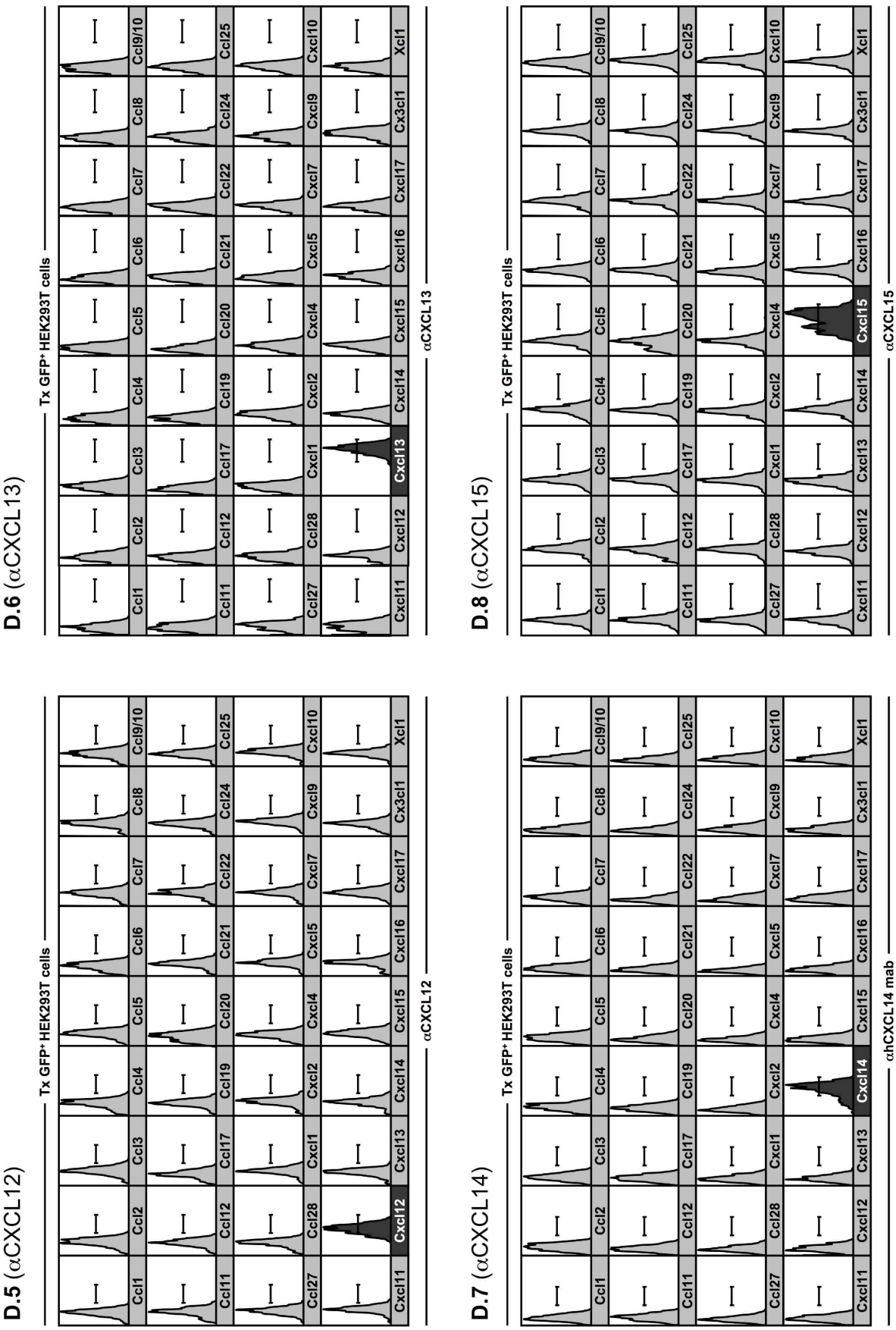

Figure 5 - continued on next page

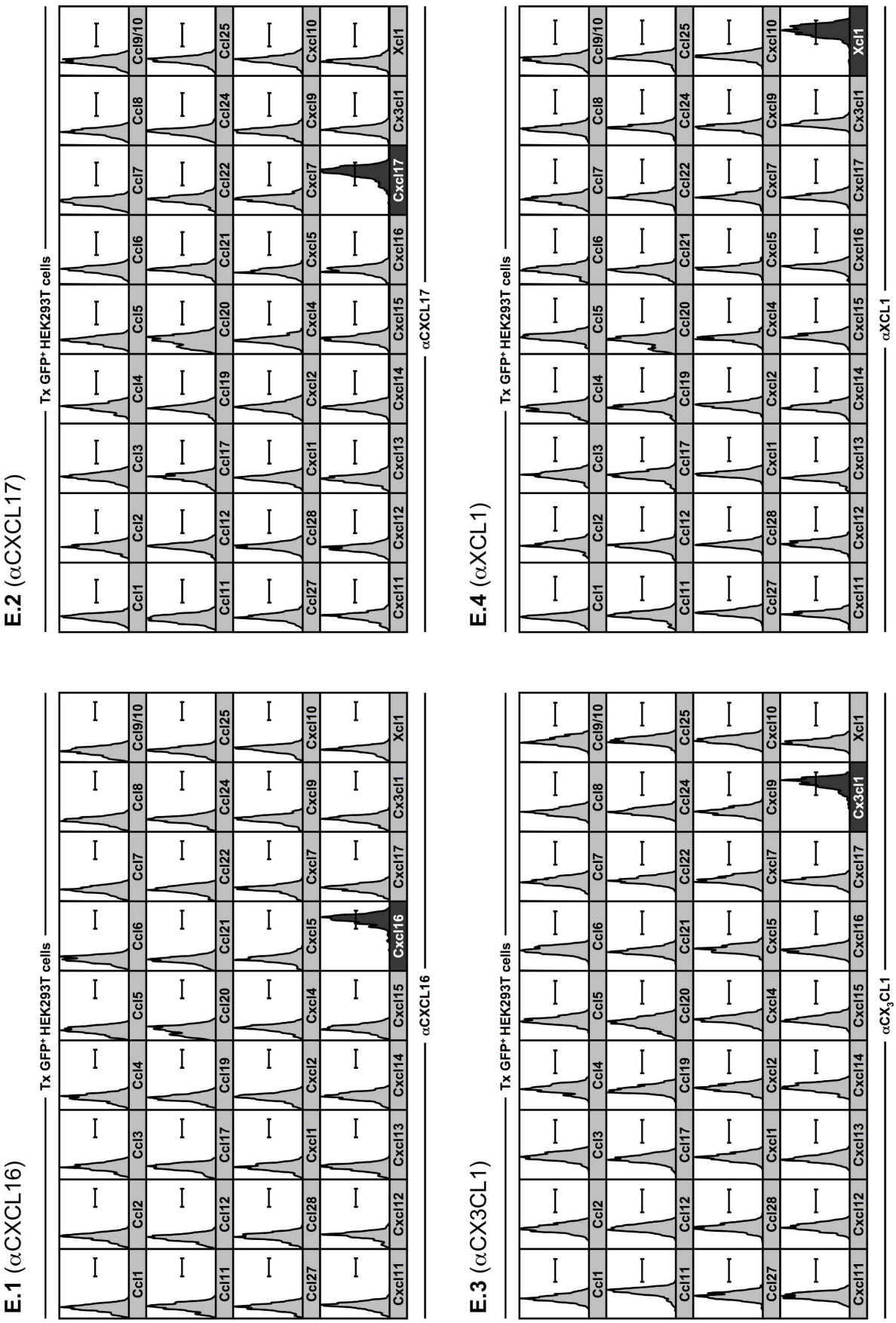

Figure 5 - continued on next page

Figure 5: ***Determination of the crossreactivity of chemokine antibodies.*** *HEK cells were transfected with 36 individual pIRES2-AcGFP1 chemokine vectors as described in Fig. 3 and stained in parallel with 36 individual chemokine-specific pabs and analyzed by FC. To reduce proteosomal degradation, Cxcl14-transfected HEK cells were cultured in the presence of a protease inhibitor (10 μM MG-132). (**A.1**) Reactivity of the CCL1-specific pab with HEK cells transfected with different chemokine vectors as indicated at the bottom of histograms. All histograms are gated on GFP$^+$cells, the black solid histogram identifies the panel depicting cognate interactions (αCCL1:CCL1) and the lack of specific staining in all other panels (gray histograms) demonstrates absence of crossreactivity of the αCCL1 pab with other chemokines. (**A.2-E.4**) Experimental procedures and data display for individual chemokine-specific pabs as detailed above. Crossrecognition of non-cognate chemokines by a given pab are highlighted by gray backgrounds (**panels A.2, A.3, A.5-7, B.1-3, B.8, C.5-C.8, D.1**) and the data are summarized in Table 1 (5th column, "partial x-reactivity"). Panel (**D.7**): staining of HEK chemokine transfectants with the αhCXCL14 mab clone 131120. A parallel evaluation of the αhCXCL14 AF866 pab also failed to reveal any apparent cross-reactivities (not shown) but this assessment has to take into account that the specific staining of Cxcl14 transfectants (positive control) is comparatively weak. Based on our identification of a cross-reactivity cluster involving several gene products of the CXCGRO group, we also included a comprehensive evaluation of CXCL3-reactivity: αCXCL1/2/5 but no other chemokine-specific pabs or mabs exhibit partial crossreactivity with CXCL3 (not shown & Table 1). All crossreactive pabs were additionally tested on HEK chemokine transfectants prepared with separate plasmid stocks to rule out accidental cross-contamination (not shown).*

Polyclonal Ab ID	Raised against	FC-approved mAbs (clone ID)	Partial x-reactivity[a]	IHC[b]
AF8452	CCL1	1A6 (hIgG)[3]	none	
AF479-NA[2]	CCL2	2H5 (hIgG1)[3,4,5]	CCL7/12	
AF450-NA[2]	CCL3	39624 (rIgG2a)[2]	CX3CL1	yes
AF451-NA[2]	CCL4		none	yes
AF4782	CCL5		CCL3	yes
AF4872	CCL6	262016 (rIgG2b)[2]	CCL9/10	
AF456-NA[2]	CCL7		CCL2/5/8/11/12	
AF7902	CCL8		none	
AF4632	CCL9/10		CCL6	
AF420-NA[2]	CCL11		CCL7/CX_3CL1	yes
AF4282	CCL12		CCL2/7	
AF5292	CCL17		none	
AF8802	CCL19		none	yes
AF7602	CCL20		none	
AF4572	CCL21a/b/c[1]		none	
AF4392	CCL22		CCL20	
AF5282	CCL24		none	
AF481-NA[2]	CCL25		none	yes
N/A	CCL26		none	
AF7252	CCL27		none	yes
AF5332	CCL28		none	

Polyclonal Ab ID	Raised against	FC-approved mAbs (clone ID)	Partial x-reactivity[a]	IHC[b]
AF453-NA[2]	CXCL1		CXCL2/3	
AF452-NA[2]	CXCL2		CXCL1/3/5	yes
N/A	CXCL3		none	
AF5952	CXCL4		CXCL1/2	
AF4332	CXCL5		CXCL1/2/3/10	
AF7932	CXCL7		CXCL2	yes
AF492-NA[2]	CXCL9		none	
AF466-NA[2]	CXCL10		none	yes
AF5722	CXCL11		none	
AF310-NA[2]	CXCL12	79018 (mIgG1)[2]	none	
AF4702	CXCL13		none	yes
AF8662	CXCL14	131120 (mIgG2a)[2,d]	none[c]	
AF4422	CXCL15		none	
AF5032	CXCL16		none	
AF42702	CXCL17		none	
AF4722	CX_3CL1		none	
AF4862	XCL1	MTAC-2 (rat Ig)[6]	none	

Table 9: ***Summary of cross-reactivities of polyclonal chemokine antibodies. a)*** *The cross-reactivities of individual chemokine-specific pAbs were determined as detailed in* ***Fig.5*** *and permit the distinction of three pAb groups: no cross-reactivity ('none'), minor cross-reactivity (cross-recognized chemokines listed in black font) and more pronounced cross-reactivity (chemokines listed in red font). This distinction is based on the fluorescence intensities (GMFI) of a given pAb comparing cross-recognized and cognate chemokines in* ***Fig.5*** *(minor: >10-fold lower GMFI in relation to cognate chemokine, more pronounced: 5-10-fold lower GMFI).* ***b)*** *Information about immunohistochemistry (IHC)-approved pAb usage as per supplier.* ***c)*** *No cross-reactivity with non-cognate chemokines observed for both αhuCXCL14 pAb (AF866) and αhuCXCL14 mAb (clone 131120).* ***d)*** *Utility of the 131120 mAb for flow cytometry determined in the present study.* ***1)*** *The AF4572 pAb does not distinguish between CCL21a and CCL21b/c as these differ only in one amino acid. Commercial or academic sources of Abs:* ***2)*** *RnD Systems,* ***3)*** *BDBiosciences,* ***4)*** *ebioscience,* ***5)*** *Biolegend,* ***6)*** *Dorner et al., PNAS 2002 [70]; mAb species* ***h)****: hamster,* ***m****: mouse,* ***r)****: rat.*

4.1.3 Profiling of splenocytes by "chemokine flow cytometry"

The unprecedented ability to visualize nearly all chemokines at the single cell level allows the re-examination of the classification into "homeostatic", "dual-use" and "inflammatory" chemokines [42]. Despite its usefulness, this classification system has several drawbacks which mainly lie in the definitions themselves. "Inflammatory chemokines" are defined as being produced by immune, epithelial and endothelial cells as well as fibroblasts and "similar cell types" upon activation whereas "homeostatic chemokines" are defined as those being expressed "in discrete locations in the absence of apparent activating stimuli" [42]. The term "homeostatic chemokine" may also refer to the simple presence of chemokine proteins under conditions of immune homeostasis but the conclusive assignment to the category "homeostatic" requires appropriate reagents to detect and measure chemokines directly in primary cells and tissues. While useful, this context-driven annotation of chemokines has not been studied in a truly comprehensive fashion. Although knockout mice for about half of the 39 murine chemokines have been developed, several strains are still lacking detailed characterization. For the purpose of this thesis, "homeostatic chemokines" are defined at the level of hematopoetic cells as those chemokines detectable in defined cellular subsets in the absence of exogenous stimuli. Furthermore, "constitutive" chemokine protein expression (detectable directly *ex vivo*) can be distinguished from "spontaneous" production (after a 5h culture in the presence of the protein transport inhibitor BFA but absence of specific stimuli) that most likely results from the translation of pre-existing chemokine transcripts. Cell preparation and culture conditions (*e.g.*, media containing fetal calf serum) could potentially lead to spontaneous chemokine production.

Figure 6: ***Visualization and identification of homeostatic chemokines in hematopoetic cells.*** *(**A & B**) Spleen cells obtained from naive B6 mice were stained directly ex vivo ("constitutive") or after a 5h culture in the presence of BFA but absence of any exogenous stimuli ("spontaneous") and stained for CD11b and indicated intracellular chemokines as detailed in Methods. All plots are gated on "live" cells as determined by FSC/SSC properties. The red dots identify chemokine^{+} staining in the respective quadrants. Data are representative for multiple independent experiments. Note that our analyses of CXCL14 expression with a preconjugated αhCXCL14 mab are associated with non-specific staining of a subset of CD11b^{++} cells (identical staining pattern observed with a preconjugated mIgG2a isotype control, not shown).*

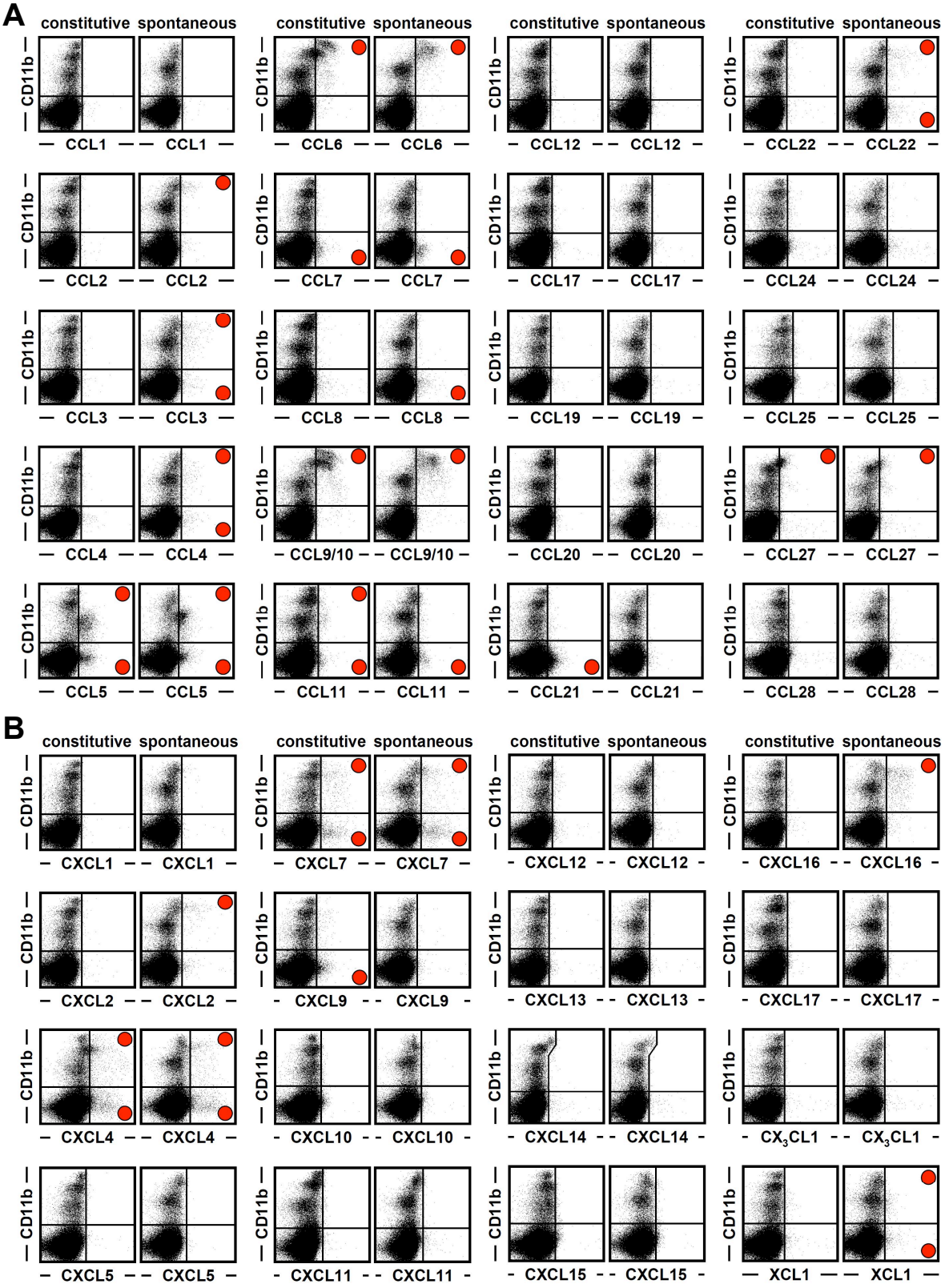
A
constitutive spontaneous
CD11b
CCL1 CCL1
CCL6 CCL6
CCL12 CCL12
CCL22 CCL22
CCL2 CCL2
CCL7 CCL7
CCL17 CCL17
CCL24 CCL24
CCL3 CCL3
CCL8 CCL8
CCL19 CCL19
CCL25 CCL25
CCL4 CCL4
CCL9/10 CCL9/10
CCL20 CCL20
CCL27 CCL27
CCL5 CCL5
CCL11 CCL11
CCL21 CCL21
CCL28 CCL28
B
constitutive spontaneous
CD11b
CXCL1 CXCL1
CXCL7 CXCL7
CXCL12 CXCL12
CXCL16 CXCL16
CXCL2 CXCL2
CXCL9 CXCL9
CXCL13 CXCL13
CXCL17 CXCL17
CXCL4 CXCL4
CXCL10 CXCL10
CXCL14 CXCL14
CX3CL1 CX3CL1
CXCL5 CXCL5
CXCL11 CXCL11
CXCL15 CXCL15
XCL1 XCL1

Evaluation of the protein expression of 37 murine chemokines by flow cytometry revealed constitutive expression of 12 chemokines and/or spontaneous expression of six chemokines in splenocytes recovered from unmanipulated B6 mice (**Fig.6A/B**).

Pronounced constitutive chemokine expression was observed for CCL5, CCL6, CCL9/10, CCL21, CCL27, CXCL4 and CXCL7. In contrast, only low-level expression of CCL7, CCL8, CCL11, CXCL9 and XCL1 is detectable directly *ex vivo* in smaller hematopoetic cell subsets whereas several additional chemokines are synthesized after a brief *in vitro* culture in a spontaneous manner (CCL2, CCL3, CCL4, CCL22, CXCL2 and CXCL16).

Two thirds of these 18 chemokines (CCL2/3/4/5/6/7/8/11 and CXCL2/7/9/16) are traditionally regarded as inflammatory [42] and their constitutive and/or spontaneous expression indicates that these chemokine may also exert previously unrecognized homeostatic functions. If the presence of the latter chemokines under conditions of immune homeostasis in fact warrants their re-classification as dual-function members of the chemokine superfamily may remain a matter of debate. However, it is important to emphasize that the mere presence of many inflammatory chemokines does not necessarily reflect activation of immune cells in response to pathological processes.

4.1.4 Identification of cellular sources of homeostatic chemokine production

Stratification of the homeostatic chemokine production utilizing the αM integrin CD11b (**Fig.6**) provided a general overview of chemokine expression. CD11b is expressed by granulocytes, Mo/MΦ and DC subsets but also by activated T cells, small B cell subsets and mature NK cells [133–136] (**Fig.7A**). A more detailed demarcation of specific cell populations can therefore be achieved by analytical exclusion of B cells ($CD19^+$), T cells ($CD3\epsilon^+$), NK cells ($NK1.1^+$) and NKT cells ($NK1.1^+CD3\epsilon^+$) and expression analysis of two additional markers (Gr-1, composed of Ly6C and Ly6G antigens, and the glycoprotein F4/80) (**Fig.7B**). The resulting delineation of six cellular subsets, combined with a determination of CD11c expression levels (**Fig.7C**), permits the identification of granulocytes, Mo/MΦ, conventional DCs ($CD11c^+$ and $CD11c^{++}$ cDC subsets), CD45R/$B220^+$ plasmacytoid DCs (pDC), a small population of $F4/80^{++}$ Mo/MΦ and a group of $CD11b^-$Gr-1^-F4/80^-CD11c^- cells, many of which lack expression of CD45 (**Fig.7D**). These dis-

tinctions correspond well to a contemporary phenotypic differentiation of Mo/MΦ, DC and granulocyte subsets [137, 138]. For those homeostatic chemokines preferentially expressed by cells that lack CD11b, complementary analyses stratify the CD11b$^-$ population according to B and T cell markers.

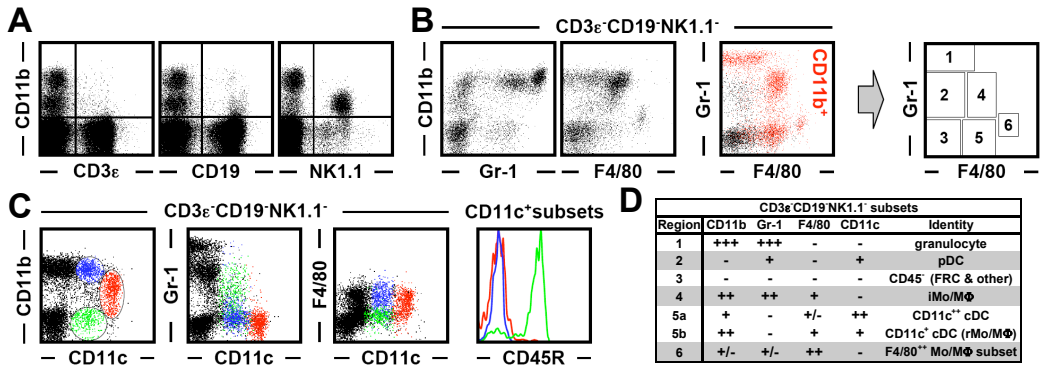

Figure 7: ***Stratification of CD3ϵ^-CD19$^-$NK1.1$^-$ immune cell subsets.*** *Single cell suspensions prepared from the spleens of naive B6 mice were analyzed directly ex vivo for expression of various cell surface markers.* ***(A)*** *CD11b expression by small subsets of CD3ϵ^+T and CD19$^+$B cells as well as mature NK cells.* ***(B)*** *Analytical exclusion of T cells (CD3ϵ^+), B cells (CD19$^+$), NK cells (NK1.1$^+$) and NKT cells (NK1.1$^+$CD3ϵ^+) permits the delineation of 6 cellular subsets according to expression of CD11b, Gr-1 (Ly6C/G) and F4/80 antigens. In the 2-color dot plot, CD11-expressing cells are identified as red events. Numbers in the right hand plot diagram demarcate regions corresponding to the 6 distinct cell populations in the 2-color dot plot. The identities of these cell subsets are summarized in panel D.* ***(C)*** *Three major DC subsets, color-coded in red, blue and green are distinguished based on CD11b and CD11c expression patterns. Their Gr-1, F4/80 and CD45R (B220) expression profiles are shown in adjacent dot plots or histograms (each of the 3 DC subsets identified by colored events or histogram tracings).* ***(D)*** *Identity of the CD3ϵ^-CD19$^-$NK1.1$^-$ immune cell subsets stratified according to Gr-1 and F4/80 expression. Numbers in first column correspond to regions demarcated in the plot diagram above. pDC: plasmacytoid DC; FRC: fibroblastic reticular cells; iMo/MΦ: 'inflammatory' monocytes/macrophages; cDC: conventional DC, rMo/MΦ: 'resident' rMo/MΦ. Note that the specifications 'inflammatory' and 'resident' Mo/MΦ are used to emphasize the close relationships of monocytes, MΦ and DCs: the iMo/MΦ described here resemble 'inflammatory' monocytes found in the blood and the CD11b^{++}F4/80$^+$Gr-1$^-$ rMo/MΦ can differentiate into CD11c-expressing DCs in the absence of inflammation [128].*

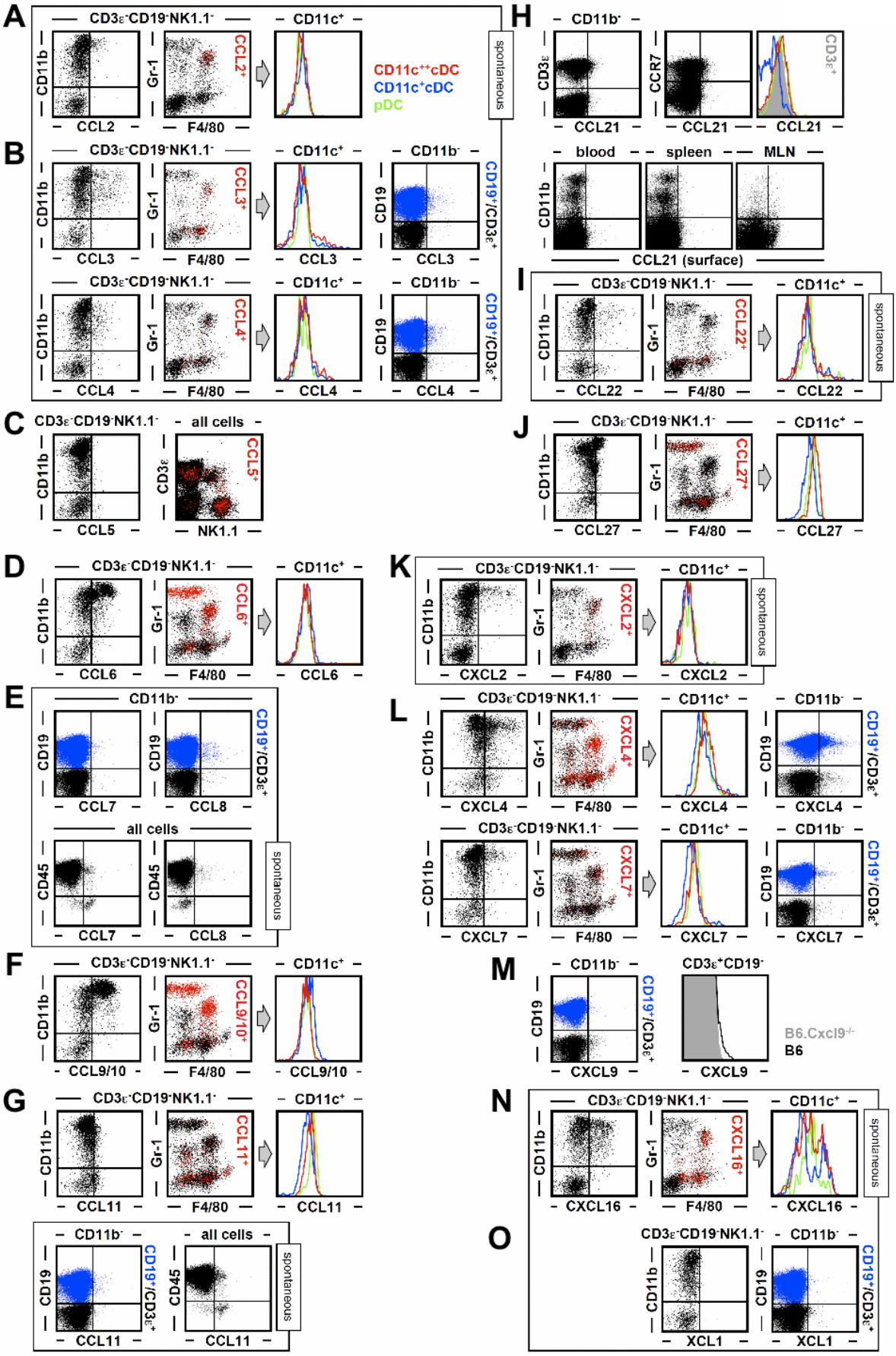
A
CD3ε-CD19-NK1.1-
CD11b
Gr-1
CCL2+
CCL2
F4/80
CD11c+
CD11c++cDC
CD11c+cDC
pDC
spontaneous
B
CCL3+
CCL3
CD11b-
CD19
CD19+/CD3ε+
CCL4+
CCL4
C
all cells
CD3ε
CCL5+
CCL5
NK1.1
D
CCL6+
CCL6
E
CD19
CCL7
CCL8
all cells
CD45
F
CCL9/10+
CCL9/10
G
CCL11+
CCL11
H
CD11b-
CD3ε
CCR7
CD3ε+
CCL21
blood
spleen
MLN
CCL21 (surface)
I
CCL22+
CCL22
J
CCL27+
CCL27
K
CXCL2+
CXCL2
L
CXCL4+
CXCL4
CXCL7+
CXCL7
M
CXCL9
B6.Cxcl9-/-
B6
N
CXCL16+
CXCL16
O
XCL1

Figure 8: ***Delineation of celluar subsets expressing homeostatic chemokines.*** *(**A-O**) Spleen cells obtained from naive mice were analyzed directly ex vivo (constitutive) or after 5h in vitro culture in the presence of BFA (spontaneous, indicated by boxed plots). For chemokines preferentially expressed by CD11b$^+$ cell subsets, dot plots are gated on CD3ϵ^-CD19$^-$NK1.1$^-$as indicated. In the adjacent 2-color dot plots (black/red), chemokine-expressing cells are identified as red events; the histograms are gated on CD11c-expressing cells and color-coded as described in panel **A**. For chemokines expressed by CD11b$^-$ cells, 2-color dot plots are gated on B cells (CD19$^+$CD3ϵ^-CD11b$^-$: blue) and T cells (CD19$^-$CD3ϵ $^+$CD11$^-$: black). Note the partially different gating strategies employed for analysis of CCL5/7/8/11 and CCL21 expression (panels **C**, **E**, **G** and **H**; all cells refers to populations gated on lymphocytes according to FSC/SSC properties): (**C**) Constitutive CCL5 is not detectable in CD3ϵ^-CD19$^-$NK1.1$^-$ cells (left) but in NK cells, subpopulations of T cells and some NKT cells (right). (**E**, **G**) Spontaneous CCL7/11 but not CCL8 production is observed in cell subsets lacking CD45 expression. (**H**) Top row: ex vivo detectable CCL21 expression by T cells (left) and CCR7$^+$ cells (middle). The histograms (right) are gated on the three DC subsets (red, blue and green) and CD3ϵ^+T cells (gray solid). Bottom row: CCL21 surface stains of cells recovered from blood, spleen and mesenteric lymph node (MLN).*

The following patterns of *homeostatic* chemokine expression can be discerned in splenic hematopoietic cells taking into account considerations and experimental strategies that address the partial crossrecognition of non-cognate chemokines by several of the pAbs (**Fig.8, Table 9**). Where applicable, the discussion of homeostatic chemokine expression is complemented with an evaluation of induced chemokine production.

CCL1: no homeostatic expression in hematopoetic cells (**Fig.6A**). However, CCL1 is readily produced by subpopulations of activated T_E and T_M as will be discussed in the next section on T cell produced chemokines (pg.91).

CCL2: in the absence of *ex vivo* detectable CCL2, spontaneous production of this chemokine is restricted to a subset of Mo/MΦ (**Fig.8A**). Lipopolysaccharide (LPS) stimulation enhances the fraction of CCL2$^+$Mo/MΦ only slightly but increases CCL2 expression levels and also induces production in a minor CD11c$^+$ cDC subset (**Fig.9A**). These findings are confirmed by the absence of detectable CCL2 in tissues from B6.CXCL2$^{-/-}$ mice (**Fig.9B**), yet the αCCL2 pAb also exhibits more pronounced crossreactivity with CCL7/12 (**Fig.5**). We therefore conducted corresponding analyses with the αCCL2 mAb 2H5 and observed similar but notably weaker CCL2 expression

patterns in B6 mice (**Fig.9C**). Unexpectedly, however, the αCCL2 mAb, which does not react with CCL7, also recognizes CCL12, a chemokine that is not spontaneously synthesized by spleen cells (**Fig.9C**). The fact that the specificity of a widely used mAb is not limited to its cognate chemokine provides an example that the phenomenon of crossreactivty is not restricted to pabs and illustrates the need to extent comprehensive specificity analyses to mAbs.

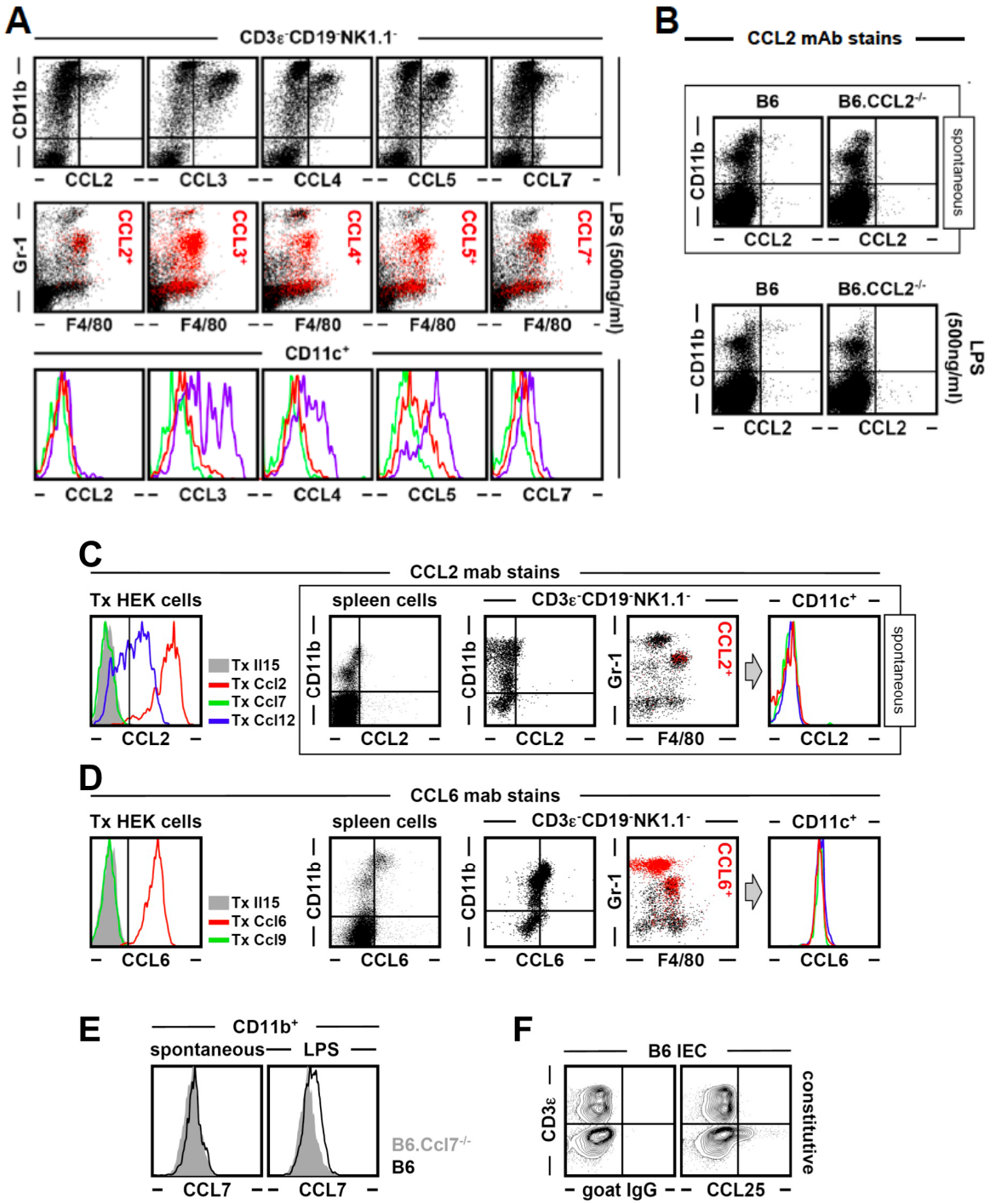

Figure 9: ***Antibody specificity controls and constitutive, spontaneous and/or induced expression patterns for selected CC chemokines.*** *(**A**) Splenocytes from naive B6 mice were cultured for 5h with BFA plus 500ng/ml LPS and subsequently stained for surface markers and intracellular chemokines. Dot plots are gated on CD3ϵ^- CD19$^-$ NK1.1$^-$ cells; the histograms depict induced chemokine production by DC subsets within the CD3ϵ^- CD19$^-$ NK1.1$^-$ population and are color-coded as in (**Fig.8A**) (red: CD11c^{++}DC, blue: CD11c$^+$DC, green: pDC). Data not shown: LPS but not IFNγ-stimulation also increases CCL6 and CCL9/10 expression by CD11b$^+$ cell subsets (data representative for 2-3 independent experiments analyzing 3 mice each). (**B**) Specificity controls for αCCL2 pAb stains: spontaneous and LPS-induced CCL2 expression analysis of B6 vs. B6.Ccl2$^{-/-}$ mice. (**C**) Characterization of αCCL2 clone 2H5 specificity with indicated HEK transfectants (left panel) and homeostatic CCL2 expression as revealed with the αCCL2 mAb. Gating strategies are indicated above the dot plots and the overlaid histograms in the right hand panel demonstrate absence of spontaneous CCL2 production by DC subsets stratified according to CD11b/c expression levels as in panel A. (**D**) Characterization of αCCL6 clone 262016 specificity with indicated HEK transfectants (left panel) and constitutive CCL6 production determined with the αCCL6 mAb; gating and data display as in panel C. (**E**) Specificity control for αCCL7 pAb stains. Spleen cells from B6 & B6.Ccl7$^{-/-}$mice were cultured in the absence or presence of LPS prior to surface and intracellular CCL7 stains; histograms are gated on CD11b$^+$ cells as Mo/Mϕ constitute the major population of LPS-induced CCL7 producers (panel A). (**F**) Small intestinal epithelial cells (IEC) were prepared as detailed in methods, stained and analyzed for constitutive CCL25 expression by FC (representative data for 3 independent analyses of individual mice).*

CCL3 and CCL4: spontaneous expression of CCL3 and CCL4 occurs in both CD11b$^+$ and CD11b$^-$ populations (**Fig.8B**). In the former group, CCL3/4 production is observed in subsets of Mo/MΦ and cDCs (**Fig.8B**), cell types that also respond with significantly increased CCL3/4 synthesis upon LPS stimulation (in particular Mo/MΦ and CD11c$^+$cDCs, also some granulocytes) (**Fig.9A**). As demonstrated in the next chapter on T cell-produced chemokines, inducible CCL3/4 production is a major component of the pathogen-specific T cell response, but constitutive expression is only observed at a very low level in T_E but not T_M populations. In agreement with this finding, only marginal spontaneous CCL3/4 expression is found in T cells of undefined specificity. Rather, B cell subsets constitute the largest CD11b$^-$ cell type capable of spontaneous CCL3/4 synthesis (**Fig.8B**). Lastly, minor crossreactivity of the αCCL3 pAb with CX_3CL1 is observed, a chemokine not produced by hematopoetic cells (**Fig.6B**) and not revealed as a 'false positive' in CCL3-deficient cells stained with this pAb (data not shown).

CCL5: CCL5 is identified as one of the most prominent homeostatic chemokines (**Fig.6A)** and its constitutive expression is largely restricted to NK cells and several T cell subsets (note the absence of constitutive CCL5 in the CD3ϵ^-CD19$^-$NK1.1$^-$ population) (**Fig.8C)**. This contention is not compromised by the weak CCL3-reactivity of the αCCL5 pAb as demonstrated by the absence of staining in CCL5-deficient cells analyzed with the αCCL5 pAb (**Fig.18A**, see page 97). Notwithstanding the fact that CCL5 can be induced in many cell types including Mo/MΦ and DCs (**Fig.9A)**, it is worth mentioning that the lack of constitutive CCL5 expression by the latter cells is systemic since it applies to lymphatic and non lymphatic tissues alike (blood, spleen, lymph nodes, bone marrow, peritoneal cavity, liver and lung; not shown). Experimental data and discussion will be provided in the next chapter in regards to T cell-produced CCL5 expression. Briefly, CD44^{hi} memory-phenotype (MP) CD8$^+$T cells represent the major population of T cells featuring constitutive CCL5 expression while subsets of $\gamma\delta$ TCR$^+$T cells and, to a much lesser extent also MP CD4$^+$ and NKT cells, are also CCL5$^+$. Interestingly, pathogen-specific CD8$^+$T$_M$ within the MPCD8$^+$ population express particularly high levels of constitutive CCL5 and account for the largest source for *ex vivo* detectable CCL5 in pathogen-immune animals.

CCL6 and CCL9/10: the murine chemokines CCL6 and CCL9/10, together with their closest human homologues (CCL23 and CCL15), belong to the N6 subfamily of proteins that have an N-terminal extension relative to other β-chemokines [42]. The constitutive expression of both chemokines is rather pronounced and confined to the same cell subsets (granulocytes, Mo/MΦ and some CD11c$^+$cDCs (**Fig.8D/F)**, but their spontaneous secretion appears to be regulated in a differential manner: the homeostatic chemokine CCL9/10 can be found at extraordinarily high levels in the circulation of normal mice (1μg/ml, [139]) but serum levels of the inflammatory chemokine CCL6 [140] are estimated to be more than 10,000-fold lower (A. Coelho, personal communication). The above considerations, however, have to take into account that the complementary cross-reactivities αCCL6 and αCCL9/10 pAbs are in fact the most pronounced of all chemokine pAb evaluated here (**Fig.5**, panels **A.6/B.1**). Nevertheless, the expression pattern described above for CCL6 is confirmed with a non-crossreactive αCCL6 mAb (**Fig.9D)** and even though part of the αCCL9/10 pAb staining may be due to CCL6-reactivity, we believe that most of the chemokine$^+$ cells in fact express CCL9/10 based on the apparent phenotype of CCL9/10$^+$ cells as well as the

intensity of the pAb staining signal. In other cell subsets, attribution of the αCCL9/10 pAb signal to CCL9/10 production may in fact be unequivocal if CCL6 expression can be ruled out by mAb stains. The next chapter will apply and discuss this strategy in regards to T cell-expressed CCL9/10.

CCL7, CCL8, CCL11: αCCL7 and αCCL11 are part of a group comprising four pAbs that feature non-cognate interactions with "CC-MCP" chemokines. The former pAb in particular exhibits an unusually broad spectrum of mostly low-level crossreactivities including recognition of CCL2/11/12 the pAbs specific for which also partially recognize CCL7 (**Table 9**). In spite of these caveats, the complementary evaluation of CCL7/8/11 and other cross-recognized chemokine expression permits the following conclusions: production of CCL7/8/11, detectable *ex vivo* at low levels preferentially in the CD11b$^-$ compartment, remains largely unchanged after short-term in vitro culture (**Fig.6A)** and it appears that some of the CCL7$^+$, CCL11$^+$ and CCL8$^+$cells are B cells (**Fig.8E/G**). Although borderline expression can be found in T cells, we note that pathogen-specific T cells neither contain *Ccl7/8/11* mRNA transcripts nor produce the corresponding proteins upon TCR engagement as will be discussed in the next chapter. In addition, constitutive CCL11 is found in some CD11b$^+$ cells but its expression, mostly excluded from granulocytes and slightly more pronounced in pDCs, is not preferentially associated with a specific immune cell subset (**Fig.8G**). Upon stimulation with LPS, induced chemokine expression is observed for CCL7 (mostly in Mo/MΦ and some DCs) but not CCL8/11 (**Fig.9A** and not shown). Lastly, about half of the CCL7$^+$ and $\sim$1/3 of CCL11$^+$ cells, but no CCL8$^+$ cells, analyzed for constitutive and spontaneous chemokine production lack expression of CD45, a population that remains to be defined in detail but does include fibroblastic reticular cells (FRC) as determined by CD31 and/or gp38/podoplanin expression (**Fig.8E/G** and not shown). However, the apparent CCL7/11 production by CD45$^-$ cells needs to be interpreted with caution as *Ccl7*-deficient mice, which demonstrate the expected lack of LPS-induced CCL7 expression in CD11b$^+$populations (**Fig.9E)**, nevertheless exhibit higher background staining in non-hematopoetic cells (not shown) and further analyses of FRCs will require optimized cell dissociation protocols [141].

CCL12, CCL17, CCL19 and CCL20: no homeostatic expression in splenic hematopoetic cells (**Fig.6A**). The absence of CCL12 is of note since the chemokines weakly cross-recognized by the αCCL12 pab (CCL2/7) are in fact expressed under homeostatic conditions. We also evaluated

CCL17 expression in LN DCs that are reported to constitutively express *Ccl17* mRNA [142] but did not detect any protein (not shown). The apparent absence of homeostatic CCL19 in spleen and LNs (**Fig.6A** and not shown) is of note since a recent publication has proposed that CCL19 is surface-bound to T cells expressing its receptor CCR7 [143]. This conclusion was based on differential staining intensities using a CCR7-specific antibody vs. CCL19 fusion protein and although the fusion protein may well constitute a more sensitive reagent for the indirect determination of CCR7 occupancy by CCL19, direct evidence for surface-bound CCL19 was not provided [143].

CCL21: CCL21 exhibits a peculiar expression pattern in that *ex vivo* detectable CCL21 in $CD11b^-$ cells disappears after 5h *in vitro* culture (**Fig.6A**). This observation suggests that CCL21 may be acquired rather than produced by $CD11b^-$ cells and is supported by a recent report that documents the capture and surface immobilization of CCL21 by a variety of immune cells in the LN [119]. Subset analyses demonstrate that T cells constitute the major population of $CCL21^+$ cells in the spleen and likely bind CCL21 via its receptor CCR7 (**Fig.8H**). The notion that T cell CCL21 is preferentially captured is also supported by observation that pathogen-specific T cells neither contain CCL21 message nor upregulate mRNA or protein expression after specific *in vitro* stimulation (see next chapter). However, our conclusions are in seeming contradiction to the finding by Friedman et al. who determined that $CD11c^+$ DCs bind CCL21 at higher levels than any other immune cell subset [119]. We therefore evaluated surface CCL21 expression in LNs, spleen and blood, tissues that have been shown to contain a wide range of distinct CCL21 levels ($\sim$2000ng/g, $\sim$300ng/g and less than 10ng/ml in serum, respectively [144, 145]). Indeed, the level of detectable surface CCL21 declines in the expected order (LN $>$ spleen $>$ blood) and although few $CD11c^+$ cells are $CCL21^+$ in the spleen, the overall mean fluorescence intensity of CCL21 stains (the parameter measured in by Friedman et al. [119]) is higher in the $CD11c^{++}$cDC subset than in other cells (**Fig.8H**). Since CCL21 capture and presentation by DCs facilitates the specific priming of T cells by establishing initial antigen non-specific interactions [119], it is well possible that the reciprocal interaction, namely the binding of CCL21-bearing T cells to $CCR7^+$ DCs, may also contribute to improved T cell activation.

CCL22: in the absence of constitutive expression, CCL22 is spontaneously synthesized by cDC subsets and to a lesser degree by $CD45^+CD11b^-$Gr-1-$F4/80^-$ cells (**Fig.8l** and not shown); B cells

as a source for induced CCL22 synthesis are discussed below. None of these or other hematopoetic cells produce CCL20, the chemokine with which the αCCL22 pAb demonstrates weak crossreactivity.

CCL24, CCL25 and CCL28: no homeostatic expression in hematopoetic cells (**Fig.6A**). However, in agreement with the reported spontaneous secretion of CCL25 by *in vitro* cultured small intestinal epithelial cells [146], constitutive CCL25 expression by these cells can be readily visualized by FC (**Fig.9F**).

CCL27: based on its homeostatic expression primarily in keratinocytes, CCL27 appears to be a tissue-specific chemokine [147]. The unique expression pattern of CCL27 described here, *ex vivo* detectable CCL27 in splenic granulocytes accompanied by weaker expression in DC subsets, is therefore rather surprising (**Figs.6A & 8J**). This observation is of particular interest in light of a recent publication on the differential expression of CCL27 protein and mRNA in skin-draining LNs: even under homeostatic conditions, CCL27 protein is transported by yet undetermined mechanisms from the epidermis to the LNs where it may assist in the recruitment of CCR10-bearing T cells [148].

CXCL1, CXCL2 and CXCL3: the determination of CXCL1/2 expression patterns is complicated by the partial cross-reactivity of αCXCL1/2 pAbs (**Table 9**), a likely consequence of the pronounced homology among these chemokines [42]. Yet, while no gene products are detected in hematopoetic cells analyzed directly *ex vivo* with αCXCL1/2 pAbs, distinct expression patterns can be discerned for spontaneous chemokine production as CXCL2 but not CXCL1 is detected in Mo/MΦ subsets (**Fig.6B & 8K**) even though the αCXCL1 pAb exhibits the highest degree of CXCL2 cross-reactivity (**Fig.5, panel C.5**). As expected, LPS stimulation results in the rapid and robust upregulation of both CXCL1/2 by Mo/MΦ, some CD11c$^+$cDC subsets and, in the case of CXCL2, granulocytes (**Fig.10A**).

CXCL4 and CXCL7: The constitutive expression of CXCL4 and CXCL7 by a wide variety of immune cells (Mo/MΦ, granulocytes, DCs and B cells, also some T cells but less than 2% of CD45$^-$ cells) is unexpected (**Figs. 6B & 8L**). In spite of the weak crossreactivity of αCXCL4/7 pAbs with CXCL1/2, we note that the αCXCL1/2 pAbs do not reveal any constitutive chemokine expression (**Table 1 & Fig.6B**). Although recent work has identified monocytes as an auxiliary CXCL4/7

source and blood-borne DC subsets constitutively transcribe *Cxcl4/7* mRNA [149–151], CXCL4/7 expression is usually regarded to be an exclusive feature the megakaryocyte lineage [152]. In fact, CXCL4/7 are the two most abundantly expressed chemokines in platelets and are detectable in normal sera at micromolar concentrations [152]. It is thus conceivable that CXCL4 and CXCL7 are in part captured rather than synthesized by the different immune cell subsets: the CXCL7 receptors CXCR1/2 are preferentially expressed by Mo/MΦ and granulocytes and these cells constitute the majority of CXCL7$^+$cells in the CD11b$^+$'myeloid' compartment (**Fig.8L**).

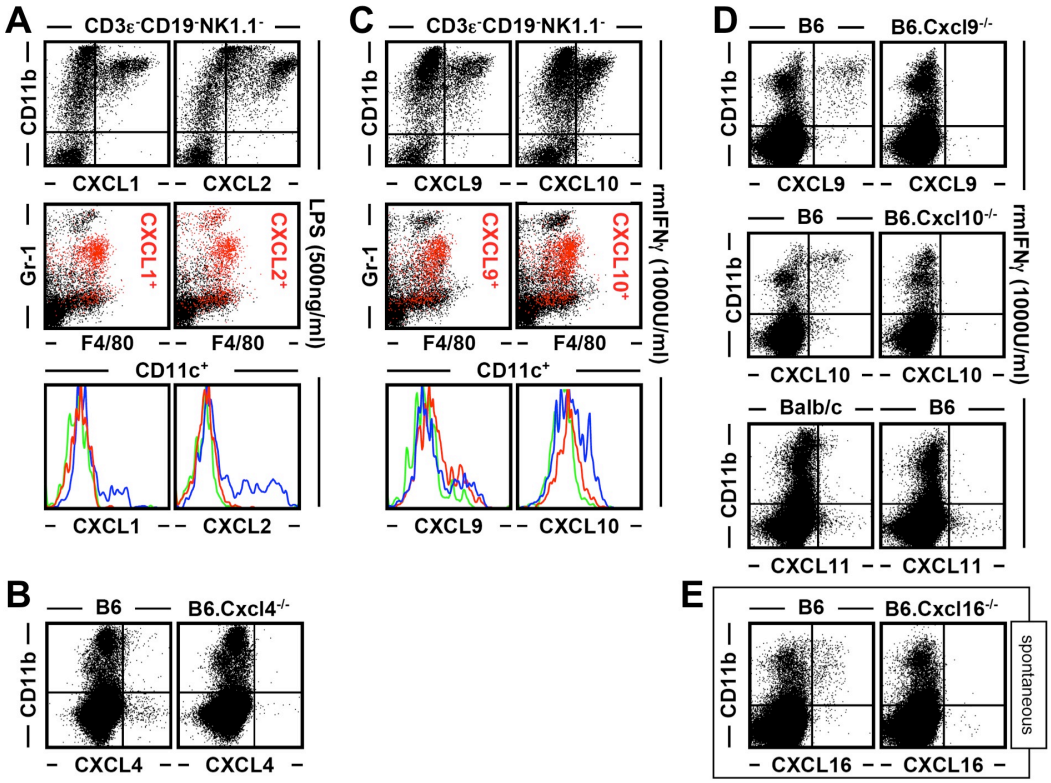

Figure 10: Antibody specificity controls, chemokine capture & constitutive, spontaneous and/or induced expression patterns for selected CXC chemokines.*(**A**) Splenocytes were analyzed for induced CXCL1/2 expression after 5h stimulation with BFA plus 500ng/ml LPS and subsequent staining for surface markers and intracellular chemokines. Dot plots are gated on CD3ϵ^-CD19$^-$NK1.1$^-$ cells; the histograms depict induced chemokine production by DC subsets within the CD3ϵ^-CD19$^-$ NK1.1$^-$ population and are color-coded as in **8A** (red: CD11c^{++} DC, blue: CD11c$^+$DC, green: pDC). The data is representative for 2-3 independent experiments analyzing 3 mice each. **(B)** Left panels: validation of αCXCL4 pab specificity as determined in direct ex vivo stains of spleen cells from B6.Cxcl4$^{-/-}$ vs. wt littermates ('B6'). Right panels: capture of CXCL4 by Cxcl4-deficient cells. 3 x 1010^7 splenocytes obtained from B6.Cxcl4$^{-/-}$or wt littermates (both CD45.2$^+$) were transferred i.v. into B6.CD45.1-congenic recipients and PBMCs analyzed 24h later. Dot plots are*

*gated on respective CD45.2$^+$ donor cells in the blood and demonstrate equivalent CXCL4 expression levels. Similar data were obtained in analyses of donor cells obtained from recipient spleens (not shown). (**C**) B6 spleen cells were cultured for 5h in the presence of 1000U/ml recombinant murine IFNγ (rm) and BFA and analyzed for induced CXCL9/10 expression as detailed in (**A**). The data is representative for 4 independent experiments analyzing 2-3 mice each. (**D**) Specificity controls for αCXCL9/10/11 pAbs. Spleen cells from B6, B6.Cxcl9$^{-/-}$, B6.Cxcl10$^{-/-}$ and Balb/c mice were stimulated with rmIFNγ as above and analyzed for induced CXCL9/10/11 expression. In contrast to the robust CXCL9/10 production, rmIFNγ induces only very modest levels of CXCL11 as evaluated in Balb/c mice (note that regular B6 mice, due to their lack of a functional Cxcl11 gene, are used here as a negative control). (**E**) Analysis of spontaneous CXCL16 synthesis (5h BFA culture of splenocytes) in B6 vs. B6.Cxcl16$^{-/-}$ mice confirms the specificity of the αCXCL16 pAb. Data not shown: LPS but not IFNγ stimulation also increases CXCL16 expression by CD11b$^+$ cell subsets.*

The identity of the murine CXCL4 receptor remains at present unknown. CXCR3 appears to be a promising candidate because in humans, CXCL4 binds CXCR3 [153] and its splice variant CXCR3B [154]. Among murine CXCR3 expressing cells, there appears indeed to be direct correlation between CXCR3 and CXCL4 expression levels (not shown) but high levels of CXCL4 are also detected in CXCR3$^-$ cells, most notably B cells (**Fig.8L**). To determine the possibility of CXCL4 capture by immune cells, I adoptively transferred splenocytes from *Cxcl4*-deficient or their *wt* littermate into congenic mice and stained for CXCL4 24h later (**Fig.10B**). Indeed, CXCL4-deficient cells were staining positive for CXCL4 indicating that chemokine capture might contribute to some extend to the observed CXCL4 expression profile. However, the rather high expression levels of CXCL4 in multiple cell subsets will require further investigation. Finally, the preservation of CXCL4 and CXCL7 expression after 5h *in vitro* culture is in contrast to the loss of surface CCL21 and indicates that potential surface capture of CXCL4 and CXCL7 has different consequences, *e.g.* the potential internalization of bound chemokines. **CXCL5:** no homeostatic expression in hematopoetic cells was observed (**Fig.6B**).

CXCL9, CXCL10 and CXCL11: in accordance with the published literature [155], our FC analyses of primary murine spleen cells stimulated with IFNγ identify Mo/MΦ as a principal source for induced CXCL9/10 production. Furthermore, DCs constitute an additional source for these inflammatory chemokines and the CD11c$^+$cDC subset consistently demonstrates the highest level of induced CXCL10 expression (**Fig.10C**). Interestingly, we also find that a small population of

T cells is characterized by weak constitutive CXCL9 expression (**Fig.8M)**. Similar to CCL21, detectable CXCL9 disappears after *in vitro* culture (**Fig.6B)** and pathogen-specific T cells do not synthesize Cxcl9 mRNA or protein (see next chapter). Thus, it is possible that T cell CXCL9 is also preferentially surface-bound, perhaps through its receptor CXCR3, one of the most prominently T_M-expressed chemokine receptors (not shown). In contrast to the robust CXCL9/10 production following IFNγ stimulation, induced CXCL11 expression, as analyzed in spleen cells of Balb/c origin, remains comparatively weak (**Fig.10D)**. Lastly, using mice deficient for *Cxcl9* or *Cxcl10* and regular B6 mice that lack a functional *Cxcl11* gene [156], we confirmed the specificity of our pAb stains (**Figs.8M & 10D**).

CXCL12, CXCL13, CXCL14, CXCL15: no homeostatic expression in hematopoetic cells was observed (**Fig.6B)**.

CXCL16 and CX_3CL1: CXCL16 and CX_3CL1 share the distinction of being the only cell membrane-anchored chemokines [42, 116]. However, whereas CX_3CL1 is not expressed by hematopoetic cells under homeostatic conditions, robust spontaneous CXCL16 production is observed for Mo/MΦ and cDCs and, to a lesser extent, also pDC subsets (**Fig.8N)**. In agreement with earlier findings [116], LPS stimulation enhances CXCL16 expression by DCs and Mo/MΦ (not shown).

CXCL17: no homeostatic expression in hematopoetic cells was observed (**Fig.6B)**.

XCL1: The constitutive and spontaneous XCL1 expression found in some $CD11b^-$ and $CD11b^+$cells (**Fig.6B)** can be narrowed down to be contained within one or more of the B, T and NK cell populations. Experiments described in subsection 4.1.6 indeed demonstrate that NK cells exhibit low-levels of constitutive and spontaneous XCL1 expression **(Fig.12C/D, pg.84)** as do small subsets of T and B cells (**Fig.8O)**. A more detailed analysis of XCL1 production by pathogen-specific T cells will be discussed in the next chapter.

In summary, the comprehensive analysis of homeostatic chemokine expression by splenocytes of hematopoietic origin demonstrates the general utility of 'chemokine flow cytometry' as it confirmed and extended the expression pattern of 18 chemokines (**Table 9**). While the focus of this thesis was clearly limited to hematopoietic cells, further investigation of homeostatic chemokine production of other cell types are generally feasible as demonstrated by the analysis of CCL25 expression by

intra-epithelial cells of the small intestine (IEC) (**Fig.9F**). Furthermore, our laboratory is currently testing some of these chemokine antibodies for suitability in IHC and preliminary data demonstrated that all tested antibodies so far indeed work using PFA-fixed tissues. This also demonstrates the use of intracellular flow cytometry as a screening tool to quickly identify the suitability of antibodies for the use in IHC of PFA-fixed tissues.

4.1.5 The dendritic cell chemokine response to infection

Dendritic cells are the principal APCs inducing the adaptive immune response and the importance of DCs as chemokine producers is beginning to emerge [54, 148]. The broad spectrum of chemokines produced by *endogenous* DCs spontaneously and after stimulation (**Fig.8-9D/E/F**) led to the investigation of chemokine production by bone marrow-derived DCs (BMDCs) in response to an *in vitro* infection with the bacterium L. *monocytogenes* (LM) (**Fig.11**). Comparison of chemokine production by uninfected BMDCs with *ex vivo* splenic DCs reveals an overall similar pattern, although additional expression of CCL5, CCL17, CXCL1 and CXCL2 is observed in BMDCs which is most likely due to partial activation due to the culturing and/or harvesting conditions. Chemokine expression of BMDCs after LM infection (**Fig.11**, black tracing) resembles the observed profile of splenic DCs stimulated with LPS (**Fig.9**) or IFNγ (data not shown): high expression of CCL2/3/4/5 and CXCL1/2/5/10, moderate synthesis of CCL11/CXCL9 and only marginal upregulation of CCL7/8/12/27 and CXCL11. However, six additional chemokines are highly expressed in uninfected BMDCs but differentially regulated upon infection: increased CCL17/22 production contrasts with unaltered CXCL16 levels and the down-modulation of CCL6, CCL9/10 and CXCL4 (and perhaps CXCL7). Thus, the DC response to infection is distributed over 20 distinct chemokines and comprised of two major components: 1., the modulation of homeostatic chemokine expression (potentiation: CCL3/4/5/11/17/22 and CXCL1/2; no change: CXCL16; inhibition: CCL6, CCL9/10 and CXCL4/7) and 2., the *de novo* induction of inflammatory chemokines generally found at somewhat lower levels (CCL2/7/8/12/27 and CXCL5/9/10/11).

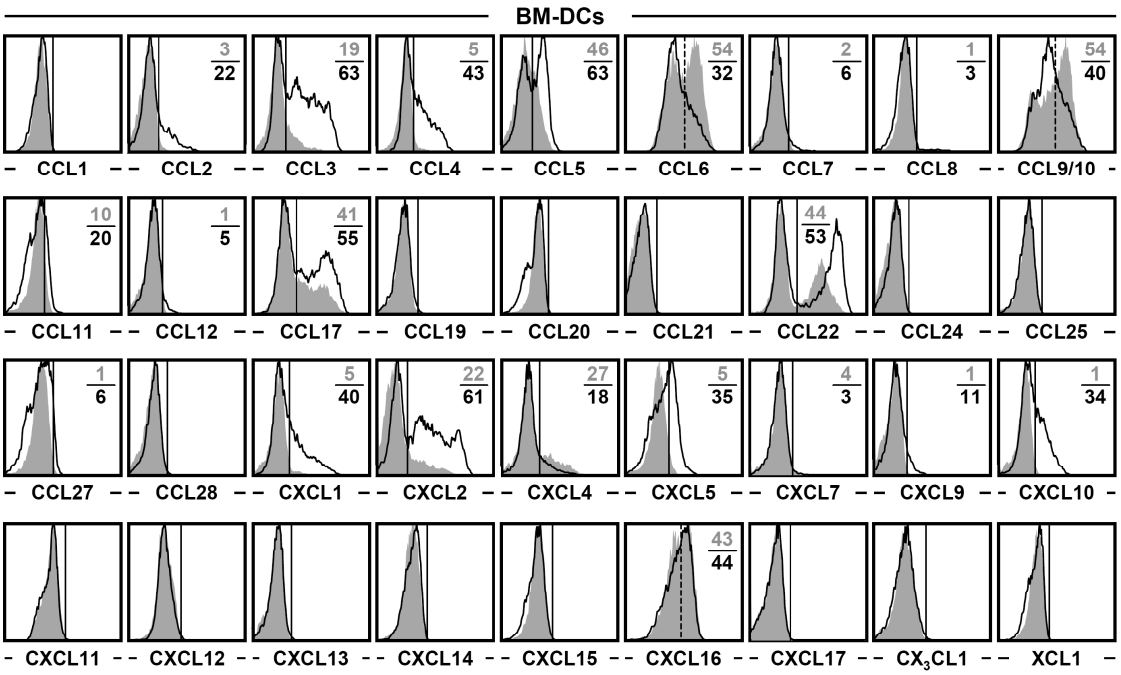

Figure 11: ***The DC chemokine response to bacterial infection.*** *Bone marrow DCs were obtained from B6 mice, propagated by culture in GM-CSF and infected with rLM-OVA at an MOI of 1 as described in Methods. Four hours after LM or mock infection, BFA was added to cultures for an additional 5h followed by the quantitation of chemokine expression by uninfected vs. infected DCs. The histograms are gated on CD11c^{+}BM-DCs and display chemokine expression by uninfected (gray solid) and infected (black tracing) cells. The solid vertical marker demarcates chemokine-expressing from non-expressing cells, the dashed marker featured in CCL6, CCL9/10 and CXCL16 histograms distinguishes chemokine^{++} and chemokine$^{+/-}$ cells. The numbers indicate the percentage of chemokine expression in the absence (gray font) or presence (black font) of infection; values are the average of duplicate experimental samples. Data are representative for 1 out of 2 experiments. Similar results were obtained after 24h of rLM-OVA infection and prevention of cell death by addition of antibiotics after initial establishment of infection (not shown).*

Interestingly, several of these chemokines (CCL2/5/17, CXCL1/2/10) were reported to be spontaneously produced by CD11b^{hi} cDCs isolated from the lungs of naive mice [117]. Since these chemokines are not produced by primary splenic DCs in the absence of stimulation (**Fig.8 & Fig.9A**), peripheral DCs residing in an organ exposed to the exterior environment apparently exhibit a 'chemokine signature' consistent with heightened activation and a predisposition to readily process inflammatory insults.

4.1.6 Chemokine profiles of murine and human NK cells

NK cells are at the interface of innate and adaptive immunity as they are capable of recognizing infected cells via TLRs, but also directly attack IgG-coated virus-infected cells via FCγR (CD16) engagement [4]. One of the best studied mouse models of NK biology is the MCMV model demonstrating the ability of NK cells to produce abundant amounts of CCL3/4/5 and XCL1 following *ex vivo* and *in vitro* infection with the virus [70, 114, 162]. The application of our chemokine flow cytometry protocol validated the expression of CCL3/4/5 and XCL1 in response to PMA/Ionomycin treatment and extended the expression profile to CCL9/10 and CXCL2 which were produced by a small subset of murine NK cells (**Fig.12A)**. Furthermore, co-staining with multiple chemokine antibodies shows the simultaneous production of CCL3/4/5 and XCL1 and identifies the IFNγ^+ cells as high chemokine producers (**Fig.12F)**. The analysis of NK-produced chemokines was extended to include blood from healthy human donors (**Fig.12B)**. In addition to the aforementioned chemokines, CCL1, CCL22 and CXCL8 (IL-8, no murine homolog) were included in the analysis as previous reports indicated their expression in human NK cells [162]. Since no FC-approved anti-human CCL1 and XCL1 antibodies were available, pAbs from R&D Systems were tested for suitability, as well as the anti-human polyclonal antibody against CCL5, due to inconsistent results obtained with FC-approved monoclonal αCCL5. To this end, we found that the CCL5-specific pAb provided more consistent results than fluorochrome-conjugated CCL5 mAbs (**Fig.12B** and not shown). Analysis of human blood-borne NK cells revealed constitutive expression of CCL3 and CCL4 in a small subset ($\sim$5%) and spontaneous expression of these chemokines ($\sim$30-40%) with $\sim$10% of NK cells being XCL1$^+$ (**Fig.12B)** which was also observed, although to a lesser extend, in murine NK cells from the blood (**Fig.12C**). Almost all human NK cells express CCL3 and CCL4 after stimulation and about half of the NK cells express XCL1. Noteworthy is the observation that IFNγ production is generally limited to less than 10% of NK cells after PMA/Ionomycin stimulation indicating that chemokine production is more readily induced. Similar to our observation in mice, CCL5 expression in human NK cells is constitutive, but differs in response to stimulation: In the presence of BFA, net accumulation of intracellular CCL5 occurs in murine NK cells upon stimulation whereas human NK cells deplete their CCL5 stores. These species-specific differences were also observed in T cells and are described in more detail in the next chapter.

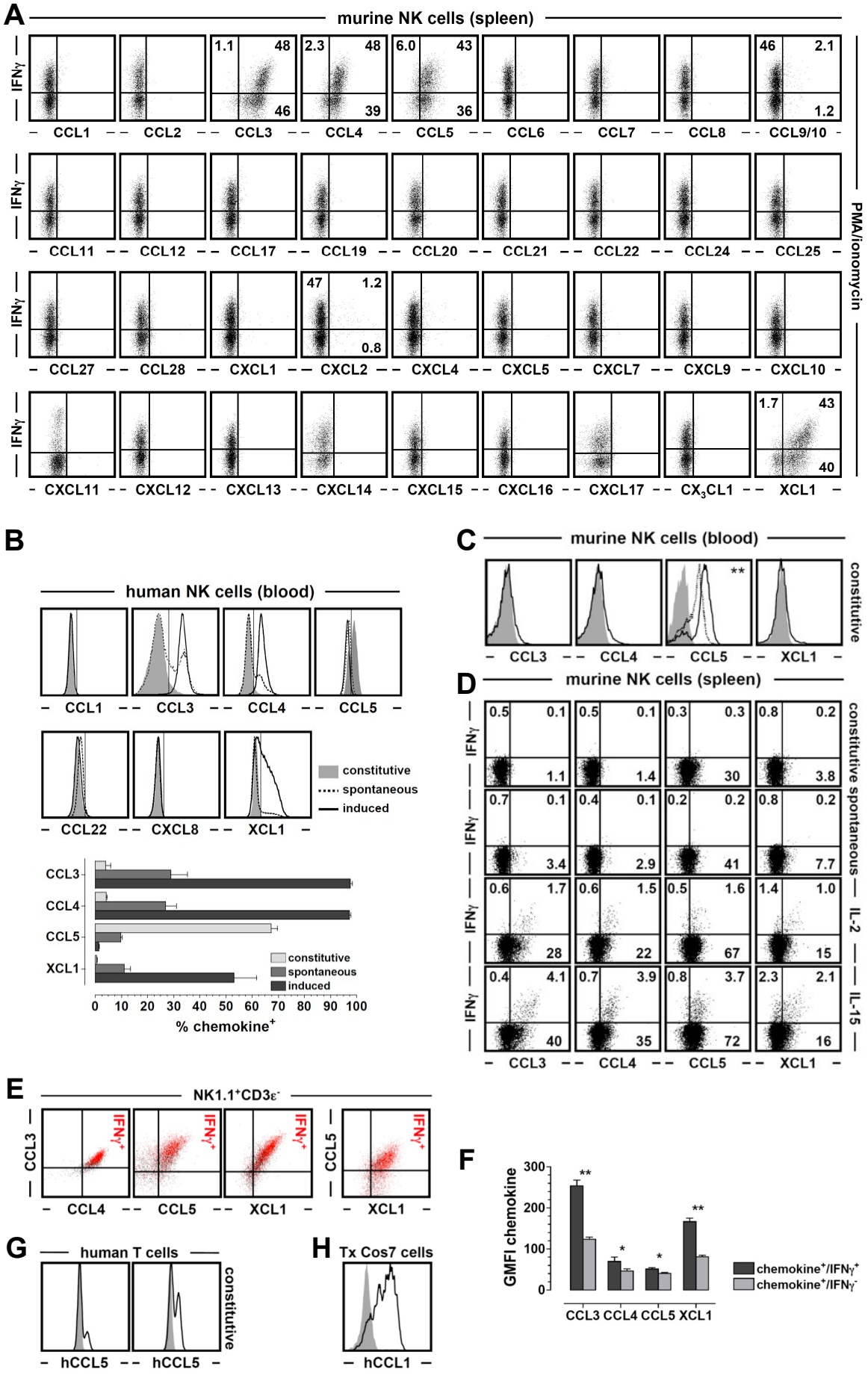
A
murine NK cells (spleen)
IFNγ
CCL1 CCL2 CCL3 CCL4 CCL5 CCL6 CCL7 CCL8 CCL9/10
CCL11 CCL12 CCL17 CCL19 CCL20 CCL21 CCL22 CCL24 CCL25
CCL27 CCL28 CXCL1 CXCL2 CXCL4 CXCL5 CXCL7 CXCL9 CXCL10
CXCL11 CXCL12 CXCL13 CXCL14 CXCL15 CXCL16 CXCL17 CX3CL1 XCL1
PMA/ionomycin
B
human NK cells (blood)
CCL1 CCL3 CCL4 CCL5
CCL22 CXCL8 XCL1
constitutive
spontaneous
induced
% chemokine+
C
murine NK cells (blood)
CCL3 CCL4 CCL5 XCL1
constitutive
D
murine NK cells (spleen)
constitutive
spontaneous
IL-2
IL-15
E
NK1.1+CD3ε-
IFNγ+
F
GMFI chemokine
chemokine+/IFNγ+
chemokine+/IFNγ-
G
human T cells
hCCL5 hCCL5
H
Tx Cos7 cells
hCCL1

Figure 12: Chemokine profiles of murine and human NK cells. *(**A**) B6 spleen cells were cultured for 5h with PMA/ionomycin and BFA and stained for surface and intracellular markers. All plots are gated on NK1.1$^+$CD3ϵ^- cells; the numbers are average percentages of IFNγ^+ and/or chemokine$^+$ cells in the respective quadrants. **(B)** Chemokine expression by human NK cells was determined directly ex vivo ("constitutive"), after 5h culture in the presence of BFA ("spontaneous") or 5h stimulation with PMA/ionomycin plus BFA ("induced") as detailed in the Methods section. Representative histograms are gated on CD56$^+$CD3$^-$ NK cells (gray solid: constitutive, dashed line: spontaneous, black tracing: induced). The vertical markers were set according to goat IgG or isotype control stains. The bar diagram depicts the fraction of chemokine$^+$ NK cells obtained from four healthy volunteers (representative data from 3-5 independent experiments). (**C**) Blood-borne murine NK cells (NK1.1$^+$ CD3ϵ^-) were analyzed for constitutive chemokine expression (black tracings). Note that different control stains (gray histograms) are featured in the individual plots (CCL3 control: CCL3 stains of B6.CCL3$^{-/-}$ NK cells; CCL4 and XCL1 controls: goat IgG stains; CCL5 controls: CCL5 stains of B6.CCL5$^{-/-}$ [gray] and B6.CCL5$^{+/-}$ [dashed line] NK cells). The CCL5 expression level (GMFI) of heterozygous CCL5$^{+/-}$ NK cells are slightly but significantly lower than those of wild-type NK cells (p=0.01 [**]). (**D**) CCL3/4/5 and XCL1 expression by splenic NK cells was determined in conjunction with IFNγ directly ex vivo ("constitutive"), after 5h culture with BFA ("spontaneous") or 5h stimulation with 100ng/ml IL-2 or IL-15 plus BFA. As above, the numbers are average percentages of IFN$\gamma^+$and/or chemokine$^+$ cells in the corresponding quadrants. All data obtained for murine NK cells are representative for multiple independent experiments with 2-3 mice analyzed in each experiment. (**E**) Induced chemokine co-expression by murine NK cells. Following a 5h culture with PMA/ionomycin and BFA, B6 spleen cells were stained for surface and intracellular markers using pre-conjugated chemokine-specific pAbs and/or the CCL3-specific mAb clone 39624 in conjunction with αIFNγ as detailed in Methods. All plots are gated on NK1.1+CD3ϵ^- cells and IFNγ-expressing NK subsets (40-50% of NK cells) are indicated as red events. Data are compiled from 4 independent experiments evaluating 2-3 mice each. (**F**) Comparison of induced chemokine production (PMA/ionomycin) by IFNγ^+ vs. IFNγ^- NK cell populations. The bar diagram displays the GMFI (geometric mean of fluorescence intensity) of indicated chemokine stains in NK subsets demonstrating IFNγ co-expression (black) and NK cells with detectable chemokine but no IFNγexpression (gray) (n=3, one of 3 similar experiments). Asterisks indicate statistical significance as determined by paired t-tests. (**G**) Constitutive CCL5 expression by human T cells. Representative histograms are gated on CD3$^+$CD56$^-$ PBMC from 2 healthy volunteers (gray: goat IgG, black: CCL5). (**H**) Cos7 cells were transfected with empty or human Ccl1 containing pIRES2-AcGFP1 vector and stained for expression of CCL1. Histograms are gated on GFP$^+$ Cos7 cells (gray: empty vector, black: Ccl1 vector; 24h Tx with BFA for final 5h).*

Lastly, human NK cells do not exhibit constitutive, spontaneous or induced expression of CCL1, CCL22 or CXCL8 (**Fig.12B**, control stains for αhCCL1 in subpanel **H**).The lack of induced CCL1 synthesis in mouse and human NK cells is of particular interest as this chemokine distinguishes the otherwise identical set (CCL3/4/5, XCL1) of abundantly produced chemokines expressed by murine NK and $CD8^+$ T cells. The overlapping chemokine repertoire even applies to a certain degree to the weakly expressed CXCL2 and CCL9/10 chemokines. As will be shown in the next chapter on T cell-produced chemokines, CXCL2 expression is restricted to a small set of stimulated $CD4^+$T cells and CCL9/10 expression is expressed by a subset of stimulated murine $CD4^+$and $CD8^+$T cells. Furthermore, quantitative differences among constitutively NK cell-expressed murine chemokines in different anatomic compartments was observed. In comparison to the spleen, blood-borne NK cells contained high amounts of constitutive CCL5 and exhibited somewhat more pronounced constitutive CCL3/4 and XCL1 expression (**Fig.12C/D)**, a finding that complements the constitutive and spontaneous production of the same chemokines by human NK cells.

In a recent study, the 'functional status' of resting murine NK cells has been characterized at the mRNA level for several cytolytic effector molecules (granzyme A [GzmA], granzyme B [GzmB] and perforin) [157]. However, while GzmA protein is expressed in a constitutive fashion, *GzmB* and perforin are translated from pre-existing mRNA species only upon stimulation with cytokines such as IL-2 and IL-15 [157]. My analysis of microarray data generated by Fehniger *et al.* [157] indicated that of all chemokine probesets, only *Ccl3/4/5* and *Xcl1* transcripts are expressed at high levels in resting NK cells and that prolonged stimulation (24h) with IL-15 did not change transcript levels of these chemokines (data not shown). Interestingly, short-term (5h) stimulation of murine NK cells with IL-2 or IL-15 (**Fig.12D)** revealed robust upregulation of chemokine proteins when compared to constitutive or spontaneous protein expression indicating post-transcriptional regulation of chemokine expression in NK cells. The post-transcriptional regulation of these chemokines will be further explored in the next chapter utilizing transcriptional and translational inhibitors. In summary, the integration of Fehninger *et al.*'s data with our experimental data indicates that the murine and human NK cell response is dominated by the synthesis and secretion of chemokines that precede IFNγ production and the eventual acquisition of cytolytic effector functions mediated by GzmB and perforin [157].

4.1.7 The chemokine profile of *activated* murine B cells

Although B cells are recognized as a biologically relevant source of cytokines and chemokines [157–159], the spectrum of chemokines synthesized by stimulated B cells remains incompletely defined. In order to determine the chemokine expression profile of B cells from unmanipulated mice, splenocytes were either stimulated via the Toll-like receptor TLR4 or via BCR signaling/co-signaling using LPS or αIgM/αCD40, respectively (**Fig.13**). LPS stimulation led to a weak but significantly increased synthesis of CCL3, CCL4 and CCL22 in a small fraction of B cells when compared to the "spontaneous" production (**Fig.13A**) and no other chemokines were detected at the protein level (data not shown). Interestingly, the increase in CCL3 and CCL4 protein production is most likely regulated post-transcriptionally as their mRNA-levels did not change after LPS stimulation [159–161] whereas *Ccl22* mRNA has shown to increase after LPS stimulation [160]. The absence of induced CCL6 and CXCL1/2 production should be emphasized here given the reported upregulation of corresponding chemokine mRNA transcripts [161]. Upregulation of chemokine mRNA after stimulation through the BCR (αIgM / αCD40) or antigen differs from LPS-stimulation in respect to the spectrum of chemokine transcripts produced (*Ccl2/3/4/5/6, Ccl9/10, Ccl22, Cxcl16,* Cx_3cl1 and/or *Xcl1* [159–161]). In contrast, analysis of the protein production (**Fig.13B**) 5 hours after IgM/CD40 engagement indicates that CCL3 and CCL4 expression resembles that of LPS-stimulated cells (**Fig. 13A**) whereas CCL22 expression is marginal at best. Of particular note is further the absence of spontaneous or induced CCL5 expression under any experimental conditions in spite of the fact that *Ccl5* is the most abundantly expressed chemokine mRNA transcript in purified B cells [66, 158]. In comparison to the rapid production of multiple chemokines by innate immune cells (NK cells, Mo/MΦ, DCs) and pathogen-specific T cells (see next chapter), the B cell chemokine response is therefore rather limited in regards to both the spectrum (CCL3/4/22) and the quantity of chemokines produced.

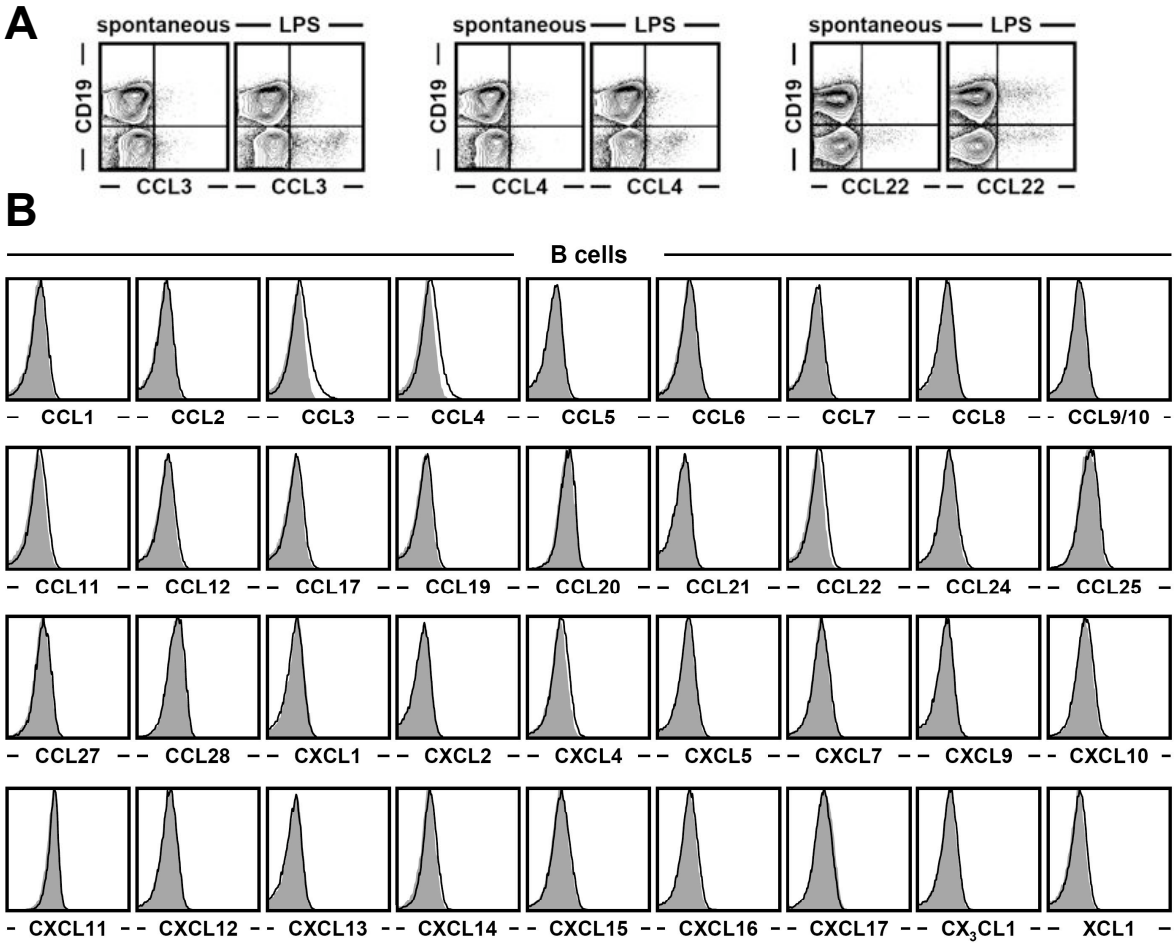

Figure 13: ***Spontaneous and induced chemokine production by murine B cells.*** ***(A)*** *Spleen cells were cultured for 5h in the presence of BFA ("spontaneous") or 500ng/ml LPS and BFA and stained for CD19 and indicated chemokines. 5% probability contour plots are gated on live cells based on FSC/SSC properties; data are representative for at least 3 independent experiments. Similar results were obtained in stimulation cultures containing 5μg/ml LPS (not shown).* ***(B)*** *After 5h culture of spleen cells with BFA only (gray histograms) or B cell stimulation with αIgM (10μg/ml) and αCD40 (15μg/ml) abs plus BFA, cells were stained for surface markers and intracellular chemokines. All histograms are gated on CD19$^+$ CD3ϵ^- cells; data are representative for 2-3 independent experiments analyzing 3 mice each.*

4.1.8 Summary of the establishment of the "chemokine flow cytometry assay"

The first part of this thesis established the use of polyclonal antibodies for the detection of nearly all (37 of 39) murine chemokines by flow cytometry. Systematic testing of cross-reactivities and specificity was performed by utilizing a combination of transiently transfected cell lines and select chemokine-deficient mouse strains.

To demonstrate the utility of the "chemokine flow cytometry assay" established in this thesis work, the chemokine profiles of primary splenocytes and BMDCs was determined under different experimental conditions as summarized in table 10.

While intracellular flow cytometry itself is not a novel technique and some flow cytometry-approved chemokine-specific antibodies exist, the ability to visualize almost all murine chemokines using flow cytometry offers a unique tool to determine the chemokine expression at the single cell level.

Until now, the measurement of mRNA abundance has commonly been used to infer the expression profile of the entire chemokine family in a given cell sample. However, the mRNA expression of a gene might not correlate well with the protein expression due to complex post-transcriptional regulatory networks therefore limiting inferences based on mRNA profiling. To this end, the ability to visualize almost all murine chemokines using flow cytometry offers the opportunity to determine the full spectrum of chemokines produced by a given cell type or population under defined conditions and further facilitates the simultaneous detection of several chemokines within a single cell. Arguably equally important, it is now possible to determine which chemokines are *not* expressed at the *protein level* within the constraints of the experimental conditions. In summary, the method developed in the first part of this thesis research provides a simple, yet novel approach to determine cell-associated chemokine expression profiles using flow cytometry.

	Homeostatic		Inflammatory
Name	**Constitutive (*ex vivo*)**	**Spontaneous (5h culture with BFA)**	**induced/stimulated**
CC family			
CCL1	—	—	T_E, T_M
CCL2	—	Mo/MΦ	Mo/MΦ, cDC, BMDC
CCL3	—	Mo/MΦ,cDC,BMDC, B	Mo/MΦ, cDC, BMDC, B
CCL4	—	Mo/MΦ,cDC,BMDC, B	Mo/MΦ, cDC, BMDC, B
CCL5	T_E, T_M, NK	T_E, T_M, NK, BMDC	Mo/MΦ, cDC, BMDC
CCL6	Gr, Mo/MΦ,cDC	Gr, Mo/MΦ,cDC, BMDC	Mo/MΦ
CCL7	[B], $CD45^-$	[B], $CD45^-$	Mo/MΦ,cDC, BMDC
CCL8	B	B	[BMDC]
CCL9/10	Gr, Mo/MΦ,cDC	Gr, Mo/MΦ,cDC, BMDC	T_E, T_M, [NK], Mo/MΦ,cDC
CCL11	DC, $CD11b^+$, [B], $CD45^-$	Mo/MΦ, DC, BMDC, [B], $CD45^-$	BMDC
CCL12	—	—	BMDC
CCL17	—	BMDC	BMDC
CCL19	—	—	No increase
CCL20	—	—	No increase
CCL21a	T, DC (captured)	—	No increase
CCL21b/c	T, DC (captured)	—	No increase
CCL22	—	cDC, BMDC	cDC, BMDC, B
CCL24	—	—	—
CCL25	—	—	—
CCL26			
CCL27	Gr, DC	Gr, DC	BMDC
CCL28	—	—	No increase
CXC family			
CXCL1	—	BMDC	Mo/MΦ,cDC, BMDC
CXCL2	—	Mo/MΦ, BMDC	T_E, [NK], Mo/MΦ,cDC, BMDC, Gr
CXCL3			
CXCL4	Mo/MΦ, DC, Gr, B (captured)	Mo/MΦ, DC, BMDC, Gr, B [$CD45^-$]	No increase
CXCL5	—	—	BMDC
CXCL7	Mo/MΦ, DC, Gr, B (captured)	Mo/MΦ, DC, [BMDC], Gr, B [$CD45^-$]	No increase
CXCL9	T (captured)	—	Mo/MΦ, cDC, BMDC
CXCL10	—	—	Mo/MΦ, cDC, BMDC
CXCL11	—	—	[Mo/MΦ, cDC]
CXCL12	—	—	No increase
CXCL13	—	—	No increase
CXCL14	—	—	No increase
CXCL15	—	—	No increase
CXCL16	—	Mo/MΦ, DC, BMDC	Mo/MΦ, DC
CXCL17	—		No increase
CX3C family			
CX_3CL1	—	—	No increase
C family			
XCL1	—	T, NK, [B]	T_E, T_M, NK

Table 10: ***Summary of the observed chemokine expression patterns by primary spleen cells and BMDCs.*** *In the case of T cell-produced chemokines, findings from LM-specific $CD8^+T_E$ cells [68] and findings from the next chapter of this thesis on LCMV, VSV and LM-specific $CD8^+$ and $CD4^+T_E$ and T_M cells were combined. No suitable reagents could be identified for the specific detection of CCL26 and CXCL3. Stimulation protocols used for cellular subsets were as follows: For pathogen-specific T_E and T_M viral and bacterial pathogen-derived peptides; for NK cells, PMA/ionomycin, IL-2, or IL-15; for Mo/MΦ and primary splenic DCs, LPS or IFNγ; for BMDCs, LM infection; for B cells, LPS or anti-IgM/anti-CD40. Negative data are categorized as absence of detectable chemokine expression (–) and no increase in chemokine production after stimulation with any agent. Cell subsets listed in brackets exhibit marginal chemokine expression under the indicated experimental conditions.*

4.2 Chemokine profiling of pathogen-specific T cells

The second part of this thesis focusses on the biology of T cell-produced chemokines. Its aim is to determine the complete spectrum of chemokines produced by T cells in response to intracellular-replicating pathogens using flow cytometry, to determine their co-expression profiles, kinetics and activation thresholds. Specifically, the chemokine-production of antigen-specific $CD4^+$ and $CD8^+$ T cells in response to three different pathogens (LCMV, VSV, rLM-OVA) will be compared. As a first step, the chemokine expression profile of LCMV-specific T cell receptor (TCR) transgenic p14 T_E and T_M will be analyzed to identify chemokine and chemokine receptors expressed at the mRNA level. Subsequently, the chemokine protein profile of p14 T cells will be determined and compared to endogenously-generated LCMV-specific T cells using flow cytometry and the analysis will be extended to T cells specific for other intracellular-replicating pathogens (VSV, rLM-OVA). Lastly, kinetic aspects of cytokine production and release as well as co-expression patterns of select T-cell-produced chemokines will be determined in the LCMV model.

4.2.1 Chemokine mRNA expression profiles of LCMV-specific effector and memory $CD8^+$ T-cells utilizing the p14 mouse model

As a foundation for this thesis, as well as for various other research projects in our laboratory, I performed a microarray experiment using the Affymetrix platform (M430.V2) to analyze the mRNA expression profile of epitope-specific $CD8^+$ T_E and T_M cells in response to an acute LCMV infection. LCMV Armstrong infection induces a strong $CD8^+$ T cell-dependent primary response leading to efficient virus clearance and memory formation. As described in detail in the Materials & Methods section, the established p14 mouse model was used to generate epitope-specific $CD8^+T_E$ and T_M cells by adoptively transferring transgenic p14 $CD8^+$ splenocytes bearing an invariant TCR specific for the GP_{33-41} epitope into naive wt mice [90,163]. The expression of the congenic marker CD90.1 on the p14 cells allowed their purification from the host spleen by sequential magnetic and fluorescent-activated cell sorting (FACS). mRNA from p14 effector p14 T cells (T_E) 8 days after LCMV infection or mRNA from early memory T cells (T_M) 46 days after LCMV Armstrong infection was extracted either directly after sorting (*ex vivo*) or after a 3 hour re-stimulation with αCD3

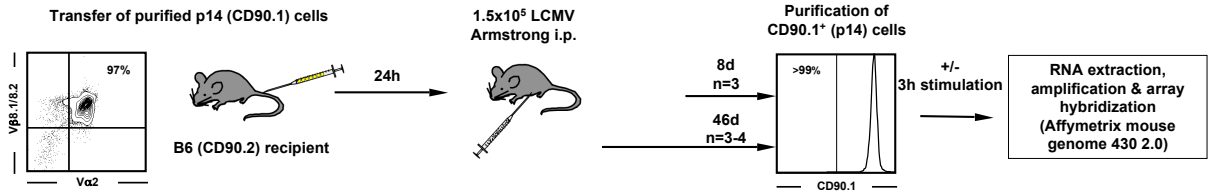

Gene Symbol	Unigene ID	Affymetrix ID	Gene Symbol	Unigene ID	Affymetrix ID
CC family			**CXC family**		
CCL1	Mm.1283	1421688_a_at	CXCL1	Mm.21013	1419209_at
CCL2	Mm.290320	1420380_at	CXCL2	Mm.4979	1449984_at
CCL3	Mm.1282	1419561_at	CXCL3	Mm.244289	1438148_at
CCL4	Mm.244263	1421578_at	CXCL4	Mm.332490	1448995_at
CCL5	Mm.284248	1418126_at	CXCL5	Mm.4660	1419728_at
CCL6	Mm.137	1417266_at	CXCL7	Mm.293614	1418480_at
CCL7	Mm.341574	1421228_at	CXCL9	Mm.766	1418652_at
CCL8	Mm.42029	1419684_at	CXCL10	Mm.877	1418930_at
CCL9/10	Mm.416125	1448898_at	CXCL11	Mm.131723	1419697_at
CCL11	Mm.4686	1417789_at	CXCL12	Mm.303231	1417574_at
CCL12	Mm.867	1419282_at	CXCL13	Mm.10116	1417851_at/1448859_at
CCL17	Mm.41988	1419413_at	CXCL14	Mm.30211	1418457_at
CCL19	Mm.426373	1449277_at	CXCL15	Mm.64326	1421404_at
CCL20	Mm.116739	1422029_at	CXCL16	Mm.425692	1418718_at
CCL21a	Mm.407493	see CCL21b	CXCL17	Mm.10545	1451610_at
CCL21b	Mm.220853	1445238_at			
CCL21c	Mm.407493	see CCL21b	**C family**		
CCL22	Mm.12895	1417925_at	XCL1	Mm.190	1419412_at
CCL24	Mm.31505	1450488_at			
CCL25	Mm.7275	1418777_at/1458277_at			
CCL26L	Mm.376459	not on chip	**CX3C family**		
CCL27	Mm.335946	1430375_a_at	CX3CL1	Mm.103711	1415803_at/
CCL28	Mm.143745	1450218_at/1455577_at			1415804_at/1421610_at

Figure 14: ***Microarray experimental design and probeset identifiers.*** *(**A**) Naive p14 TCR transgenic CD8$^+$T cells were purified from the spleens of naive p14 mice (CD90.1 background) by negative selection and transferred i.v. into congenic B6 recipients (CD90.2) that were challenged 24h later with 1.5x10^5 pfu LCMV Armstrong. Eight days (CD8^+T_E) and 46 days (CD8^+T_M) later, p14 were re-purified by combined magnetic and fluorescence activated cell sorting to >99% purity; RNA was extracted either immediately or after 3h stimulation with αCD3/αCD28 antibodies, processed for hybridization to Affymetrix Mouse Genome 430 2.0 arrays and data analyzed as detailed in Experimental Procedures (n=3-4 individual mice).(**B**) Murine chemokine IDs and Affymetrix IDs. If more than one Affymetrix ID is listed, the data presented in (**Fig.15**) displays the average of the respective chemokine mRNA levels.*

and αCD28 (**Fig.14**). This approach not only generated a complete overview of chemokine mRNA expression (**Fig.15**), but also of their receptors (**Fig.16**).

Of the 38 chemokine genes represented on the chip, six were expressed *ex vivo* above background in T_E and T_M cells (*Ccl3, Ccl4, Ccl5, Ccl6, Ccl9/10, Xcl1*) and four genes (*Ccl3, Ccl4, Ccl9/10, Xcl1*) were further upregulated after restimulation. *Ccl25, Ccl27* and *Cxcl10* showed only marginal gene expression above background. Ccl5 and Ccl6 were downregulated upon restimulation whereas *Ccl1* was the only chemokine not expressed *ex vivo* but strongly upregulated upon restimulation.

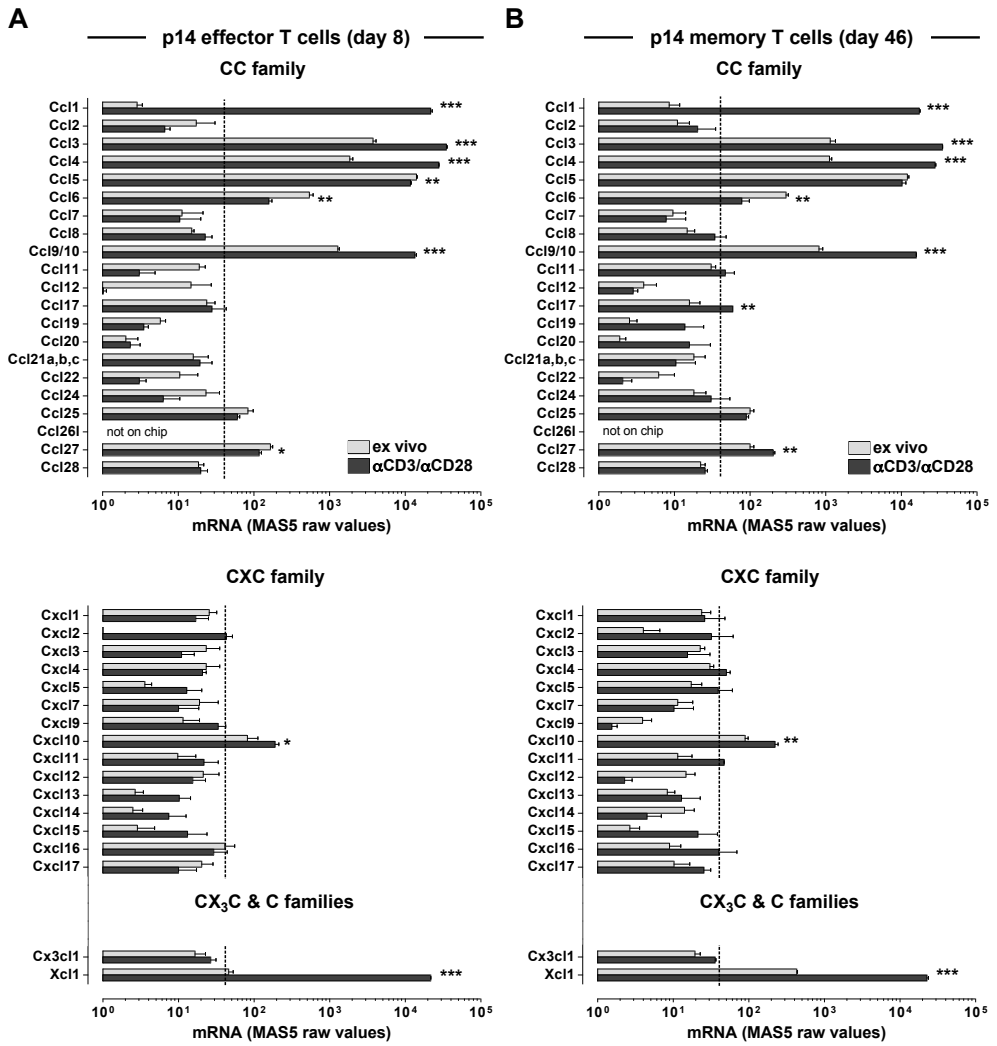

Figure 15: ***Chemokine mRNA profiles of p14 effector and memory T cells.*** *The experiment was performed as described in (**Fig.14**). (**A**) MAS5-normalized values of chemokine gene expression by p14 T_E analyzed ex vivo (gray bars) or after TCR stimulation (black bars). Statistically significant ex vivo or induced chemokine expression above the threshold is demonstrated for CCL1, CCL3, CCL4, CCL5, CCL6, CCL9/10 and Xcl1. Marginal, but significant expression above the average background is found for CCL25, CCL27 and CXCL10. Statistically significant differences between ex vivo and TCR-induced chemokine mRNA levels are indicated by asterisks. (**B**) Chemokine mRNA expression in p14 T_M (46 dpi) is displayed as in A. Coverage: 39/40 murine chemokines genes (Ccl26 not on chip, three distinct Ccl21 genes give rise to two unique proteins, CCL21a[Ser^{65}] and the identical gene products CCL21b and CCL21c [Leu^{65}] all of which are represented by one mRNA probeset.)*

Ccl17 was the only chemokine that was only expressed in T_M, albeit at marginal levels and only after restimulation. In summary, 10 of the 38 chemokines analyzed were expressed at the mRNA-level in T_E. Eight of these genes were expressed *ex vivo* as well as after restimulation. *Ccl1* was

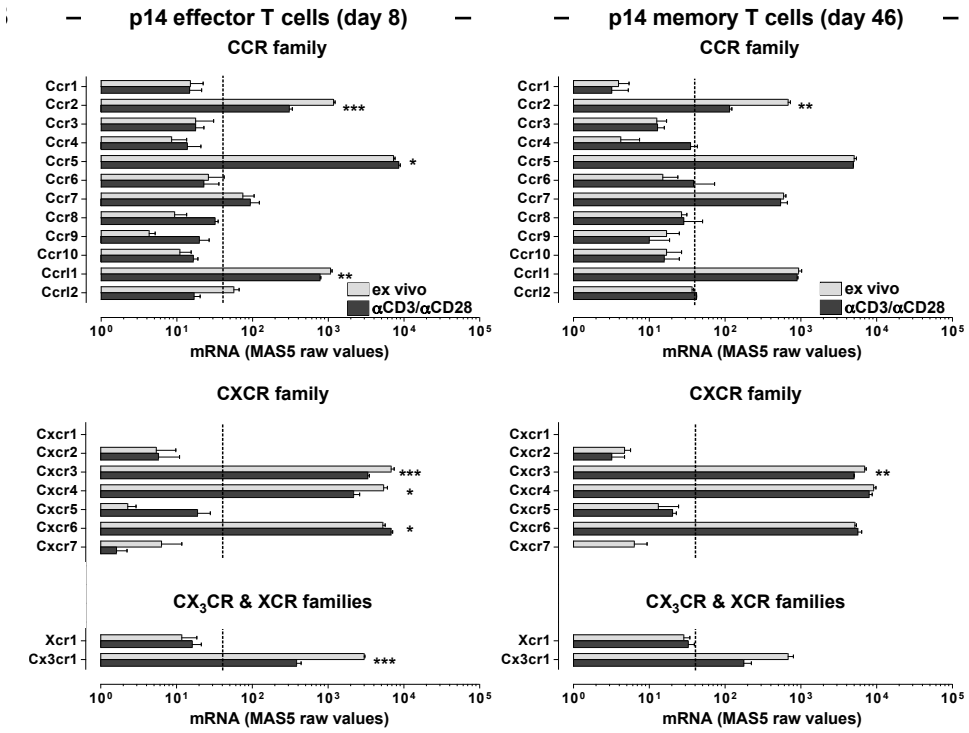

Figure 16: ***Chemokine receptor mRNA expression by virus-specific CD8$^+$T$_E$ and T$_M$.*** *Summary of chemokine receptor genes detected ex vivo and after TCR stimulation in p14 CD8$^+$T$_E$ and p14 CD8$^+$T$_M$ (MAS5-normalized values). The dotted line represents average background signal and genes at or below this threshold are termed absent.*

only expressed after restimulation and *Xcl1* expression *ex vivo* was marginal, if at all, but showed robust upregulated after restimulation. Comparison of these results with a recent publication of microarray expression profiles of p14 T$_E$ and T$_M$ by Wherry *et al.* [164] indicated the presence of additional chemokine mRNAs *ex vivo* (*Ccl8, Ccl19, Ccl21, Ccl22, Cxcl1, Cx$_3$cl1*). However, we were not able to detect these chemokines at the protein level in p14 T$_E$ and T$_M$ either *ex vivo* or after re-stimulation (data not shown).

Lastly, possible auto- or paracrine mechanisms of T cell-produced chemokines were evaluated (**Fig. 16**): mRNA expression for 9 chemokine receptors were found in both T$_E$ and T$_M$ for (*Ccr2, Ccr5, Ccr7, Ccrl1, Cxcr3, Cxcr4, Cxcr6,Cx$_3$cr1*) as well as marginal expression of *Ccrl2* restricted to *ex vivo* T$_E$. Expression of the corresponding receptor proteins by flow cytometry varied widely and was in part restricted to intracellular compartments (CCR5, CXCR4, CXCR6; not shown). Of note is that the only receptor specific for any of the T cell-produced chemokines is CCR5, the receptor for CCL3/4/5.

4.2.2 Protein expression profiles of LCMV-specific p14 T_E and T_M cells

Although T cells have been described as a source of some chemokines, the complete spectrum produced by *pathogen-specific* T cells remains to be determined. Furthermore, our current knowledge of T cell-produced chemokines has been derived from heterogeneous experimental methods, e.g. RT-PCR, Western blotting, ELISA and, to a limited extend, by flow cytometry. The application of "chemokine flow cytometry" allows for a consistent evaluation of T cell-derived chemokines at the single cell level.

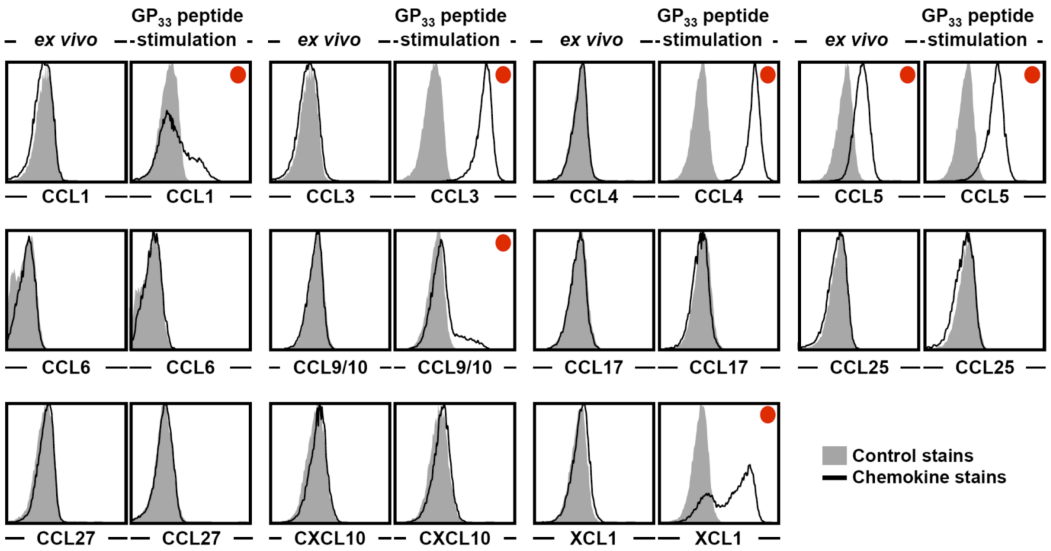

Figure 17: ***Constitutive and induced chemokine protein expression by virus-specific CD8$^+$ T cells.*** *P14 CD8$^+$ T_E (d8) were analyzed for chemokine protein expression using flow cytometry ex vivo or after a 5h stimulation with GP_{33-41} peptide. Histograms are gated on p14 cells (gray histograms: IgG control stains, black tracings: indicated chemokine stains; red dots identify panels demonstrating detectable chemokine expression).*

Analogous to the microarray experiment, p14 chimera were generated and infected with LCMV Armstrong to measure the chemokine protein profile of p14 T_E either *ex vivo* or after a five hour *in vitro* restimulation with GP_{33-41} peptide (**Fig.17**). Only six out of the eleven chemokines expressed at the mRNA level were present at the protein level after 5 hours of restimulation with GP_{33-41} peptide (CCL1, CCL3, CCL4, CCL5, CCL9/10 and XCL1). CCL5 was the only chemokine found to be present *ex vivo* and its expression was further increased upon re-stimulation. Although *Ccl3* and *Ccl4* mRNA was present *ex vivo* in p14 T_E, translation only occured after re-stimulation. While

CCL3 and CCL4 protein was essentially expressed by all p14 T_E after re-stimulation, expression of CCL1, CCL9/10 and XCL1 was only observed in a subset of cells with roughly ∼60% of cells being $XCL1^{hi}$.

Five chemokines (CCL6, CCL17, CCL25, CCL27 and CXCL10) were not detected at the protein level. From our previously established HEK293T stains, as well as control stains using murine primary cells (**Figs.9, 10C & 8J**) it can be deduced that these chemokines are indeed not expressed in p14 T_E at the protein level, neither *ex vivo* nor after restimulation.

4.2.3 Constitutive and induced chemokine expression profiles of endogenous, pathogen-specific $CD8^+$ and $CD4^+$ T_E

The number of endogenous naive GP_{33}-specifc T cells is estimated to be less than 200 [165]. Transferring higher amounts of TCRtg T cells can skew several aspects of immune response to a given pathogen as, on a per cell basis, less cell cycles are required to reach the maximum T cell titer constituting the effector response [166]. However, the p14 adoptive transfer model is relatively unaffected over a wide range of transferred p14 cells when compared to other model systems [166]. To determine if our findings in the p14 model system reflect that of endogenously-generated LCMV-specific T cells, we next examined the chemokine expression profile of endogenously-generated LCMV-specific $CD8^+$ T_E and extended the analysis to include LCMV-specific $CD4^+$ T_E. The constitutive chemokine profile of $CD8^+T_E$ (d8) is mainly restricted to CCL5 as determined by MHC-tetramer staining of the NP_{396}- and GP_{276}-specific population (**Fig.18A**). CCL5 protein was detected *ex vivo* in $CD4^+T_E$ (d8) as well (**Fig.18B**), albeit only in ∼60% of the population compared to ∼90% in $CD8^+T_E$ and the amount of protein is also significantly lower (∼20% less) as determined by the geometric mean fluorescence intensity (GMFI).

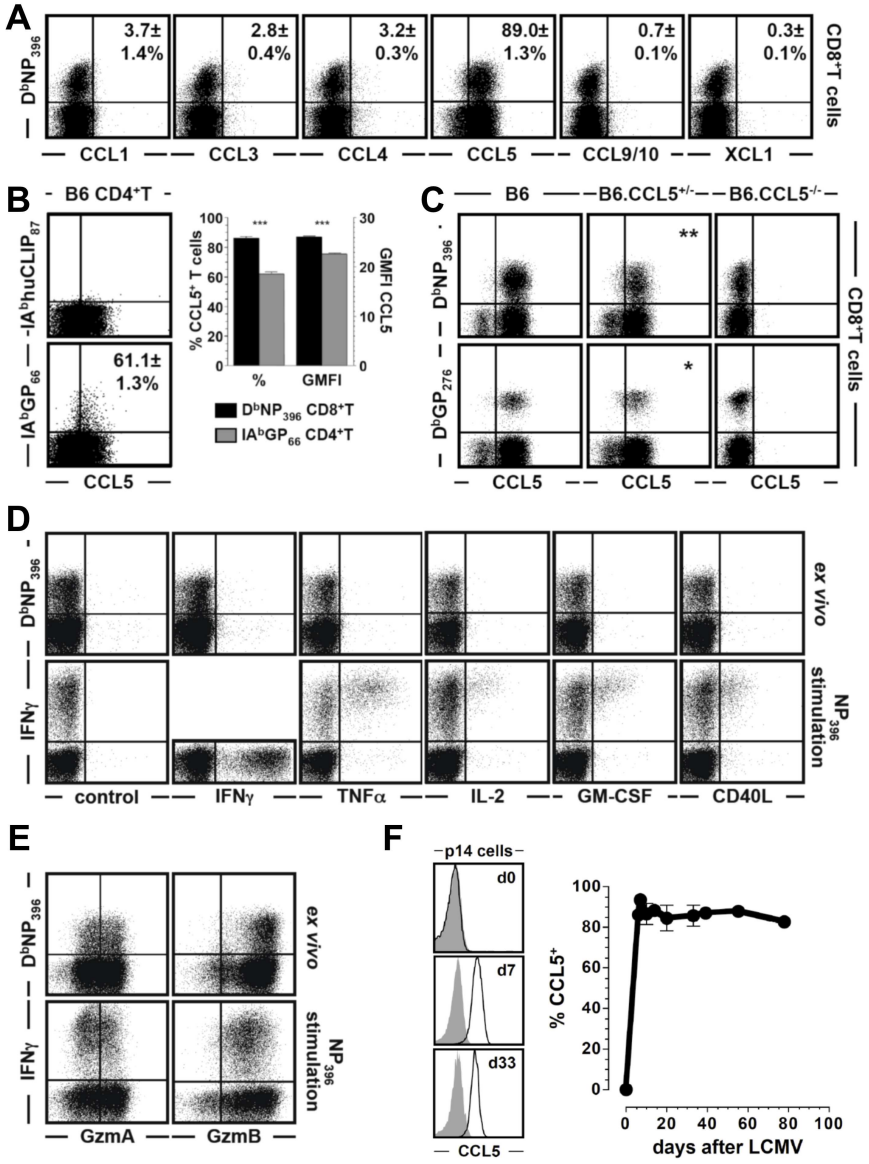

Figure 18: Constitutive chemokine expression by endogenous LCMV-specific T_E . *(**A**) Endogenously generated (plots gated on splenic $CD8^+$ T cells); values indicate SEM of chemokine$^+$ subsets among NP_{396}-specific $CD8^+$ T_E. (**B**) Ex vivo detectable CCL5 expression by LCMV-specific $CD4^+$ T_E 8 days after LCMV Arm infection. The adjacent bar diagram compares the fractions (%) and CCL5 expression levels (GMFI) of CCL5-specific $CD8^+$ and $CD4^+$ T cells; statistical differences are indicated by asterisks. For the purpose of this direct comparison, MHC-I and - II tetramer stains were performed under the same experimental conditions (90 min incubation at 37°C). (**C**) Comparison of constitutive CCL5 expression by LCMV-specific $CD8^+$ T_E subsets (d8) of . (**D**) Induced vs. constitutive expression of effector molecules by virus-specific $CD8^+$T cells. Eight days after LCMV infection of B6 mice, NP_{396}-specific $CD8^+T_E$ were analyzed directly ex vivo or after 5h peptide stimulation for the presence effector molecules (dot plots gated on $CD8^+$T cells). Note that IFNγ , TNFα, IL-2, GM-CSF and CD40L are not constitutively expressed by $CD8^+T_E$ and require a brief period of TCR stimulation to initiate protein neosynthesis. In contrast, detection of constituents in the perforin/granzyme pathway does not require prior activation of specific $CD8^+T_E$ and even re-*

*sults in a slight reduction of GzmA and B expression levels after stimulation (**E**) Interestingly, nearly all virus-specific CD8$^+$T$_E$ contain ex vivo detectable GzmB but only ∼50% of the cells express in addition GzmA (data are representative for 2 or more independent experiments performed with 3 mice/group). (**F**) p14 CD8$^+$T cells obtained from peripheral blood of naive p14 mice (day 0) or LCMV-infected p14 chimeras (days 6-78) were analyzed directly ex vivo for constitutive CCL5 expression (gray histograms: goat IgG, black tracing: CCL5 stains; data are SEM with 3-4 individual mice evaluated per time point).*

Very weak *ex vivo* chemokine expression in a small subset of NP$_{396}$-specific T$_E$ was also observed for CCL1, CCL3 and CCL4 while CCL9/10 and XCL1 was below the background threshold (**Fig.18A**). An explanation for the residual chemokine expression could be a delayed downregulation after cessation of TCR signals as compared to effector molecules like IFNγ [167] in combination with the possibility that these cells have been the last cells engaged in the waning immune response to LCMV. The relative lack of CCL1, CCL3 and CCL4 chemokine expression *ex vivo* in aged T$_M$ (**Fig.21A, pg.103**), as compared to d8 T$_E$ (**Fig.18A**), validates this hypothesis, as these T$_M$ have not encountered any antigen for an extended period of time ($>$ 160 d.p.i.).

As constitutive CCL5 expression presents a rather unusual feature, we further assured ourselves that the antibody is highly specific by comparing the staining pattern of T$_E$ of LCMV-infected wt, CCL5$^{+/-}$ and CCL5$^{-/-}$ mice. Besides establishing the specificity of the antibody, we also observed a small, but significant gene-dosage effect. In the same experiment, two different epitope-specific CD8$^+$T$_E$ subpopulations (NP$_{396}$, GP$_{276}$) were analyzed by co-staining with the respective MHC tetramers (**Fig.18C**) demonstrating that constitutive CCL5 expression is a feature shared among different LCMV-specific CD8$^+$ T$_E$ clonotypes. The robust expression of constitutive CCL5 by virus-specific CD8$^+$T$_E$ may in fact be unique for cytokines at large, since none of the effector molecules readily detected in re-stimulated CD8$^+$T$_E$ (IFNγ, TNFα , IL-2, GM-CSF and CD40L) are expressed in a constitutive fashion (**Fig.18D**). Rather, CCL5 expression resembles that of constituents of cytolytic granules such as GzmA, GzmB and perforin (**Fig.18E**). [167–169].

Endogenously generated LCMV-specific CD8$^+$T$_E$ (d8) exhibited the same profile as the GP$_{33-41}$-specific T$_E$ in the p14 system upon *ex vivo* re-stimulation (**Fig.19A/B**). Almost all NP$_{396}$-specific ($>$ 98%) IFNγ-positive cells expressed CCL3, CCL4, CCL5 whereas only a fraction of cells expressed CCL1 (∼32%), CCL9/10 (∼10%) and XCL1 (∼60%), which was restricted to the IFNγ^{hi} popula-

tion. $CD4^+$ and $CD8^+$ T_E cells produced the same six chemokines after re-stimulation (**Fig.19A**), although the fraction of chemokine-positive $CD4^+$ cells was significantly reduced for all chemokines except CCL1 (**Fig.19A/B**). Comparison of the effect of functional avidity (*i.e.* peptide concentration required to induce IFNγ-production in 50% of a given epitope-specific population), dominance (*i.e.* relative population size) and epitope-specificity on the fraction of chemokine-positive cells revealed no significant differences among LCMV-specific $CD8^+$ T cells (**Fig.19B)** and were independent of the mouse strain as demonstrated by chemokine staining of NP_{118} -specific Balb/c T_E (**Fig.19B)**.

To evaluate if the chemokine production differs qualitatively and quantitatively in response to different intracellular pathogens, the chemokine production in response vesicular stomatitis virus (VSV) and recombinant *Listeria monocytogenes* (rLM-ova) [110] was characterized. Both pathogens were chosen because of their distinct pathogen biology therefore complementing the data generated using the LCMV model. VSV is a cytopathic, enveloped Rhabdovirus capable of producing infections in many species and is occasionally transmitted to humans. Related to the rabies virus, VSV is capable of inducing a rabies-like infection in immunodeficient mice [91, 92], but is also known to infect a wide range of different cell types [170]. In contrast to the natural murine pathogen LCMV, VSV is an abortively-replicating cytopathic virus in mouse. The Gram-positive *Listeria monocytogenes* (LM) is a facultative intracellular organism and, although a rare event, can cause severe infections (listerosis) in immuno-compromised individuals. The mouse model of listerosis is one of the best characterized models of bacterial infection in mice allowing us to compare and contrast our findings to the literature.

Analogous to LCMV infections, both pathogens induce $CD8^+$ and $CD4^+$ T cell responses during acute infections and pathogen-specific T cells are readily detected *ex vivo* using MHC tetramers, or, after peptide restimulation, by intracellular IFNγ-staining [105, 109, 171]. Recombinant rLM-ova constitutively expresses a truncated ovalbumin (amino acids 134-387) generating a traceable OVA_{257}-specific $CD8^+$ T cell population [105].

The results indicate that endogenously generated VSV- and LM-ova-specific $CD4^+$ and $CD8^+$ T cells expressed the same chemokines identified in the LCMV system (CCL1, CCL3, CCL4, CCL5,

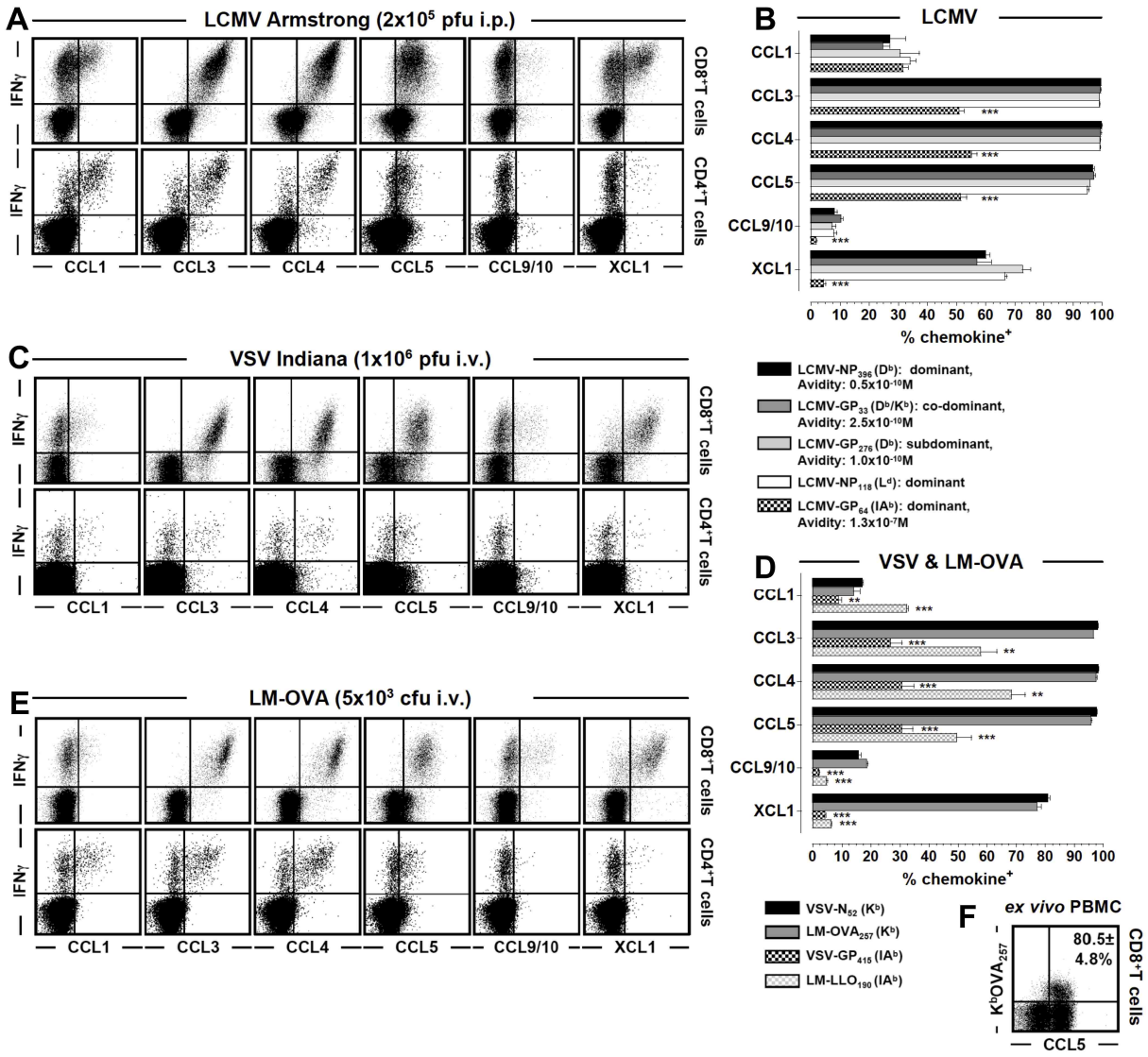

Figure 19: Chemokine expression in response to different pathogens. *(**A**) Induced chemokine production by NP_{396}-specific $CD8^+$(top row) and GP_{64}-specific $CD4^+$ (bottom row) T cells. (**B**) Summary of induced chemokine expression by LCMV-specific T_E subsets stratified according epitope specificity; their restriction elements, relative size (immunodominance) and functional avidities (peptide concentration required to induce IFNγ production in 50% of a given epitope-specific population) are indicated. Significant differences between chemokine-expressing $CD8^+$ and $CD4^+$ T_E subsets are identified by asterisks. (**C-E**) B6 mice challenged with VSV or LM-OVA were analyzed on d8 for induced chemokine expression by VSV-N_{52}-specific $CD8^+$ and GP_{415}-specific $CD4^+$ T cells or LM-OVA_{257}-specific $CD8^+$ and LLO_{190}-specific $CD4^+$ T cells. Asterisks indicate differences between $CD8^+$ and $CD4^+$ T_E specific for the same pathogen. (**F**) Constitutive CCL5 expression by blood-borne LM-OVA_{257}-specific $CD8^+$ T_E. All data are representative for multiple experiments comprising groups of at least 3 mice.*

CCL9/10 and XCL1). Overall, the fraction of chemokine-producing CD4$^+$ cells was reduced as compared to the CD8$^+$ T_E population (**Fig.19C/D**). Significant differences between the CD4$^+$ T_E cell responses were observed: CCL9/10 was the only chemokine differentially expressed between LCMV and LM. However, comparing LCMV and VSV chemokine expression, a significant reduction in the percentage of chemokine-positive cells was found for all chemokines except CCL9/10 and XCL1. Comparing VSV and LM, only differences in XCL1 expression were not significant.

Although LM and LCMV predominantly elicit a T_H1 response, a small subset of pathogen-specific (IL-4-producing) T_H2 -type CD4$^+$$T_E$ cells have been described in both model systems [172, 173], but whose existence has since been contested by others [109, 174] due to the lack of IL-4 expression by these cells. To address these conflicting results, and based upon the use of CXCL2-production as a functional readout for *in vitro* -generated CD4$^+$$T_H2$ cells [70], CXCL2-production by peptide-specific CD4$^+$T cells was measured via flow cytometry (**Fig.20**). Polyclonal activation with PMA/Ionomycin induces CXCL2-expression in predominantly IFNγ-negative CD4$^+$T cells. CXCL2 expression by LCMV-specific, but not by LM-specific, CD4$^+$ T_E cells was detect in a very small percentage (0.2%) of cells.

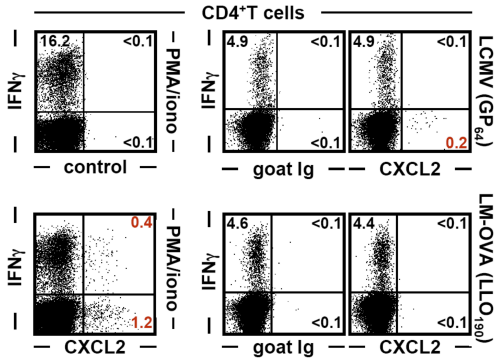

Figure 20: ***CXCL2-production by primary CD4$^+$$T_E$.*** *Left panels: spleen cells obtained from Balb/c mice were stimulated for 5h in the presence of BFA and subsequently stained for surface and intracellular markers (all plots gated on CD4$^+$T cells). Note the presence of CXCL2$^+$CD4$^+$T cells preferentially in the IFNγ-compartment. Middle and right panels: B6 mice infected with LCMV Armstrong or LM-OVA were restimulated with GP_{64} or LLO_{190} peptides and analyzed by cytokine/chemokine flow cytometry. LCMV-specific but not LM-specific CD4$^+$T cells contain a small subset of CXCL2-expressing T_H2-like cells ($\sim$5%). Data is representative for multiple experiments comprising groups of at least 3 mice.*

However, given the clearly predominant "T_H1 phenotype", of LCMV- and LM-specific $CD4^+T$ cells [109, 174], no further characterization of the "T_H2 chemokines" was performed. In summary, the chemokine profile identified in the p14 model was also found in endogenously generated LCMV- , VSV- and LM-specific T_E thus identifying a general pattern of chemokine expression in response to intracellular pathogens. Differences were mainly restricted to a reduction in chemokine$^+$ $CD4^+T_E$ in VSV-infected mice which could have been due to a reduced overall pro-inflammatory response observed in the VSV model system [170].

4.2.4 Constitutive CCL5 expression by virus-specific T_M

Analogous to the experiments performed on $CD8^+T_E$, we next examined the profile of splenic T_M cells in regards to constitutive (*ex vivo*) chemokine expression (**Fig.21A)**. Similar to the T_E chemokine profile, T_M cells expressed large amounts of CCL5 protein *ex vivo* but only neglegible amounts of the other $CD8^+$T cell-produced chemokines. As constitutive expression of CCL5 is a rather unique feature, we further characterized CCL5 expression of NP_{396}-specific T_M cells in lymphatic and non-lymphatic tissues (**Fig.21A/B)**. With the notable exception of a heterogeneous T_M population in the mesenteric lymphnodes (MLN) T_M containing $CCL5^+$ ($\sim 60\%$) as well as $CCL5^-$ ($\sim 40\%$) subsets, all other T_M populations examined expressed CCL5 constitutively at high levels ($> 95\%$).

Since the lymph nodes are enriched for $CD62L^+$/$CCR7^+$ central memory T cells (T_{CM}), we evaluated the possibility that T_{CM} express lower levels of CCL5 than effector memory T cells (T_{EM}). While this was indeed the case (**Fig.21A, bottom row)**, the differences were small and, importantly, the progressive conversion of T_{EM} to T_{CM} T cells [168] was associated with only a slight reduction of the overall T_M CCL5 content and not with a significant decline of the dominant $CCL5^+$ $CD8^+T_M$ subset in the spleen (**Fig.21C)**.

Interestingly, the constitutively high CCL5 expression was in stark contrast to the decaying protein levels of the cytolytic effector molecules GzmA and GzmB in the progression to longterm memory of NP_{396}-specific $CD8^+$T cells (**Fig.21C)** previously reported for LCMV-, LM- and to some extend for VSV, specific T_M populations [83, 175–177] recovered from lymphatic tissues.

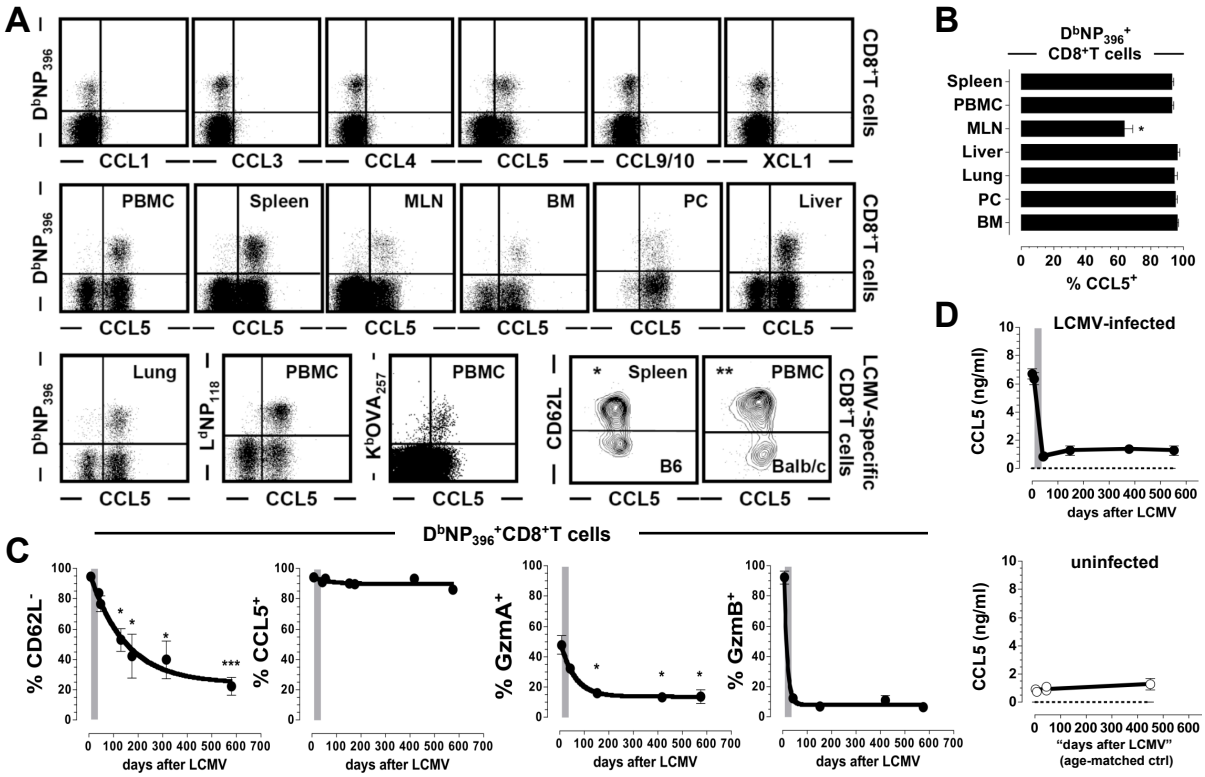

Figure 21: ***Constitutive chemokine expression by virus-specific T_M.*** *(**A**) Constitutive chemokine expression by LCMV-specific CD8^+T_M cells was analyzed in different tissues at d175 (top row, spleen) or d55 (middle and bottom rows) after acute LCMV infection. For analyses of T_M cells in non-lymphatic tissues, mice were treated with whole-body PBS perfusion prior to organ harvesting and tissue processing. Two additional contour plots gated on epitope-specific CD8^+T_M populations recovered from LCMV-immune B6 (d175, spleen) or Balb/c (d174, PBMC) mice demonstrate a slight but significant reduction of constitutive CCL5 expression levels by CD62L^{hi} vs. CD62L^{lo} subsets. (**B**) Summary of constitutive CCL5 expression by LCMV-specific CD8^+T_M recovered from lymphatic and non-lymphatic organs (SEM, 3 mice/group). (**C**) Kinetics of CD62L^{lo} to CD62L^{hi} conversion, stability of CCL5$^+$phenotype and loss of constitutive GzmA and GzmB expression among NP$_{396}$-specific CD8$^+$T cells (spleen) as a function of time after LCMV challenge. The gray-shaded area identifies the transitional period from effector (d8) to early memory (d42) stage and asterisks identify significant differences comparing young (∼d42) vs. older CD8^+T_M (SEM, 3-4 mice analyzed per time point). (**D**) Serum CCL5 levels were determined by ELISA as a function of time after LCMV infection of B6 mice (left panel). Age-matched uninfected B6 mice were analyzed in parallel (right panel). The broken line indicates the detection threshold as determined in LCMV-immune B6.CCL5$^{-/-}$ mice.*

Our finding that constitutive GzmA expression was only detectable in half of the LCMV-specific CD8$^+$T$_E$ (8 d.p.i) and subject to delayed down-modulation as compared to GzmB (**Fig.21B/C**) provides further evidence for the differential regulation of cytolytic effector mechanisms [178], but

also emphasizes the fact that the molecular components of this pathway are subject to progressive "silencing". Thus, the robust CCL5 expression by virus-specific $CD8^+T_M$ in the absence of inflammatory stimuli constitutes a unique functional "signature" that *suggest a particular importance for T cell-expressed CCL5 in secondary T cell immunity*. These findings are in apparent contrast to the reported presence of *Ccl5* mRNA but absence of protein in murine MPCD8$^+$T cells [63, 64]. To reconcile these discrepancies, we evaluated constitutive CCL5 expression in cell subsets isolated from lymphatic and non-lymphatic organs of naive mice (**Fig.22**).

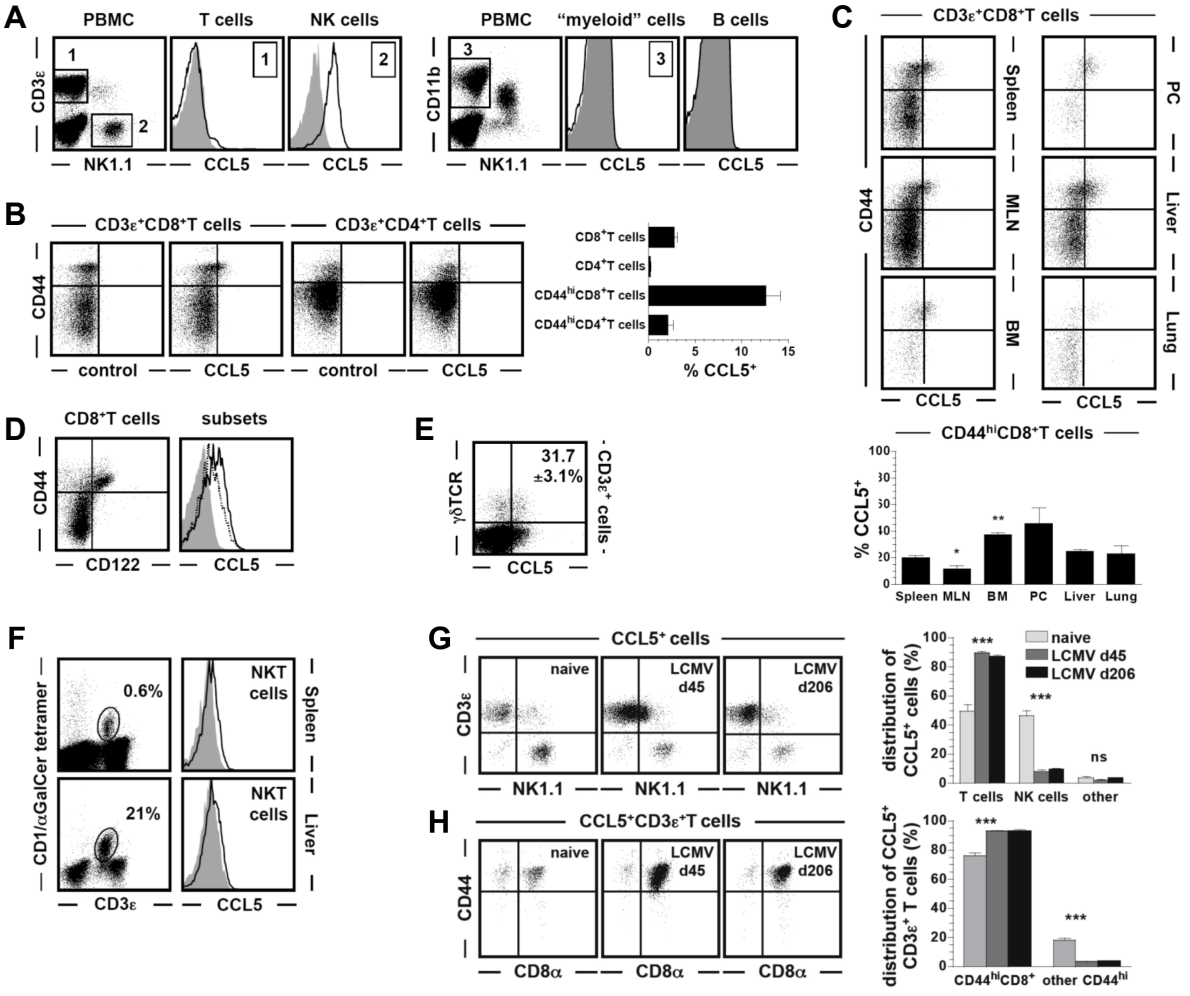

Figure 22: Hematopoetic sources of constitutively expressed CCL5. *Unless noted otherwise, all data were generated with cells obtained from naive B6 mice and analyzed directly ex vivo for expression of various surface markers and intracellular chemokines.* ***(A)*** *Dot plots demonstrate gating strategies to identify blood-borne T cells, NK cells and CD11b-expressing myeloid cells; numbers in plots refer to gates employed in adjacent histograms (black tracing: CCL5 stains, gray-shaded histograms: control stains). The CD11b-expressing cells, excluding mature CD11b$^+$NK cells, comprise monocytes, macrophages, neutrophils and DC subsets. Lack of CCL5 expression*

by B cells is demonstrated after gating on CD19$^+$ cells. ***(B)*** *Dot plots are gated on the indicated blood-borne T cell subsets. The adjacent bar diagram displays the frequencies of CCL5$^+$T cells among the indicated T cell subsets.* ***(C)*** *Naive B6 mice were perfused with PBS and spleen, MLN, BM, PEC, lung and liver were processed according to Experimental Procedures to yield single cell suspension. Dot plots demonstrate constitutive CCL5 expression in the CD44^{hi}CD8$^+$T cell compartment of cells recovered from all organs; the corresponding bar diagram summarizes these data, statistical differences were calculated in comparison to spleen.* ***(D)*** *Plot gated on splenic CD8$^+$T cells; histograms show CCL5 expression of CD8$^+$T cell subsets: CD44^{lo} (gray shaded), CD44^{hi}CD122^{lo} (broken tracing) and CD44^{hi}CD122^{hi} (black tracing). The difference between the CCL5 GMFI of CD44^{hi}CD122^{lo} vs. CD44^{hi}CD122^{hi} cells is small but significant (*p=0.0132, paired t-test).* ***(E)*** *Gated on splenic CD3ϵ^+cells, the dot plot identifies CCL5$^+$ γ:δTCR$^+$T cells; value indicates the frequencies of γ:δT cells expressing ex vivo detectable CCL5 (SEM).* ***(F)*** *Spleen and liver from PBS-perfused B6 mice were processed and NKT cells identified by combined CD3 and CD1/αGalCer tetramer stains. Histograms are gated on CD3ϵ^+ and CD1/αGalCer tetramer$^+$ NKT cells (black tracing: CCL5 stains, gray-shaded histograms: control stains).* ***(G)*** *PBMCs obtained from naive as well as young and aged LCMV-immune B6 mice were analyzed for their relative contribution to the CCL5$^+$ compartment. Note that a sizable fraction of CCL5$^+$T cells in the LCMV d45 group expresses low levels of NK1.1. Therefore, no clear distinction between conventional T cells expressing NK1.1 and NKT cells can be made in the LCMV d45 group, and the corresponding bar diagram distinguishes T cells (CD3ϵ^+), NK cells (NK1.1$^+$/CD3ϵ^-) and other cells (NK1.1$^-$/CD3ϵ^-); p values pertain to differences among indicated populations in naive vs. LCMV d45 or d206 groups (p0.001; ns: not significant; no significant differences between LCMV d45 and d206 groups). Note that a history of LCMV infection permanently alters the distribution of CCL5$^+$ cells by making T cells its primary source.* ***(H)*** *Exemplary data and summary of CCL5 distribution among T cell subsets; CCL5$^+$ CD44^{hi}T cells not expressing CD8α belong mostly to the CD4 compartment (not shown and panel B); p values pertain to differences among indicated populations in naive vs. LCMV d45 or d206 groups (p<0.001; no significant differences between LCMV d45 and d206 groups).*

As detailed in the first part of this thesis, NK cells are the predominant producers of *ex vivo*-detectable (homeostatic) CCL5 of the hematopoetic compartment of antigen-inexperienced mice. The only other hematopoietic source of *ex vivo* CCL5 was restricted to a small fraction of CD3ϵ^+T cells. Our data indicated a weak CCL5 expression in MP CD8$^+$T cells which was slightly more pronounced in the CD122$^+$(IL-2Rb$^+$) subset (**Fig.18A-D**). Additional minor CCL5$^+$ T cell subsets included γ:δ TCR$^+$T cells as well as MP CD4$^+$T and NKT cells that harbor constitutive CCL5 at marginal levels (**Fig.18B/E/F**)). The low-level CCL5 content of MPCD8$^+$T cells in naive mice

provides an explanation for the seeming absence of CCL5 in these cells [63, 64] and is in stark contrast to the robust CCL5 expression patterns of MPCD8$^+$T cells in age-matched, LCMV-immune mice (**Fig.21D**). In fact, a viral infection can leave a permanent trace of prior infection by shifting the relative distribution of constitutive CCL5 expressors from both NK cells and MPCD8$^+$T cells (each contributing 45-50% to the CCL5$^+$ population in naive mice) to MPCD8$^+$T cells as the predominant constituent of CCL5$^+$ cells (>90%) (**Fig.22G/H**). However, CCL5 serum levels after cessation of an acute LCMV infection did not differ from that found in LCMV-inexperienced mice indicating that neither T_M nor MPCD8$^+$T cells contribute significantly to the homeostatic CCL5 serum levels. The relatively high serum levels (1ng/ml (**Fig.21E**)), as compared to other chemokines, are most likely maintained by other cell lineages (**Fig.21E**) which is in agreement with the requirement of TCR stimulation to induce CCL5 secretion [63, 64].

4.2.5 Induced chemokine profiles of virus-specific T_M

Although the transition from T_E to T_M stage is associated with profound molecular and phenotypic changes [163, 164], the functional profiles of pathogen-specific T_E are often maintained or only modestly altered in the T_M population. Two notable changes pertaining to the elicitation of "immediate" effector activities distinguish CD8$^+$$T_M$ from CD8$^+$$T_E$ the progressively increasing ability to produce IL-2 and the loss of constitutive GzmB expression [83] that correlates with a decline of *ex vivo* detectable CTL activity [179]. Thus, as expected, the induced chemokine profiles of LCMV-specific T_M determined were very similar to T_E (**Fig.23A/B**): chemokine expression was limited to the same six chemokines found in T_E (no induction of CCL6, CCL17, CCL27 or CXCL10) and the quantitative differences between specific CD8$^+$and CD4$^+$T cells were largely preserved in the memory stage. A more detailed analysis performed at various timepoints ranging from effector stage to long-term T cell memory, however, revealed a certain extent of functional plasticity (**Fig.23C**). Production of CCL3/4/5 by practically all LCMV-specific CD8$^+$$T_E$ and CD8$^+$$T_M$ as well as CCL1 expression in a subset of these cells (25-30%) is readily demonstrated beyond 1.5 years after infection. In contrast, inducible CCL9/10 production increases during the transition from effector to early memory stage ($\sim$6 weeks) but subsequently declines progressively.

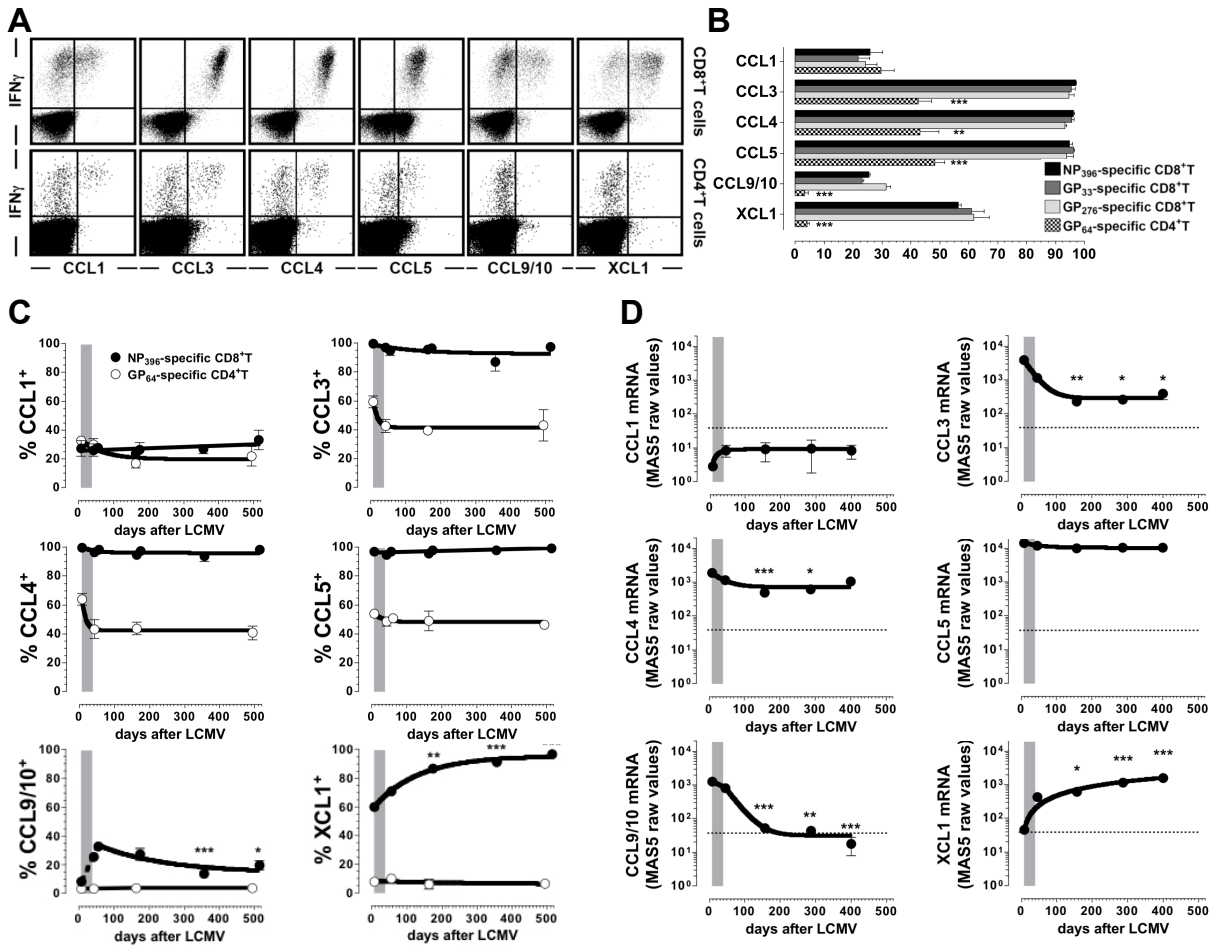

Figure 23: ***Induced chemokine expression by splenic LCMV-specific T_M.*** ***(A&B)*** *Induced chemokine expression by splenic GP_{33}-specific $CD8^+$(top row) and GP_{64}-specific $CD4^+$T cells (bottom row) evaluated 42 days after acute LCMV challenge of B6 mice.* ***(B)*** *Summary in the corresponding bar diagram (SEM, 3 mice/group); asterisks indicate significant differences between specific $CD4^+$ and $CD8^+$T cells.* ***(C)*** *Induced chemokine production by NP_{396}- specific $CD8^+$ and GP_{64}-specific $CD4^+$T cells (spleen) as a function of time after challenge; details for data display and statistics as in legend to Fig.21C on page 103 (SEM of 3-6 mice analyzed per time point; asterisks indicate statistical differences of chemokine expressing $CD8^+$T cell subsets comparing young [d56] and older [>d150] $CD8^+T_M$).* ***(D)*** *Longterm changes in chemokine mRNA expression detected directly ex vivo in purified p14 cells ranging from effector (d8) to aged memory (d400) stage as determined by microarray analyses detailed in Materials & Methods. Dotted lines mark the detection threshold; gray shaded areas identify the transitional period from effector (d8) to early memory (d42) stage. Asterisks indicate significantly different expression levels of the same chemokine mRNA in young (d46) vs. aging (≥5 months) p14 T_M cells.*

While the mechanistic foundation for this unusual expression pattern and the contribution of T cell-produced CCL9/10 to antiviral immunity remain obscure, we note that the decrease of induced CCL9/10 protein production during the memory phase correlated with a similar decline of *Ccl9/10*

mRNA (**Fig.23D**). Perhaps more importantly, $CD8^+T_M$ exhibited improved XCL1 production over time, a pattern that again correlated with a significant rise of *Xcl1* mRNA in aging T_M (**Fig.23C/D**). Despite the fact that our current knowledge about the biological relevance of T cell-produced XCL1 is rather limited [70], it should be emphasized that the gradual increase of $XCL1^+CD8^+T_M$ subsets shown here constitutes, together with the increasing ability to express IL-2, the only known functional gain bestowed on established $CD8^+T_M$. In contrast, no functional gain was observed for $CD4^+T_M$ and apart from a small drop of CCL3/4$^+$ subsets during the transition from $CD4^+T_E$ to $CD4^+T_M$ stage, the fraction of chemokine producing $CD4^+$T cell subsets remained relatively stable (**Fig.23C**).

4.2.6 Induced CCL1 expression as a determinant for "polyfunctional" T_M subsets

The measurement of six T cell-produced chemokines as detailed above provides a significant addition to the repertoire of pathogen-specific T cell activities measurable in short-term *ex vivo* assays. Inducible IFNγ, TNFα and IL-2 production are the most frequently analyzed T cell functions and can be complemented by an evaluation of GM-CSF production and CD40L upregulation [80, 180]. Virus-specific T cells producing other cytokines such as IL-4, IL-5, IL-10 and IL-13 are rare, if present at all under conditions of natural or experimental viral infections but may be found in vaccinated individuals [181]. The extent to which individual effector molecules contribute to primary T cell-mediated pathogen control has been delineated in multiple experimental systems, yet comparatively little information is available about their precise role in immune protection afforded by secondary T cell responses. Rather, the emerging concept of T cell "polyfunctionality" argues that the presence of T_M with a diversified and robust functional repertoire correlates with better pathogen control irrespective of the mechanisms by which the analyzed T cell functions may in fact contribute to this task [180, 182]. Some of the most compelling data in support of this hypothesis has come from R. Seders group who identified a simple metric (composed of the number of IFNγ^+/TNFα $^+$/IL-2$^+$-specific $CD4^+T_M$ ("triple producers") as well as the amount of cytokines produced by these cells (measured by the MFI of the cytokine stains) that can predict the extent of immune protection in a model for *L. major* infection [183]. Although similar correlations remain to be established for specific $CD8^+T_M$ and other model systems, it would appear that T cell "poly-

functionality" constitutes the first conclusive "correlate for immune protection" at the T cell level. Furthermore, the predictive value of such a metric may be improved by inclusion of chemokine production profiles (readily achieved by polychromatic flow cytometry), yet it would also be desirable to identify a single T_M function that by itself delineates "polyfunctional" T cell subsets.

Here, we demonstrate that induced CCL1-expression by virus-specific $CD8^+T_M$ and $CD4^+T_M$ identified a subset characterized by highly diversified effector functions and increased production of multiple effector molecules (**Fig.24A-D**). In addition to IFNγ, LCMV-specific $CD8^+T_M$ subsets rapidly synthesized TNFα, IL-2, GM-CSF and CD40L but not IL-4 or IL-10 [80]. Interestingly, the level of IFNγ expression in TNFα $^+$, IL-2^+, GM-CSF^+ and $CD40L^+$ subsets (double producers) was consistently and significantly higher than in corresponding T_M subpopulations producing IFNγ only ($p<0.05$, analysis of $NP_{396}{}^-$, $GP_{33}{}^-$ and GP_{276}-specific $CD8^+T_M$). Combined analysis of these functions by polychromatic flow cytometry demonstrated that IL-2^+ and $CD40L^+$, but not GM-CSF^+CD8^+T cell populations, belong to T cell subsets that also produced IFNγ and TNFα at higher levels. However, among the IL-2 and CD40L producers, only $\sim$25% exhibit co-expression while another $\sim$25% were IL-2^+/$CD40L^-$ and $\sim$50% expressed CD40L in the absence of IL-2 (**Fig.24A**). The "diagonal" distribution of events observed for IFNγ/CCL3 and IFNγ/CCL4 stains of stimulated T_E and T_M indicated that high levels of IFNγ production were associated with increased CCL3 or CCL4 expression which implies a direct correlation of CCL3/4 expression levels (**Fig.18C/E/F)** & (**Fig.23A**). Indeed, a particularly "tight" association of CCL3 and CCL4 expression (**Fig.24B)** was observed that might in part be due to the formation of intracellular CCL3/4 heterodimers as detailed in (**Fig.26)** and as reported for human CCL3 and CCL4 [184]. Comparing the extent of induced CCL3 production in subsets expressing additional chemokines with those that do not, CCL3 was significantly increased in $CCL1^+$ and $XCL1^+$ and to a lesser extent also CCL9/10^+ populations (**Fig.24B, upper panels**). In fact, the $CCL1^+$population was identified as a subset of $XCL1^+$ cells that produced significantly more CCL3 and IFNγ compared to the $XCL1^+$/$CCL1^-$ cells which in turn exhibited higher CCL3/IFNγ levels than the $XCL1^-$/$CCL1^-$ population.

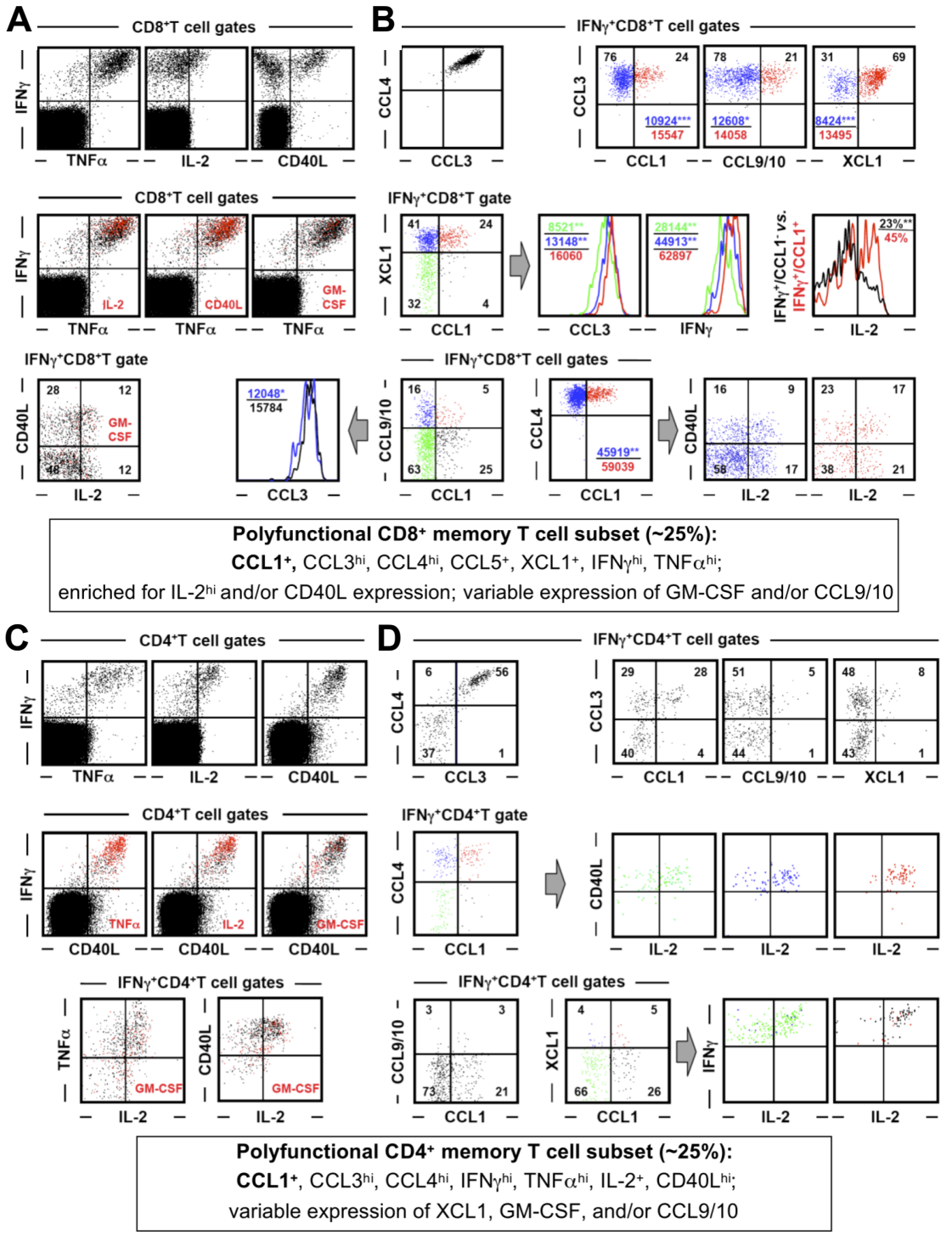

Figure 24: Polyfunctional subset analysis. *Experiments displayed in panels (**A-D**) were performed by stimulation of spleen cells from LCMV-immune mice (d67) with GP_{33} or GP_{64} peptides and determination of T_M-induced cytokine, CD40L and chemokine expression in complementary samples using polychromatic flow cytometry. All values listed in panels **D-G** are the average of 3 mice analyzed. (**A**) Patterns of induced cytokine and CD40L expression by GP_{33}-specific $CD8^+T_M$. Middle and bottom rows: red dots designate specific $CD8^+$T cells producing a third cytokine (identified*

*in red font) in addition to IFNγ/TNFα (or CD40L/IL-2) expression displayed in conventional dot plots. (**B**) Top row: specific CD8$^+$T$_M$ subsets producing CCL1, CCL9/10 or XCL1 also express higher levels of CCL3 (the color-coded CCL3 GMFI values refer to cells identified with the same color; statistical significance is indicted by asterisks). Middle row: induced CCL1/XCL1 expression and corresponding CCL3 and IFNγ expression levels in subpopulations identified by color-coded histograms and corresponding GMFI values. In addition, IL-2 production by CCL1$^-$ (black tracing) vs. CCL1$^+$ (red tracing) subsets is shown. Bottom row, left: 80% of CCL1$^+$ cells fail to induce CCL9/10 expression suggesting that XCL1 and CCL9/10 are expressed in a reciprocal fashion in CCL1$^+$ subsets (compare to above CCL1/XCL1 plot). Lack of CCL9/10 production is associated with higher CCL3 (as well as IFNγ and IL-2) expression. Bottom row, right: CCL4 GMFI values and IL-2/CD40L expression patterns by CCL1$^-$ (blue) vs. CCL1$^+$ (red) subsets. (**C**) Patterns of induced cytokine and CD40L expression by specific GP$_{64}$specific CD4$^+$T$_M$. Middle and bottom rows: red dots designate specific CD4$^+$T cells producing a third cytokine (identified in red font) in addition to effector functions displayed on the axes of the dot plots. Note that IL-2$^+$ cells are CD40L$^+$ and TNFα^{hi}. (**D**) Top row: co-production of CCL3/4 by a major CD4$^+$T$_M$ subset and enrichment of CCL1, CCL9/10 and XCL1 expression in the CCL3/4$^+$ subpopulation. Middle row: progressive enrichment of CD40L$^+$ IL-2 producers in CCL1$^-$/CCL4$^-$ > CCL1$^-$/CCL4$^+$ > CCL1$^+$/CCL4$^+$ subsets (color-coded gating strategy). Bottom row: no clear association of induced CCL9/10 and XCL1 production with CCL1 expression. However, CCL1$^+$ CD4$^+$T$_M$ not only contain more IL-2 producers, the latter cells are also enriched for a pronounced IFNγ^{hi} phenotype. The text boxes below the figures summarize the functional characteristics of LCMV-specific CD8$^+$T$_M$ and CD4$^+$T$_M$ subsets identified by induced CCL1 expression.*

Furthermore, while IL-2 producers were found in both CCL1$^-$ and CCL1$^+$ populations, the latter subset was significantly enriched for IL-2$^+$ cells ($\sim$45% vs. 23%) that also produced IL-2 at higher levels (p=0.0206) (**Fig.24B, middle panels**). CCL1$^-$ and CCL1$^+$ populations were further stratified according IL-2 and CD40L expression: the CCL1$^+$ subset is clearly enriched not only for IL-2$^+$ cells but also for IL-2$^+$CD40L$^+$ and IL-2$^+$CD40L$^+$ subsets (**Fig.24B, lower panels**). Finally, the majority ($\sim$3/4) of CCL9/10 expressors were found among CCL1$^-$ cells and, as expected, expressed significantly lower amounts of CCL3 (**Fig.24B, lower panels**). Therefore, the induced production of CCL1 defines a highly polyfunctional virus-specific CD8$^+$T$_M$ subset comprising $\sim$25% of epitope-specific cells that is defined by a CCL3^{hi}/CCL4^{hi}/CCL5$^+$/XCL1$^+$/IFNγ^{hi}/TNFα^{hi} phenotype, enriched for IL-2^{hi} and/or CD40L$^+$ cells and exhibits variable GM-CSF and/or CCL9/10 expression (CCL5 analyses not shown in (**Fig.24A/B**) as all specific CD8$^+$T$_M$ were capable of induced CCL5 production as shown in (**Fig.23A-C**).

Similar analyses were also performed for LCMV-specific CD4$^+$T$_M$ taking into account that IL-2$^+$ and CD40L$^+$ subsets are significantly larger in this population as compared to CD8$^+$ T$_M$ [80] (**Fig.24C/D**). Details of these analyses are found in the legend to **24 C/D** and demonstrate that induced CCL1 production is also useful to delineate a polyfunctional CD4$^+$T$_M$ subset ($\sim$25%). This population is characterized by a CCL3^{hi}/CCL4^{hi}/IFNγ^{hi}/TNFα^{hi}/IL-2$^+$/CD40L^{hi} expression pattern, but displays variable induction of XCL1, GM-CSF, and/or CCL9/10.

4.2.7 T$_M$-produced chemokines in context

The full spectrum of "immediate" effector functions elaborated by pathogen-specific T$_M$ remains at present unknown. While the induction of IFNγ, TNFα, IL-2, GM-CSF, CD40L and degranulation are routinely observed in short-term restimulation cultures [80, 180], virus-specific T$_M$ producing IL-4, IL-5, IL-10 and IL-13 are rare, if present at all under conditions of natural or experimental viral infections but may be found in vaccinated individuals [181]. To estimate the extent of induced T$_M$ activities at large, we evaluated the constitutive and induced expression of $\sim$150 p14 T$_M$ genes comprising the known perforin/granzymes, interferons, interleukins and related cytokines as well as TNFSF, TGFβSF and PDGF members, and $\sim$90% of all mRNA transcripts demonstrating a significant TCR-induced upregulation were further analyzed for corresponding protein expression by FC (not shown). Remarkably, these analyses suggest that chemokine synthesis may account for up to 40% of all rapidly inducible T cell effector functions and thus emphasize the potential importance of T$_M$-produced chemokines in the context of secondary responses.

4.2.8 Chemokine profiles of secondary T$_E$ and T$_M$

Several recent publications have reported that secondary T$_E$ and T$_M$ exhibit a number of properties pertaining to phenotype, function and traffic patterns that are distinct from primary T$_E$ and T$_M$. Of particular note is the reduced IL-2 production as well as increased GzmB expression by secondary CD8$^+$T$_M$ [175, 176]. To assess potential quantitative changes in chemokine expression by secondary CD8$^+$T$_E$ in relation to other T cell functions, we used an adoptive transfer system that permits the concurrent analysis of primary and secondary T cells in the same host (**Fig.25**).

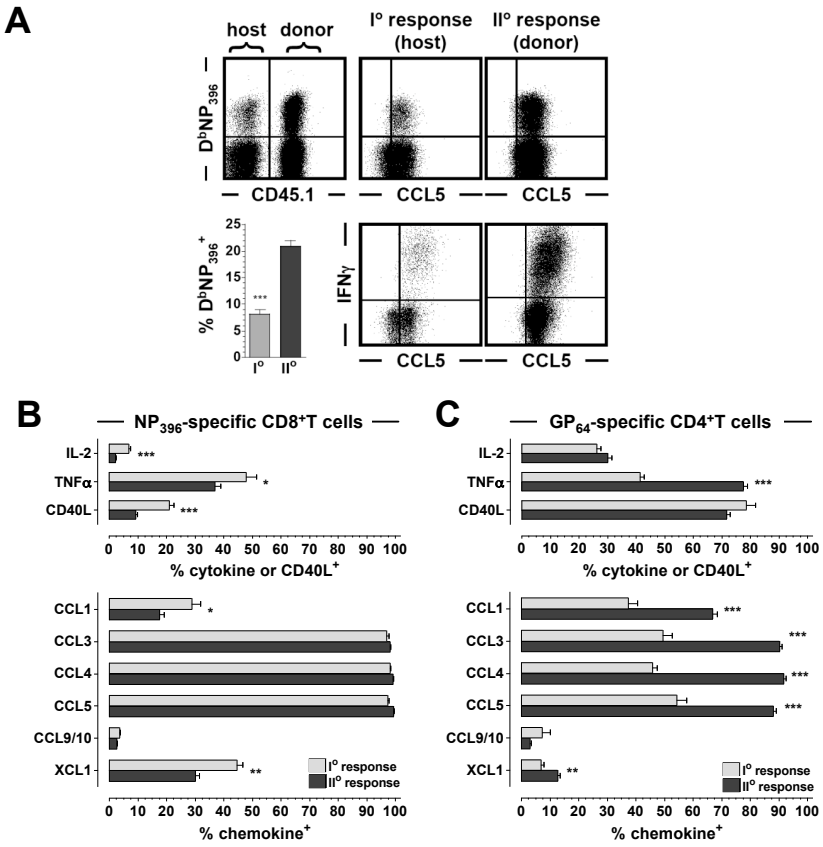

Figure 25: ***Chemokine profiles of secondary CD8$^+$T$_E$.*** *Spleen cells from LCMV-immune B6.CD45.1 donors (∼d200) were transferred into B6 recipients (5x10^6 cells i.v. per mouse) that were challenged 24h later with 2x10^6 pfu clone13 i.v. Six days later, concurrent primary and secondary responses were analyzed ex vivo in blood and after NP$_{396}$- or GP$_{64}$-peptide stimulation of spleen cells.* ***(A)*** *Upper right plot and bar diagram: presence of primary (CD45.1$^-$) and secondary (CD45.1$^+$) LCMV-specific CD8$^+$T$_E$ in the same host (plot gated on CD8$^+$T cells); the bar diagram shows frequencies of NP$_{396}$-specific CD8$^+$T$_E$ among primary vs. secondary CD8$^+$effectors (SEM, n=4 mice). Middle and right plots display constitutive (top) and induced (bottom) CCL5 expression by NP$_{396}$-specific CD8$^+$T$_E$ (plots gated on primary or secondary CD8$^+$T$_E$).* ***(B&C)*** *Frequencies of primary (gray) and secondary (black) NP$_{396}$-specific CD8$^+$T$_E$ or GP$_{64}$-specific CD4$^+$T$_E$ capable of induced cytokine, CD40L and/or chemokine production (SEM, n=4 mice). Note in particular the functional gain of secondary CD4$^+$T effectors at the level of CCL1/3/4/5 and XCL1 production; the chemokine response of concurrently generated primary CD4$^+$T effectors, however, is not significantly different from a genuine primary CD4 response to an LCMV Armstrong (**Fig.18D**) or clone13 (not shown) challenge.*

Confirming an earlier report about reduced IL-2 expression by specific CD8$^+$T cells in the LM system [175], we found that secondary LCMV-specific CD8$^+$T$_E$ expressed less IL-2 than primary T$_E$ and, in addition, also less TNFα and CD40L. Thus, our analyses demonstrated an overall trend

towards reduced functional diversity in secondary T_E , a pattern that is mostly preserved in secondary $CD8^+T_M$ (not shown). A similar loss of functional diversity extends to inducible CCL1 and XCL1 production by secondary $CD8^+T_E$ but interestingly, induced CCL3/4/5 and CCL9/10 synthesis as well as constitutive CCL5 expression is identical in primary and secondary $CD8^+T_E$ (**Fig.25A/B**). Furthermore, there was no evidence for a functional gain at the chemokine level (no induced CCL17, CCL25, CCL27, CXCL2 or CXCL10 production) and profiles of the 6 expressed chemokines were largely maintained in secondary $CD8^+T_M$ (not shown). Less information is available about functional alterations in secondary $CD4^+T_E$ and $CD4^+T_M$. We found that induced IL-2, TNFα and CD40L expression, in contrast to $CD8^+$T cells, was comparable in primary and secondary $CD4^+T_E$, but remarkably, chemokine production was significantly increased in the secondary effectors (**Fig.25C**). The enhanced functional diversity pertained to all but one chemokine (CCL9/10) and secondary $CD4^+T_E$, based on their profoundly increased CCL3/4/5 expression, in fact resemble primary $CD8^+T_E$ (**Fig.25C**) and preserve this improved chemokine profile in the secondary memory phase (not shown).

4.2.9 Subcellular localization and co-expression of constitutive and induced T cell chemokines

The precise subcellular localization of CCL5 is a matter of controversy as a reported preferential association with cytolytic granules [66, 67] contrasts with the identification of a separate subcelluar CCL5 compartment [65]. The frequent use of T cell clones or blasts and the seeming absence of constitutive CCL5 expression by murine MP$CD8^+$T cells further complicates resolution of this issue [63, 64]. Our discovery of constitutive CCL5 expression by specific T_E and T_M now offers an opportunity to determine the subcellular localization and expression patterns in primary murine virus-specific T cells. Flow cytometric analyses of LCMV-specific $CD8^+T_E$ performed directly *ex vivo* demonstrate a clear association of CCL5 and GzmB expression levels (**Fig.26A**). Further analysis of these cells by confocal microscopy reveals the existence of multiple discrete vesicles that contain both CCL5 and GzmB. Nevertheless, granules containing only CCL5 or GzmB are also readily discernible (**Fig.26A**), an overall heterogenous expression pattern that is reminiscent of the subcellular distribution of CCL5 in relation to perforin and granulysin reported for primary human

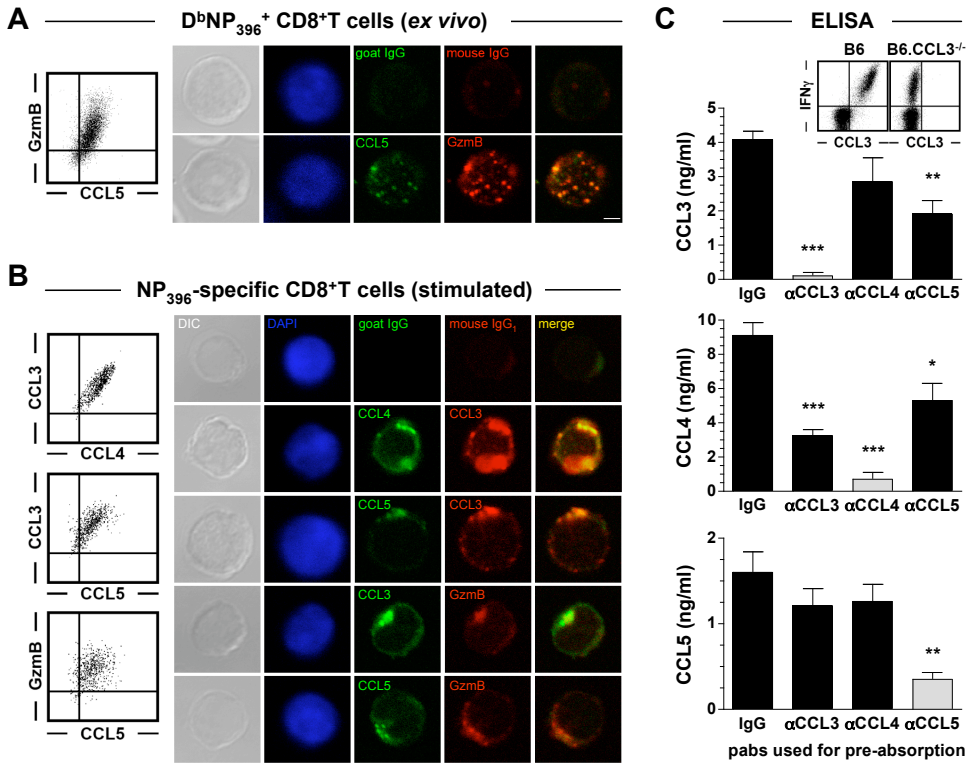

Figure 26: Subcellular localization and co-secretion of T cell-produced chemokines. *(**A**) NP_{396}-specific $CD8^+T_E$ (d8) were stained ex vivo and analyzed by flow cytometry or purified, further stained and evaluated by confocal microscopy (scale bar: 2μm). (**B**) B6 effector spleen cells were restimulated for 5h with NP_{396} peptide in the presence of BFA and analyzed for induced CCL3/4/5 and GzmB expression by flow cytometry and, after purification, also by confocal microscopy. In some cases (panel B, confocal pictures), stimulation cultures were performed in the absence of BFA to avoid interference with intracellular protein trafficking; both culture conditions gave similar results. (**C**) Equal numbers of B6 effector spleen cells (d8) were restimulated for 5h with NP_{396} peptide and supernatants were pre-absorbed with indicated polyclonal antibodies prior to quantitation of CCL3/4/5 by ELISA (gray bars indicate absorption/detection with abs of the same specificity, statistic significance was calculated in relation to IgG pre-absorption control. Data are representative for 2 similar experiments with 3-4 mice/group). The insert demonstrates specificity of the polyclonal αCCL3 antibody tested on peptide-stimulated $CD8^+T_E$ from LCMV-infected B6 and B6.Ccl3$^{-/-}$ mice.*

MPCD8$^+$T cells [66]. It is therefore possible that the generation of T cell blasts and clones selectively increases CCL5 storage in a compartment distinct from cytolytic granules by currently unknown mechanisms. Upon stimulation of LCMV-specific CD8$^+$T$_E$ CCL5 and GzmB stores are rapidly but not completely emptied and the synthesis of additional CCL5 as well as CCL3/4 is

initiated (see below). Induced CCL3/4 and interestingly also CCL5 expression evaluated by flow cytometry demonstrates a rather tight association (**26A**, see also **24B/D**); the association of induced CCL5/GzmB proteins, however, is somewhat less defined than in the *ex vivo* evaluated samples (**Fig.23A/B**). When analyzed by confocal microscopy, CCL3/4/5 as well as GzmB and IFNγ tend to cluster in a single defined location close to the plasma membrane and in immediate proximity of the immunological synapse (not shown) (**Fig.26B**). The co-localization and association of intracellular CCL3/4/5 expression in particular might provide a basis for the joint release of these chemokines bound to sulphated proteoglycans as described for an HIV-specific CD8$^+$T cell clone [67]. Moreover, human PBMC stimulated with PMA secrete CCL3/4 as heterodimeric complexes [185] and up to half of the CCL3/4 content in medium conditioned with LN cells from recently immunized mice is in a state of hetero-oligomerization [54]. To determine the extent of heterologous chemokine complex formation in the context of a virus-specific T cell response, splenic CD8$^+$T$_E$ were restimulated for 5h, the supernatants collected and pre-absorbed with αCCL3, αCCL4, αCCL5 or control antibodies prior to quantitation of CCL3/4/5 by ELISA (**Fig.26C**). Although we noted some variability in these cross-absorption experiments (and CCL5 is not reported to form heterodimers with CCL3 or CCL4 [185]), the biologically active form of CD8$^+$T$_E$-secreted CCL3/4/5 consists in part of hetero-oligomeric complexes. Beyond the apparently intimate coordination of CCL3/4/5 activities, this finding also emphasizes important limitations for the interpretation of any experiments that employ antibody-mediated *in vivo* neutralization of these chemokines.

4.2.10 Kinetics of T cell chemokine production and secretion

Having established the qualitative and quantitative aspects of chemokine expression, the next series of experiments addressed temporal dynamics of chemokine production and secretion. As previously discussed, despite high levels of *ex vivo* mRNA expression for CCL3 and CCL4 in T$_E$ and T$_M$ cells, protein production was only observed after restimulation. One advantage of pre-stored chemokine mRNA might be the ability of accelerated chemokine production upon activation as compared to *de novo* synthesis.

To determine the velocity of chemokine production/release by specific CD8$^+$T$_E$ spleen cells ob-

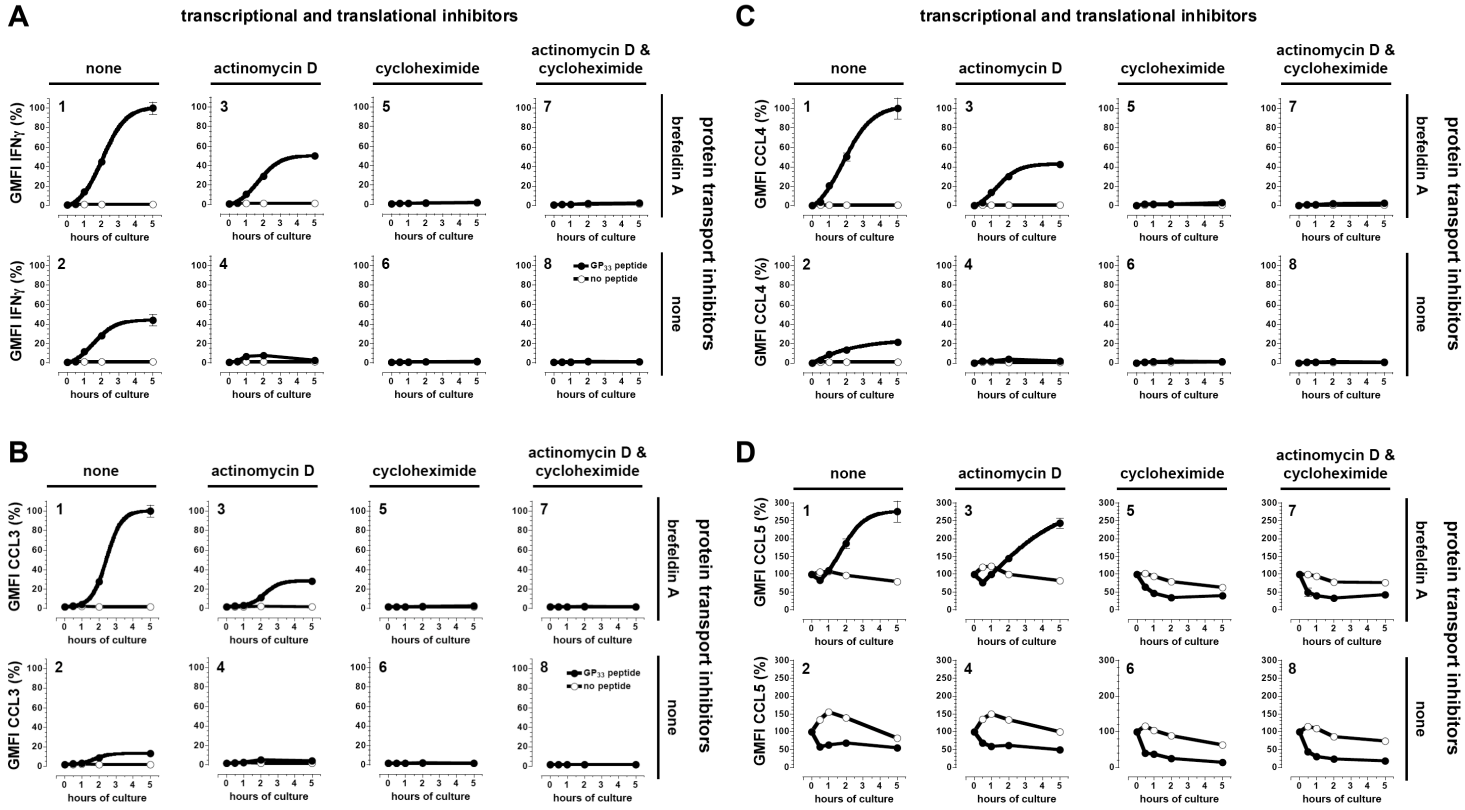

Figure 27: ***Regulation and kinetics of chemokine production by virus-specific CD8$^+$T$_E$.*** *(**A-D**) Spleen cells from LCMV-infected p14 chimeras (d8) were cultured for indicated time periods in the presence (closed symbols, -●-) or absence (open symbols, -○-) of GP$_{33}$ peptide and indicated transcriptional (ActD), translational (CHX) and/or protein transport (BFA) inhibitors. Graphs depict the GMFI of IFNγ, CCL3, CCL4 and CCL5 expression by p14 effectors as a function of culture time and inhibitor presence or absence. To better compare the kinetic regulation of cytokine and chemokine production the respective GMFI values were normalized (IFNγ: the GMFI of rat isotype control stains was subtracted from all corresponding IFNγ GMFI values and the resulting values of BFA/GP$_{33}$ cultures for the t=5.0h time point (panel A.1) were set at 100%. CCL3 and CCL4: similar normalization performed by subtraction GMFI values of goat IgG stains from corresponding CCL3 or CCL4 GMFI values. CCL5: ex vivo goat Ig control stain GMFI was subtracted from all CCL5 GMFI values and resulting normalized ex vivo CCL5 values (panel B.1) were set at 100%. The sigmoidal curve fit is based on optimal fits determined by non-linear regression analyses of samples containing additional time points. Three mice/group, data from 3 similar experiments, 2 of the 3 experiments were performed by Jessica Humann.*

tained from p14 chimeras (d8) were restimulated for 0-5h with GP_{33-41} peptide in the presence or absence of transcriptional (actinomycin D: ActD), translational (cycloheximide: CHX) and/or protein secretion inhibitors (Brefeldin A: BFA) and p14 T_E were analyzed for intracellular chemokine content by flow cytometry. Induced CCL3, CCL4 and IFNγ production became detectable after as little as 30min of stimulation and reached a maximum after 4-5h. The synthesis of these proteins was sufficiently robust to allow detection of intracellular CCL3/4 and IFNγ even in the absence of BFA (**Fig.27A.1/2 - C.1/2**). Given the presence of *ex vivo* detectable mRNA species for CCL3/4 and IFNγ (**Fig.15A and not shown**), protein synthesis, while reduced, was still observed under conditions of translational blockade in the presence but not absence of BFA (**Fig.27 A.3/4 - C.3/4**). The fact that protein synthesis increased over time in a homogenous fashion in all p14 T_E (not shown) suggests that constitutive CCL3/4 and IFNγ message was evenly distributed among individual cells rather than preferentially allocated to a particular p14 subset. As expected, inhibition of transcription or combined translational/transcriptional blockade completely prevented the accumulation of CCL3/4 and IFNγ protein (**Fig.27A.5-8 - C.5-8**). The kinetics of intracellular CCL5 accumulation are predictably more complex as TCR-induced release of prestored CCL5 and initiation of protein neosynthesis occur in parallel. In fact, a modest loss of CCL5 observed 30min after TCR stimulation was quickly compensated for by a pronounced increase of intracellular CCL5 in cultures containing BFA, a pattern that contrasts with rapid, partial and unmitigated CCL5 depletion in the absence of BFA (**Fig.27D.1/2**). It is therefore worth mentioning that induced CCL5 production, in contrast to secretion of prestored CCL5 by human T cell blasts [65], was largely inhibited by BFA. Furthermore, the kinetics of intracellular CCL5 accumulation are comparable in the presence and absence of transcriptional inhibition (**Fig.27D.1-4**) and thus in agreement with our observation that TCR stimulation does not modulate the level of CCL5 mRNA (**Fig.15A**).

The inclusion of CHX in the stimulation cultures permitted a precise determination of the kinetics and quantities of prestored CCL5 released after TCR stimulation. Remarkably, $\sim$2/3 of prestored CCL5 were released within 30-60min after TCR stimulation, to our knowledge the fastest known T cell effector response recorded *in vitro*. Additional depletion of CCL5 stores occured with slower kinetics and was inhibited by BFA (**Fig.28A**).

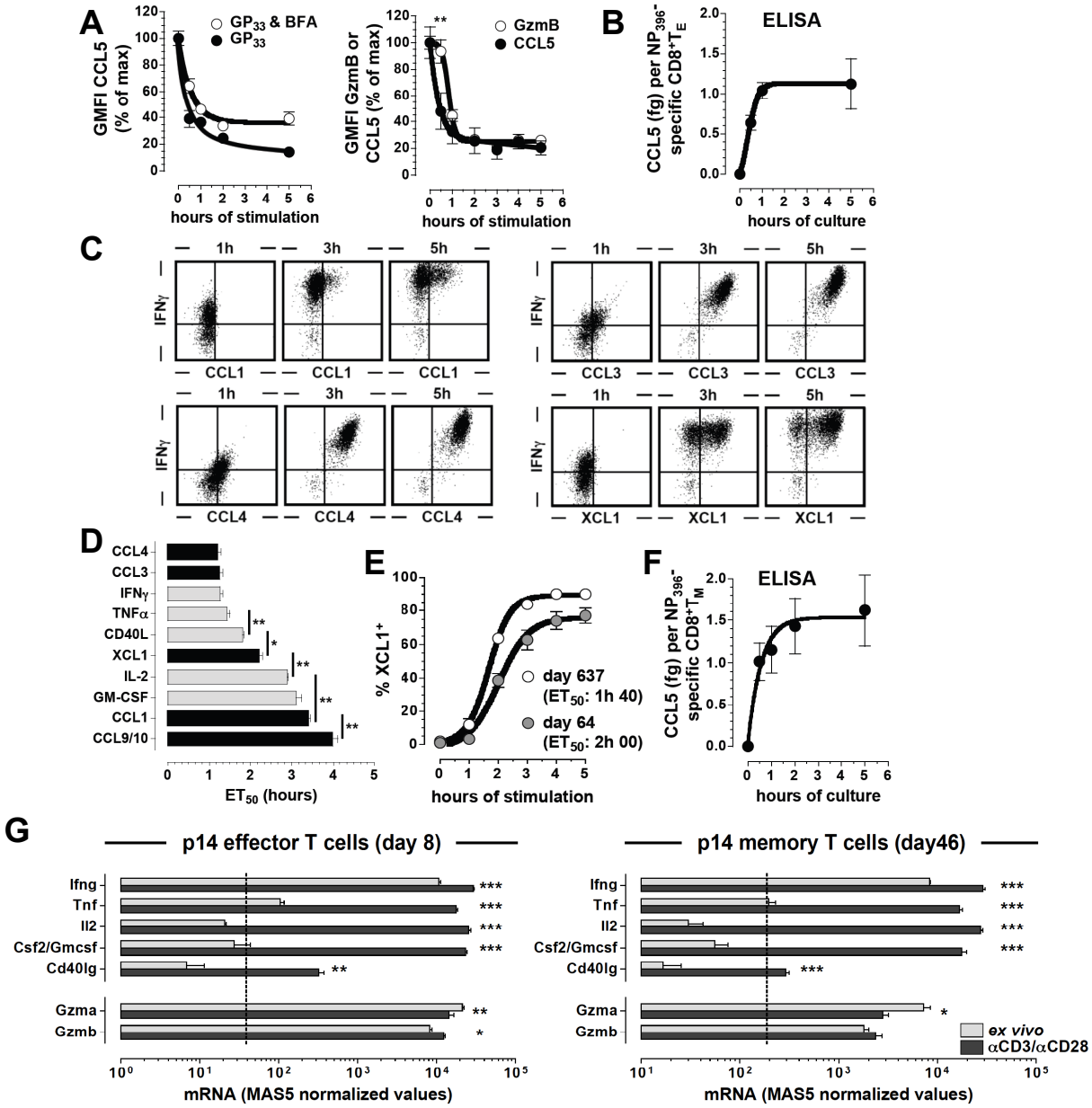

Figure 28: Kinetics and activation thresholds for induced chemokine production/release by virus-specific CD8^+T_E and CD8^+T_M. *(**A**) Spleen cells containing p14 CD8^+T_E (d8) were pre-incubated with CHX prior to initiation of TCR stimulation by addition of GP_{33} peptide and analysis of p14 cell GzmB and CCL5 content 0-5h later. GzmB and CCL5 expression levels (GMFI) were normalized such that t=0h levels correspond to 100% and the GMFI of respective control stains are set at to 0%. Left: kinetics of pre-stored CCL5 release in the presence vs. absence of BFA. Right: "immediate" depletion of CCL5 stores vs. delayed GzmB release. At t=0.5h, ∼2/3 of CCL5 but less than 10% of GzmB stores are emptied (p=0.0035, paired t-test). (**B**) Spleen cells from LCMV-infected B6 mice (d8) were pre-incubated with CHX, stimulated with NP_{396} peptide (no BFA) and CCL5 in the supernatant quantified by ELISA. To calculate the amount of pre-stored CCL5 secreted by individual NP_{396}-specific CD8^+T_E, complementary FACS analyses were performed to determine the absolute numbers of cultured specific CD8^+T_E. Further, the amount of CCL5 secreted in the absence of*

*TCR stimulation was subtracted from stimulated samples at all time points. Note that after 30min, ∼60% of total CCL5 is already secreted, at 1h, ∼90%. (**D/E**) Splenocytes from LCMV-immune p14 chimeras (∼10 wks) were stimulated for 0-5h with GP_{33} peptide and expression of indicated effector molecules was determined as a function of stimulation time. The dot plots (gated on p14 $CD8^+$T cells) show representative data for the temporal regulation of induced CCL1/3/4, XCL1 and IFNγ synthesis. The bar diagram ranks inducible chemokine (black) and other effector molecule (gray) production according to ET_{50} values calculated as detailed in Methods; significant differences are indicated by asterisks. Overall, induced CCL3/4 and IFNγ synthesis proceeds with significantly faster kinetics as compared to other effector functions ($p<0.003$) with the exception of TNFα. (**F**) ET_{50} values for induced XCL1 expression by young (d64) vs. aged (d637) p14 $CD8^+T_M$ were determined as above. (**G**) Microarray analyses: The bar diagrams display the level of T cell-expressed mRNA transcripts corresponding to the effector molecules analyzed above and detected directly ex vivo or after a 3h αCD3/αCD28 stimulation in purified p14 T_E (d8) and T_M (d46) as described in Materials & Methods. Statistically significant differences between individual mRNA species analyzed ex vivo and after stimulation are indicated by asterisks.*

The near instantaneous release of CCL5 was also distinct from the mobilization of cytolytic granules: loss of intracellular GzmB only occured after a lag period of ∼30min but then proceeded so rapidly that the extent of CCL5 and GzmB depletion was comparable by 1h after initiation of T cell stimulation (**Fig.28A, right panel**). Overall, these kinetic differences as well as the differential sensitivity of constitutive versus induced CCL5 expression to BFA were in agreement with the heterogenous distribution of CCL5 in different subcellular compartments as shown in Fig.26A. To quantify the amount of prestored CCL5 in endogenously generated LCMV-specific $CD8^+T_E$, we combined FACS analyses (to enumerate epitope-specific $CD8^+$T cells) and ELISA assays performed in the presence of CHX (**Fig.28B**). The rapid increase of CCL5 in the culture supernatant mirrored the loss of intracellular CCL5 in (**Fig.28A**) and demonstrated that an individual T cell can secrete ∼0.5fg of CCL5 within 30min after TCR triggering. Finally, the early increase of intracellular CCL5 in cultures without TCR stimulation and translational blockade emphasizes that maintenance of constitutive CCL5 expression by T cells is an active process. The eventual decline of CCL5 expression at later time points was likely due to degradation since we did not observe CCL5 secretion by unstimulated T cells (**Fig.26A**).

The presence of chemokine transcripts in T_M has been suggested to confer a kinetic advantage that permits more rapid protein synthesis [63, 186], but this hypothesis has not been experimen-

tally tested. Our observed distinct expression patterns of *ex vivo* detectable chemokine mRNA species in LCMV-specific CD8$^+$T$_M$ (absence of *Ccl1* mRNA, stable *Ccl3/4/5* mRNA and progressively increasing *Xcl1* mRNA; Fig.23D would therefore suggest that early synthesis of CCL3/4 is followed by that of XCL1 and finally CCL1 protein. Experiments performed with LCMV-immune p14 chimeras indeed confirmed this prediction: by calculating the time point at which p14 T$_M$ demonstrate detectable chemokine expression in half of the responder population ("effective time 50": ET$_{50}$), we found ET$_{50}$ values of $\sim$1h10min for induced CCL3/4 and IFNγ production while XCL1 synthesis was significantly delayed ($\sim$2.0h, p$<$0.0002) yet faster than the eventual induction of CCL1 ($\sim$3.5h, p$<$0.0001) (**Fig.28C/D)**. In fact, a direct comparison to other effector functions demonstrates that induced chemokine production dominates the earliest (CCL3/4) and later (CCL1, CCL9/10) stages of the CD8$^+$T$_M$ response (**Fig.28D)** and also illustrates that the presence/absence of preexisting mRNA species was not the sole predictor for the temporal regulation of effector functions: although absent at the mRNA level in resting T$_M$, *Il2*, *Csf2/Gmcsf* and *Cd40lg* mRNA species are rapidly transcribed following TCR stimulation (**Fig.28G)**. However, translation to CD40L, IL-2 and GM-CSF proteins occured with significantly different kinetics (**Fig.28D)**. Conversely, despite the presence of *Ccl9* mRNA (**Fig.15A)**, synthesis of the corresponding protein is a relatively late event (**Fig.28D)**. Since the differential stability of mRNA species contributes to the temporal order in which genes encoding inflammatory mediators are expressed [187], it is conceivable that this phenomenon contributes to the observed differences in translation kinetics. Nevertheless, the significant increase of *Xcl1* message in aging p14 T$_M$ (**Fig.23D, pg.107)** allowed for an analysis of the kinetics with which an individual chemokine is synthesized as a function of changing mRNA levels. As shown in (**Fig.28E)**, not only do more aged p14 T$_M$ ($\sim$21 months) produce XCL1 but they do so $\sim$20min faster (p=0.0104) than younger p14 T$_M$ ($\sim$9 weeks). In contrast, the kinetics of CCL1/3/4 and IFNγ production are not significantly different comparing young and aged CD8$^+$T$_M$ (not shown).

Lastly, we determined the secretion kinetics and quantities of CCL5 constitutively expressed by endogenously generated LCMV-specific CD8$^+$T$_M$ (d45) in an ELISA format. Interestingly, both the speed of CCL5 release and per cell amount secreted by CD8$^+$T$_M$ is similar to CD8$^+$T$_E$ (**Fig.28F**). Thus, the T$_M$ chemokine response proceeds through an ordered sequence of overlapping events that

are in part dictated by the extent of preexisting protein and/or mRNA species: CCL5 > CCL3/4 & IFNγ > TNFα > CD40L > XCL1 > IL-2 > GM-CSF > CCL1 > CCL9/10. Given the particularly rapid release of CCL3/4/5, stimulated T_M rather than DCs or other APCs [54] likely constitute the principal source of these chemokines under conditions of secondary immune responses.

4.2.11 Activation thresholds for chemokine production/secretion

In addition to the temporal regulation of the T cell chemokine response, production and secretion of individual chemokines may be controlled by distinct activation thresholds. The "functional avidities" of specific T cells are often determined by measuring the induced IFNγ-synthesis in response to graded concentrations of antigenic peptide [188]. Although the interpretation of such assays provides insights into properties intrinsic to the interaction between TCRs and peptide/MHC complexes it should be noted that the experimental readout is modulated by complex signaling events that precede the induction of a given T cell function. For example, functional avidities for induced IFNγ production were reported to be lower than those required for IL-2 production by the same cells suggesting that limiting antigen concentrations may permit the elaboration of direct T cell effector functions (IFNγ) whereas induction of proliferative T cell responses, mediated by T cell-produced IL-2, occurs only at higher antigen loads [180].

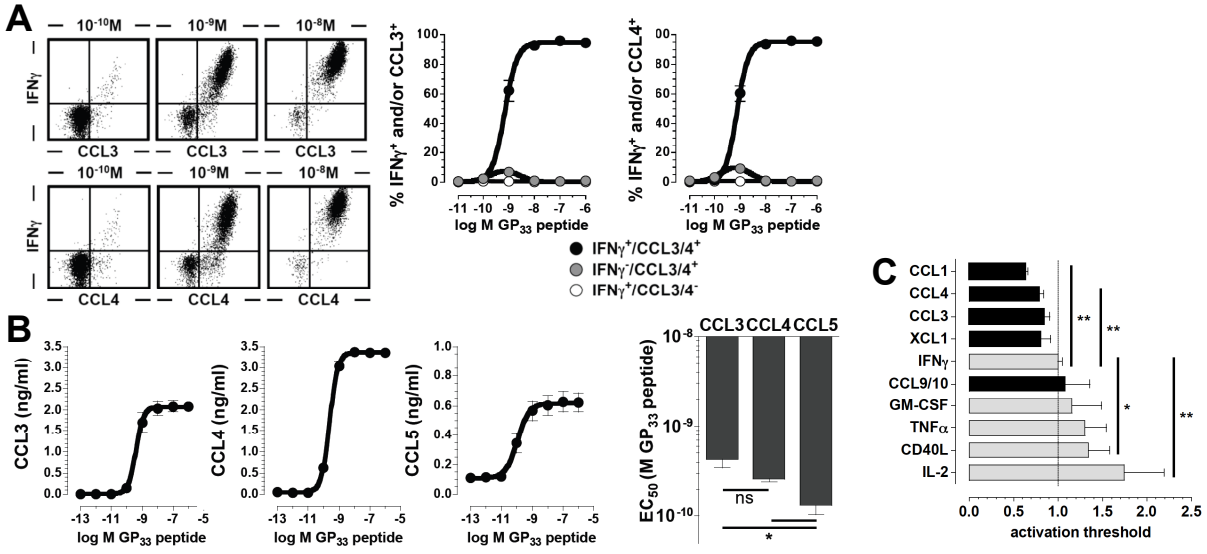

Figure 29: Kinetics and activation thresholds for induced chemokine production and release by virus-specific CD8^+T_E and CD8^+T_M. *(**A**) Intracellular IFNγ and CCL3/4 content of p14 CD8^+T_M ($\sim$9 wks) determined after 5h stimulation with graded doses of GP$_{33}$ peptide (plots gated on p14 T_M). The adjacent diagrams summarize the emergence of p14 CD8^+T_M with defined effector functions (IFNγ^-/CCL3$^+$/CCL4$^+$ vs. IFNγ^+/CCL3$^+$/CCL4$^+$ vs. IFNγ^+/CCL3$^-$/CCL4$^-$) as a function of GP$_{33}$ peptide concentration. (**B**) CCL3/4/5 secreted by p14 CD8^+T_M as a function of GP$_{33}$ peptide concentration was determined by ELISA (5h stimulation). Activation thresholds (EC$_{50}$ values) were calculated by non-linear regression analysis and are summarized in the bar diagram. All data are representative for individual experiments conducted 2-4 times (n=3-4 mice per experiment). (**C**) Activation thresholds for inducible CD8^+T_M effector functions. Spleen cells from LCMV-immune p14 chimeras (9-10 weeks after infection) were stimulated with graded doses of GP33 peptide (10^{-11}-10^{-6}M), the fraction of chemokine$^+$, cytokine$^+$or TNFSF$^+$ p14 T_M was determined 5h later by FC and EC$_{50}$ values for individual effector functions were determined as detailed in Methods. The data displayed are combined from 3 similar experiments evaluating 3 p14 chimeras each. To account for inter-experimental variability, all samples were co-stained for IFNγ, the average IFNγ EC$_{50}$ value was set at 1.0 (dotted line) and the EC$_{50}$ values of other effector functions were calculated accordingly (chemokines: black, cytokines/TNFSFs: gray). Statistically significant differences comparing the IFNγ activation threshold to CCL1, CCL4, CD40L and IL-2 are indicated by asterisks.*

We therefore compared the functional avidities/activation thresholds for induced CCL3/4 and IFNγ synthesis by LCMV-specific CD8$^+$T$_M$ (**Fig.29A**). Though not significantly different, the activation thresholds for CCL3/4 production were slightly ($\sim$1.3-1.8-fold) lower than for IFNγ induction and we consistently observed the emergence of a small CCL3$^+$ or CCL4$^+$T cell subset in the absence of detectable IFNγ at limiting peptide concentrations. In fact, at a peptide concentration of 10^{-10}M, the very small subset of responding p14 T$_M$ consists to $>$50% of CCL3/4$^+$ cells that are IFNγ -negative. In contrast, no IFNγ induction is observed in the absence of CCL3/4 production (**Fig.29A**). Parallel analyses of aged p14 T$_M$ ($\sim$21 months) yielded identical results indicating that subtle differences pertaining to the thresholds for defined effector functions are preserved in longterm memory (not shown). To directly compare the activation thresholds for CC3/4 synthesis with CCL5 release and

production, we determined the respective functional avidities by ELISA (**Fig.29B**). The activation thresholds for CCL3 and CCL4 secretion were expectedly comparable but interestingly, significantly lower than that of induced CCL5 release. In summary, at limiting antigen concentration, the IFNγ response is preceded by secretion of the chemokines CCL5 and to a certain extent also CCL3/4.

5 Discussion

The chemokines are a large family of mainly secreted molecules involved in the regulation of numerous physiological and pathophysiological processes. However, despite many years of investigation, the precise cellular sources of most chemokines have remained incompletely defined as a consequence of the limited availability of suitable reagents to visualize the expression of chemokine proteins at the single cell level. The ”chemokine flow cytometry” assay was developed to employ commercially available chemokine-specific antibodies for efficient cell-associated detection of nearly all murine chemokines (37 out of 39). To demonstrate the utility of this methodology, ”chemokine flow cytometry” was used to re-define the nature of ”homeostatic chemokines” in the hematopoetic compartment, to delineate the complete chemokine profiles of NK cells and B cells and to assess the chemokine response of dendritic cells to bacterial infection.

It is anticipated that over time, polyclonal antibodies will be replaced by newly available monoclonal antibodies suitable for intracellular flow cytometry. Until then, as demonstrated, the almost (37 of 39) complete spectrum of available polyclonal chemokine antibodies allows the profiling of virtually any murine cell provided it is in a single cell suspension. Although cross-reactivities have been observed for 14 out of 37 chemokines, most of these are only minor. Prior knowledge, e.g. mRNA expression profiles, can guide the deduction process to determine wether the signal is due to the presence of a cross-reactive chemokine, as was demonstrated with the integration of microarray data from our lab as well as microarray data from public repositories.

Probably one of the greatest benefits of this methodology lies in the ability to visualize a nearly complete spectrum of chemokines as this allows to not only identify chemokines that are expressed, but, arguably equally important, also chemokines that are *not* expressed at the protein level under the same experimental conditions and within the detection limits of flow cytometry. Although ”the absence of evidence is not the evidence of absence” applies, under carefully designed experimental conditions, which includes appropriate controls, this methodology greatly enhances the ability to comprehensively screen for chemokine expression in even small subsets of antigen-specific T cells.

Furthermore, the usefulness of polyclonal antibodies is obviously not restricted to mouse-specific antibodies as demonstrated by applying chemokine FC to human samples, but it can also apply to

virtually any set of polyclonal antibodies. An advantage of this method, compared to others like IHC, is the processing speed from cell harvest to data acquisition. Therefore this methodology provides a useful tool for the rapid testing of any new antibody in regards to their suitability for IHC as both methods require the same fixating agent (paraformaldehyde). To this end, our preliminary results (data not shown) indicate that all non-IHC-approved antibodies tested so far are indeed suitable for IHC.

Table 10 on page 90 provides a comprehensive overview of the chemokine expression profile of hematopoietic cells as determined in this thesis work. The application of chemokine FC not only validated many observations previously described in the literature, but also provided new insights into the expression of chemokines by hematopoietic cells. For example, pronounced constitutive chemokine expression was observed for CCL5, CCL6, CCL9/10, CCL21, CCL27, CXCL4 and CXCL7. In contrast, only low-level expression of CCL7, CCL8, CCL11, CXCL9 and XCL1 was detectable directly *ex vivo* in smaller hematopoetic cell subsets and several additional chemokines were synthesized after a brief (5h) *in vitro* culture in a spontaneous manner (CCL2, CCL3, CCL4, CCL22, CXCL2 and CXCL16). Two thirds of the above chemokines (CCL2/3/4/5/ 6/7/8/11 and CXCL2/ 7/9/ 16) are traditionally regarded as "inflammatory" [42] and our description of their constitutive and/or spontaneous expression indicates that these chemokine may also exert previously unrecognized homeostatic functions. One experimental caveat is the disruption and processing of tissue itself which could induce chemokine production in unstimulated cultured cells thus contributing to the spontaneous chemokine expression profile. Future studies are envisioned where *in vivo* administration of BFA into mice will allow to exclude possible effects of short-term culture conditions in the absence of stimuli. Even subtracting the number of spontaneously induced chemokines leaves six chemokines (CCL6/7/8/11 and CXCL7/9) that could be reclassified as dual-function chemokines.

The second part of the thesis focussed on the production of chemokines by pathogen-specific T cells. An important observation was the apparent disconnect between mRNA expression and protein expression exemplified by the comparison of microarray and flow cytometric data of pathogen-specific T_E and T_M p14 T cells: Only 6 of 10 chemokines expressed at the mRNA level were detectable at the protein level (CCL1,3,4,5, 9/10 and XCL1) indicating post-transcriptional regula-

tion of chemokine production. Although mRNA expression analyses are useful and often, due to the lack of suitable antibodies, the only method of measuring gene expression, this highlights the limited power of mRNA-based expression analyses and inferences based upon these.

Comparison of the endogenous $CD4^+$ and $CD8^+$T cell chemokine signature to different intracellular pathogens (LCMV, VSV, LM) demonstrated that pathogen-specific T_E and primary T_M produced the same set of chemokines and the observed quantitative differences were only relatively minor and largely independent of immunodominance and avidity of the TCR.

The magnitude of T cell responses are frequently assessed by measuring a single parameter such as the relative frequencies of antigen-specific T cells or the expression of an effector molecules such as IFNγ or granzyme. However, these measurements do not capture the full spectrum of the T cell response and might not be indicative of the quality of the immune response. Recently, Darrah *et al.* [183] described an approach where the expression of three factors, IFNγ,TNFα and IL-2, but none by themselves or in doublets, were predictive for the degree of immune protection afforded by $CD4^+$T cells in response to *L. major* infection. The high expression of this triplet correlated with enhanced protection and despite the lack of knowledge of the precise underlying mechanisms of this enhanced protection, the usefulness of "correlates of immune protection" for vaccine design and vaccination strategies are beginning to emerge [180]. To this end, we identified the chemokine CCL1 as marker for a set of highly "polyfunctional" pathogen-specific $CD4^+$ and $CD8^+$ T cells capable of producing several chemokines and effector molecules in high amounts. Clearly, further functional studies are required to determine the applicability of induced CCL1 expression as a principle predictor of immune protection. However, preliminary data from our lab (data not shown) highlights the potential of CCL1 as a marker for "superior" T_M functions: In the clone13 model of chronic LCMV infection induced CCL1 expression was quickly curtailed, abolished and not regained. In this experimental system [83], various T cell functions are impaired in a staggered fashion and it appears that CCL1 production is even more sensitive to downmodulation than that of induced IL-2 expression, currently the best functional indicator for early T cell "exhaustion" (not shown).

The presence of chemokine mRNA species in T_M has been suggested to confer a kinetic advantage

that permits more rapid protein synthesis [63, 186], but has previously not been formerly tested. This hypothesis is confirmed by a combination of experiments showing that constitutive mRNA expression of CCL3, CCL4 (and CCL5) greatly contributes to their protein syntheses (**Fig.27)** and precede the production of CCL1 (**Fig.28)** which requires *de novo* transcription (**Fig.28D)**.

The constitutive CCL5 expression by antigen-experienced T cells is only shared with NK cells and during the course of a primary infection, the cellular source of CCL5 shifts from predominantly NK cells to predominantly pathogen-specific T cells (**Fig.22G/H)**. Dorner et al. also described this phenomena as handing over the "innate chemokine response" to the "adaptive chemokine response" [70]. The constitutive CCL5 expression by pathogen-specific late T_E as well as T_M cells is rather unusual as CCL5 is generally considered as an "inflammatory" chemokine prompting further investigation of kinetics of chemokine production and release. Curiously, the velocity of CCL5 release upon T cell stimulation exceeded that of GzmB, the effector molecule with the fastest known release kinetic and the activation threshold of CCL5 was lower than CCL3/4 followed by IFNγ (**Fig.28)**. These effector molecule-like properties along with constitutive expression suggests a novel role for CCL5 which requires immediate release of pre-stored molecules and comparatively lower activation thresholds. As CCL5 is expressed by T cells relatively late during the primary response, but constitutively expressed by lymphnode-resident T_M, it is tempting to speculate that CCL5 has a role in shaping the magnitude or quality of the immune response by influencing trafficking and/or survival of APCs. Tyner et al. reported that CCL5 can prolong survival of macrophages via CCL5:CCR5 interaction [51]. A different study found that CCL5 stimulation of BMDCS and splenic DCs induced cytokine and chemokine production, including autocrine production of CCL5 [189]. The authors hypothesized that "CCL5-mediated chemokine amplification in DC may prolong inflammatory responses and shape the microenvironment, potentially enhancing acquired and innate immune responses" [189]. Evidence for a role of CCL3 and CCL4 in shaping helped T_M has been reported [54] as well as the requirement of $CD8^+$T cell-expressed CCR5 for efficient accumulation in draining lymph nodes containing activated $CD4^+$T cells.

In summary, the fast release kinetics combined with low activation thresholds of prestored CCL5, and to some extend of *de novo* -produced CCL3 and CCL4, may stabilize interactions between T cell and target cells or APCs, may provide costimulatory and/or survival signals, exert direct effector

functions [69] or mediate additional novel functions.

A possible role of XCL1:XCR1 interaction in shaping the pool-size of antigen-specific T cells has recently been proposed by Dorner *et al.* utilizing their newly generated XCL1$^{-/-}$ mouse: CD8^{+}DCs, which are capable of cross-presenting exogenous peptides in the context of MHC-I, were identified as the (presumably) only cell type expressing the cognate XCR1 receptor. Lack of XCL1 resulted in a reduced T_E pool size and reduced IFNγ production using an OT-I adoptive transfer model in conjunction with an αDEC-205:OVA immunization regiment [71]. The authors further speculate that XCL1 might serve as a factor contributing to the subdomain organization of CD8^{+}T cell:DC interaction postulated previously [190]. Interestingly, our results demonstrate that XCL1 was the only chemokine whose constitutive mRNA expression continuously increased with the age of the CD8^{+}T_M (**Fig.23D**). This upregulation correlated well with the observed increase of the fraction of aged CD8^{+}T_M capable of producing XCL1 protein upon stimulation ($\sim$70% in young vs. $\sim$95% in old T_M, **Fig.28E**) and constitutes together with IL-2 the only known functional gain by established CD8^{+}T_M. Combining our observations with those of Dorner *et al.*, one could speculate that aged CD8^{+}T_M might display a better induction of secondary immune responses than their young counterparts in the context of antigen-presentation by CD8^{+}DCs [71].

6 Future Directions

Current and future studies are aimed at further understanding the non-redundant roles of T cell produced chemokines which is inherently complicated due to the observed promiscuity of receptor-chemokine interaction as multiple chemokines can bind to multiple receptors and *vici versa*. Although knockout mice for *Ccl3* and *Ccl5* are commercially available, generation of double and triple-knockout mice (*Ccl3*$^{-/-}$*Ccl4*$^{-/-}$*Ccl5*$^{-/-}$) cannot be generated by intercrossing due to tight linkage of these loci and therefore have to be targeted as one unit. Experiments neutralizing these chemokines with antibodies are currently in progress in order to determine future directions into the role of T cell-produced chemokines. To proceed with the characterization of the ”polyfunctional” CCL1^{+}T cell population, *Ccl1*$^{-/-}$ mice are being acquired. Furthermore, the generation of a *Ccl1* reporter mouse is envisioned as the current identification of CCL1-producing cells by flow

cytometry requires PFA fixation thus rendering the identified cells unsuitable for further *in vivo* / *in vitro* studies. Lastly, the application of "chemokine flow cytometry" to the characterization of the chemokine expression profile of human pathogen-specific T cells as well as NK cells chronically infected with Hepatitis C is under way.

7 Summary

The chemokines are a large family of mainly secreted molecules involved in the regulation of numerous physiological and pathophysiological processes. However, despite many years of investigation, the precise cellular sources of most chemokines have remained incompletely defined as a consequence of the limited availability of suitable reagents to visualize the expression of chemokine proteins at the single cell level.

This thesis work describes the development and application of a simple flow cytometry-based assay that employs commercially available chemokine-specific antibodies for efficient cell-associated detection of nearly all murine chemokines (37 out of 39). To demonstrate the utility of this methodology, chemokine flow cytometry was employed to re-evaluate the classification of chemokines produced by hematopoietic cells, to delineate the complete chemokine profiles of NK cells and B cells, and to assess the chemokine response of dendritic cells to bacterial infection. The versatility of this analytical methodology was further demonstrated by its application to selected human chemokines and should greatly facilitate any future investigation into chemokine biology at large.

Although T cells are recognized as a source for some chemokines, the complete spectrum of pathogen- specific T cell-produced chemokines remains at present unknown. Here we demonstrate that T cells specific for distinct viral and bacterial pathogens produce a limited spectrum of chemokines (CCL1, CCL3, CCL4, CCL5, CCL9/10 and XCL1) and identify a unique expression pattern for CCL5 that, in contrast to all other effector molecules, is constitutively expressed by specific $CD8^+$ memory T cells. Indeed, these cells are the principal source of prestored CCL5 and the near instantaneous CCL5 release after TCR activation coupled with a low activation threshold for induced CCL3/4 production establishes the T cell chemokine response as the first step in a cascade of

temporally regulated effector activities. Synthesis of XCL1 and CCL1 occurs with delayed kinetics but exhibited two notable features: 1., aging $CD8^+$ memory T cells progressively acquired the ability for accelerated XCL1 production and 2., induced CCL1 expression by specific memory T cells identifies highly ”polyfunctional” subsets and thus may serve as a possible ”correlate of immune protection”. The results presented in this thesis provide a methodological and conceptual foundation for further investigations aimed at deciphering the non-redundant roles of T cell-produced chemokines in infectious disease.

8 Zusammenfassung

Die Mehrheit der zahlreichen Mitglieder der Chemokinfamilie werden sekretiert und sind involviert in der Regulation von vielzähligen physiologischen und pathophysiologischen Prozessen. Trotz Jahre intensiver Forschung sind die chemokineproduzierenden Zelltypen für die meisten Chemokine nur teilweise identifiziert. Der Grund liegt zumeist an der Tatsache, dass bis vor kurzem nur eine limitierende Anzahl von Reagenzien zur Visualisierung von Chemokinen in Einzelzellen zur Verfügung stand.

Die hier vorliegende Arbeit beschreibt die Entwicklung und Anwendung einer einfachen, auf Durchflusszytometrie basierenden Methode zur effizienten zellassoziierten Detektion von nahezu allen Maus-Chemokinen (37 von 39) mit Hilfe von kommerziell erhältlichen, chemokinspezifischen Antikörpern. Die hier beschriebene ”Chemokine Flow Cytometry” Methode wurde angewandt, um sowohl die bestehende funktionelle Klassifizierung von Chemokinen zu beurteilen, das Chemokinprofil von natürlichen Killerzellen und B-Zellen zu bestimmen als auch die Chemokinantwort von bakterieninfizierten dendritischen Zellen zu charakterisieren. Die Vielseitigkeit dieser analytischen Methode wurde des weiteren durch die Anwendung auf ausgewählte humane Chemokine demonstriert und sollte zukünftige Forschung im Bereich der Chemokinbiologie generell erleichtern.

Obwohl T-Zellen bereits als Quelle für einige Chemokine bekannt sind, wurde das gesamte Spektrum von T-Zell-produzierten Chemokinen bisher noch nicht systematisch charakterisiert. In dieser Doktorarbeit wurde gezeigt, dass T-Zellen spezifisch für bestimmte Viren oder Bakterien ein limi-

tiertes Spektrum von Chemokinen produzieren (CCL1, CCL3, CCL4, CCL5, CCL9/10 and XCL1). Des weiteren wurde ein besonderes Expressionsprofil für CCL5 entdeckt, welches, im Gegensatz zu anderen Effektormolekülen, konstitutiv in CD8-positiven Gedächtnis-T-Zellen (Memory T cells) exprimiert ist.

Die ”T-Zell Chemokineantwort” wurde als der erste Schritt in einer zeitlich regulierten Kaskade von Effektoraktivitäten durch die folgenden Beobachtungen etabliert: Pathogenspezifische T-Zellen sind die Hauptquelle von gespeichertem CCL5, weisen eine nahezu sofortige CCL5-Ausschüttung nach Aktivierung des T-Zellrezeptors auf und verfügen, im Vergleich zu anderen Effektormolekülen, über eine relative niedrige Aktivierungsschwelle für die Induktion der CCL3- und CCL4-Produktion.

Die Synthese von XCL1 und CCL1 geschah mit verzögerter Kinetik, zeigte jedoch zwei erwähnenswerte Eigenheiten auf: Einerseits erwarben Gedächtnis-T-Zellen mit zunehmendem Alter die Fähigkeit der beschleunigten XCL1 Produktion, andererseits identifizierte die induzierte Exprimierung von CCL1 eine ”hochpolyfunktionale” Subpopulation von Gedächtnis-T-Zellen mit dem Potential für CCL1 als ein ”Korrelat der Immunprotektion”.

Die Ergebnisse dieser Doktorarbeit bereiten ein methodisches und konzeptionelles Fundament für zukünftige Forschung mit dem Ziel der Entschlüsselung von nicht-redundanten Funktionen von T-Zell-produzierten Chemokinen im Feld der Infektionsbiologie.

9 References

[1] Kenneth M. Murphy, M. W., Paul Travers. *Janeway's Immunobiology*. 978-0-8153-4123-9 (2007), 7 edn.

[2] Wu, L. & Liu, Y.-J.: Development of dendritic-cell lineages. *Immunity* 26, 741–750 (2007).

[3] Joffre, O., Nolte, M. A., Sporri, R. & Reis e Sousa, C.: Inflammatory signals in dendritic cell activation and the induction of adaptive immunity. *Immunol Rev* 227, 234–247 (2009).

[4] Lanier, L. L.: Evolutionary struggles between NK cells and viruses. *Nat Rev Immunol* 8, 259–268 (2008).

[5] Born, W. K., Reardon, C. L. & O'Brien, R. L.: The function of gammadelta T cells in innate immunity. *Curr Opin Immunol* 18, 31–38 (2006).

[6] Blanden, R. V. *et al.*: Genes required for cytotoxicity against virus-infected target cells in K and D regions of H-2 complex. *Nature* 254, 269–270 (1975).

[7] Doherty, P. C. & Zinkernagel, R. M.: H-2 compatibility is required for T-cell-mediated lysis of target cells infected with lymphocytic choriomeningitis virus. *J Exp Med* 141, 502–507 (1975).

[8] Sigal, L. J., Crotty, S., Andino, R. & Rock, K. L.: Cytotoxic T-cell immunity to virus-infected non-haematopoietic cells requires presentation of exogenous antigen. *Nature* 398, 77–80 (1999).

[9] Huang, A. Y. *et al.*: Role of bone marrow-derived cells in presenting MHC class I-restricted tumor antigens. *Science* 264, 961–965 (1994).

[10] Zhu, J. & Paul, W. E.: Heterogeneity and plasticity of T helper cells. *Cell Res* 20, 4–12 (2010).

[11] Infante-Duarte, C., Horton, H. F., Byrne, M. C. & Kamradt, T.: Microbial lipopeptides induce the production of IL-17 in Th cells. *J Immunol* 165, 6107–6115 (2000).

[12] Lowin, B., Hahne, M., Mattmann, C. & Tschopp, J.: Cytolytic T-cell cytotoxicity is mediated through perforin and Fas lytic pathways. *Nature* 370, 650–652 (1994).

[13] van de Berg, P. J., van Leeuwen, E. M., ten Berge, I. J. & van Lier, R.: Cytotoxic human CD4(+) T cells. *Curr Opin Immunol* 20, 339–343 (2008).

[14] MacLeod, M. K. L., Clambey, E. T., Kappler, J. W. & Marrack, P.: CD4 memory T cells: what are they and what can they do? *Semin Immunol* 21, 53–61 (2009).

[15] Jabbari, A. & Harty, J. T.: The generation and modulation of antigen-specific memory CD8 T cell responses. *J Leukoc Biol* 80, 16–23 (2006).

[16] Homann, D., Teyton, L. & Oldstone, M. B.: Differential regulation of antiviral T-cell immunity results in stable CD8+ but declining CD4+ T-cell memory. *Nat Med* 7, 913–919 (2001).

[17] Veiga-Fernandes, H., Walter, U., Bourgeois, C., McLean, A. & Rocha, B.: Response of naive and memory CD8+ T cells to antigen stimulation in vivo. *Nat Immunol* 1, 47–53 (2000).

[18] Whitton, J. L. & Oldstone, M. B. *Field's Virology*, chap. The immune response to viruses., 285–320 (Lippincott Williams and Wilkins, 2001).

[19] Lanzavecchia, A. & Sallusto, F.: Understanding the generation and function of memory T cell subsets. *Curr Opin Immunol* 17, 326–332 (2005).

[20] Gunn, M. D. *et al.*: Mice lacking expression of secondary lymphoid organ chemokine have defects in lymphocyte homing and dendritic cell localization. *J Exp Med* 189, 451–460 (1999).

[21] Forster, R. *et al.*: CCR7 coordinates the primary immune response by establishing functional microenvironments in secondary lymphoid organs. *Cell* 99, 23–33 (1999).

[22] Unsoeld, H. & Pircher, H.: Complex memory T-cell phenotypes revealed by coexpression of CD62L and CCR7. *J Virol* 79, 4510–4513 (2005).

[23] Roberts, A. D. & Woodland, D. L.: Cutting edge: effector memory CD8+ T cells play a prominent role in recall responses to secondary viral infection in the lung. *J Immunol* 172, 6533–6537 (2004).

[24] Roberts, A. D., Ely, K. H. & Woodland, D. L.: Differential contributions of central and effector memory T cells to recall responses. *J Exp Med* 202, 123–133 (2005).

[25] Barber, D. L., Wherry, E. J. & Ahmed, R.: Cutting edge: rapid in vivo killing by memory CD8 T cells. *J Immunol* 171, 27–31 (2003).

[26] Kaech, S. M. & Wherry, E. J.: Heterogeneity and cell-fate decisions in effector and memory CD8+ T cell differentiation during viral infection. *Immunity* 27, 393–405 (2007).

[27] Tanaka, Y. *et al.*: T-cell adhesion induced by proteoglycan-immobilized cytokine MIP-1 beta. *Nature* 361, 79–82 (1993).

[28] Middleton, J. *et al.*: Transcytosis and surface presentation of IL-8 by venular endothelial cells. *Cell* 91, 385–395 (1997).

[29] Cinamon, G., Shinder, V. & Alon, R.: Shear forces promote lymphocyte migration across vascular endothelium bearing apical chemokines. *Nat Immunol* 2, 515–522 (2001).

[30] Swaminathan, G. J. *et al.*: Crystal structures of oligomeric forms of the IP-10/CXCL10 chemokine. *Structure* 11, 521–532 (2003).

[31] Ansel, K. M. & Cyster, J. G.: Chemokines in lymphopoiesis and lymphoid organ development. *Curr Opin Immunol* 13, 172–179 (2001).

[32] Campbell, D. J., Kim, C. H. & Butcher, E. C.: Chemokines in the systemic organization of immunity. *Immunol Rev* 195, 58–71 (2003).

[33] Kunkel, E. J. & Butcher, E. C.: Chemokines and the tissue-specific migration of lymphocytes. *Immunity* 16, 1–4 (2002).

[34] Luther, S. A. & Cyster, J. G.: Chemokines as regulators of T cell differentiation. *Nat Immunol* 2, 102–107 (2001).

[35] Rot, A. & von Andrian, U. H.: Chemokines in innate and adaptive host defense: basic chemokinese grammar for immune cells. *Annu Rev Immunol* 22, 891–928 (2004).

[36] Gerard, C. & Rollins, B. J.: Chemokines and disease. *Nat Immunol* 2, 108–115 (2001).

[37] Kunkel, S. L. & Godessart, N.: Chemokines in autoimmunity: from pathology to therapeutics. *Autoimmun Rev* 1, 313–320 (2002).

[38] Locati, M. & Murphy, P. M.: Chemokines and chemokine receptors: biology and clinical relevance in inflammation and AIDS. *Annu Rev Med* 50, 425–440 (1999).

[39] Yopp, A. C., Krieger, N. R., Ochando, J. C. & Bromberg, J. S.: Therapeutic manipulation of T cell chemotaxis in transplantation. *Curr Opin Immunol* 16, 571–577 (2004).

[40] Zlotnik, A.: Chemokines in neoplastic progression. *Semin Cancer Biol* 14, 181–185 (2004).

[41] Alcami, A.: Viral mimicry of cytokines, chemokines and their receptors. *Nat Rev Immunol* 3, 36–50 (2003).

[42] Zlotnik, A., Yoshie, O. & Nomiyama, H.: The chemokine and chemokine receptor superfamilies and their molecular evolution. *Genome Biol* 7, 243 (2006).

[43] Naumann, U. *et al.*: CXCR7 functions as a scavenger for CXCL12 and CXCL11. *PLoS One* 5, e9175 (2010).

[44] Mantovani, A., Bonecchi, R. & Locati, M.: Tuning inflammation and immunity by chemokine sequestration: decoys and more. *Nat Rev Immunol* 6, 907–918 (2006).

[45] Rot, A.: Contribution of Duffy antigen to chemokine function. *Cytokine Growth Factor Rev* 16, 687–694 (2005).

[46] Van Damme, J., Van Beeumen, J., Opdenakker, G. & Billiau, A.: A novel, NH2-terminal sequence-characterized human monokine possessing neutrophil chemotactic, skin-reactive, and granulocytosis-promoting activity. *J Exp Med* 167, 1364–1376 (1988).

[47] Colditz, I., Zwahlen, R., Dewald, B. & Baggiolini, M.: In vivo inflammatory activity of neutrophil-activating factor, a novel chemotactic peptide derived from human monocytes. *Am J Pathol* 134, 755–760 (1989).

[48] Taub, D. D. & Oppenheim, J. J.: Review of the chemokine meeting the Third International Symposium of Chemotactic Cytokines. *Cytokine* 5, 175–179 (1993).

[49] NCBI Genomic Biology [http://www.ncbi.nlm.nih.gov/Genomes/]. URL .

[50] Baekkevold, E. S. *et al.*: The CCR7 ligand elc (CCL19) is transcytosed in high endothelial venules and mediates T cell recruitment. *J Exp Med* 193, 1105–1112 (2001).

[51] Tyner, J. W. *et al.*: CCL5-CCR5 interaction provides antiapoptotic signals for macrophage survival during viral infection. *Nat Med* 11, 1180–1187 (2005).

[52] Guermonprez, P., Valladeau, J., Zitvogel, L., Thery, C. & Amigorena, S.: Antigen presentation and T cell stimulation by dendritic cells. *Annu Rev Immunol* 20, 621–667 (2002).

[53] von Andrian, U. H. & Mackay, C. R.: T-cell function and migration. Two sides of the same coin. *N Engl J Med* 343, 1020–1034 (2000).

[54] Castellino, F. *et al.*: Chemokines enhance immunity by guiding naive CD8+ T cells to sites of CD4+ T cell-dendritic cell interaction. *Nature* 440, 890–895 (2006).

[55] Belz, G. T., Wodarz, D., Diaz, G., Nowak, M. A. & Doherty, P. C.: Compromised influenza virus-specific CD8(+)-T-cell memory in CD4(+)-T-cell-deficient mice. *J Virol* 76, 12388–12393 (2002).

[56] Sun, J. C. & Bevan, M. J.: Defective CD8 T cell memory following acute infection without CD4 T cell help. *Science* 300, 339–342 (2003).

[57] Marzo, A. L. *et al.*: Fully functional memory CD8 T cells in the absence of CD4 T cells. *J Immunol* 173, 969–975 (2004).

[58] Schaerli, P. *et al.*: A skin-selective homing mechanism for human immune surveillance T cells. *J Exp Med* 199, 1265–1275 (2004).

[59] Schaerli, P. & Moser, B.: Chemokines: control of primary and memory T-cell traffic. *Immunol Res* 31, 57–74 (2005).

[60] Price, D. A., Klenerman, P., Booth, B. L., Phillips, R. E. & Sewell, A. K.: Cytotoxic T lymphocytes, chemokines and antiviral immunity. *Immunol Today* 20, 212–216 (1999).

[61] Cocchi, F. *et al.*: Identification of RANTES, MIP-1 alpha, and MIP-1 beta as the major HIV-suppressive factors produced by CD8+ T cells. *Science* 270, 1811–1815 (1995).

[62] Samson, M. *et al.*: Resistance to HIV-1 infection in caucasian individuals bearing mutant alleles of the CCR-5 chemokine receptor gene. *Nature* 382, 722–725 (1996).

[63] Swanson, B. J., Murakami, M., Mitchell, T. C., Kappler, J. & Marrack, P.: RANTES production by memory phenotype T cells is controlled by a posttranscriptional, TCR-dependent process. *Immunity* 17, 605–615 (2002).

[64] Walzer, T. *et al.*: Cutting edge: immediate RANTES secretion by resting memory CD8 T cells following antigenic stimulation. *J Immunol* 170, 1615–1619 (2003).

[65] Catalfamo, M. *et al.*: Human CD8+ T cells store RANTES in a unique secretory compartment and release it rapidly after TcR stimulation. *Immunity* 20, 219–230 (2004).

[66] Stegelmann, F. *et al.*: Coordinate expression of CC chemokine ligand 5, granulysin, and perforin in CD8+ T cells provides a host defense mechanism against Mycobacterium tuberculosis. *J Immunol* 175, 7474–7483 (2005).

[67] Wagner, L. *et al.*: Beta-chemokines are released from HIV-1-specific cytolytic T-cell granules complexed to proteoglycans. *Nature* 391, 908–911 (1998).

[68] Cook, D. N., Smithies, O., Strieter, R. M., Frelinger, J. A. & Serody, J. S.: CD8+ T cells are a biologically relevant source of macrophage inflammatory protein-1 alpha in vivo. *J Immunol* 162, 5423–5428 (1999).

[69] Narni-Mancinelli, E. *et al.*: Memory CD8+ T cells mediate antibacterial immunity via CCL3 activation of TNF/ROI+ phagocytes. *J Exp Med* 204, 2075–2087 (2007).

[70] Dorner, B. G. *et al.*: MIP-1alpha, MIP-1beta, RANTES, and ATAC/lymphotactin function together with IFN-gamma as type 1 cytokines. *Proc Natl Acad Sci U S A* 99, 6181–6186 (2002).

[71] Dorner, B. G. *et al.*: Selective expression of the chemokine receptor XCR1 on cross-presenting dendritic cells determines cooperation with CD8+ T cells. *Immunity* 31, 823–833 (2009).

[72] Borrow P, O. M. *Viral Pathogenesis*, chap. Lymphocytic choriomeningitis virus., 593–627 (Lippincott-Raven, 1997).

[73] Lau, L. L., Jamieson, B. D., Somasundaram, T. & Ahmed, R.: Cytotoxic T-cell memory without antigen. *Nature* 369, 648–652 (1994).

[74] Murali-Krishna, K. *et al.*: Persistence of memory CD8 T cells in MHC class I-deficient mice. *Science* 286, 1377–1381 (1999).

[75] Selin, L. K., Vergilis, K., Welsh, R. M. & Nahill, S. R.: Reduction of otherwise remarkably stable virus-specific cytotoxic T lymphocyte memory by heterologous viral infections. *J Exp Med* 183, 2489–2499 (1996).

[76] von Herrath, M. G., Yokoyama, M., Dockter, J., Oldstone, M. B. & Whitton, J. L.: CD4-deficient mice have reduced levels of memory cytotoxic T lymphocytes after immunization and show diminished resistance to subsequent virus challenge. *J Virol* 70, 1072–1079 (1996).

[77] Janssen, E. M. *et al.*: CD4+ T cells are required for secondary expansion and memory in CD8+ T lymphocytes. *Nature* 421, 852–856 (2003).

[78] Bevan, M. J.: Helping the CD8(+) T-cell response. *Nat Rev Immunol* 4, 595–602 (2004).

[79] Sun, J. C., Williams, M. A. & Bevan, M. J.: CD4+ T cells are required for the maintenance, not programming, of memory CD8+ T cells after acute infection. *Nat Immunol* 5, 927–933 (2004).

[80] Lenz, D. C. *et al.*: IL-7 regulates basal homeostatic proliferation of antiviral CD4+T cell memory. *Proc Natl Acad Sci U S A* 101, 9357–9362 (2004).

[81] Sevilla, N. *et al.*: Immunosuppression and resultant viral persistence by specific viral targeting of dendritic cells. *J Exp Med* 192, 1249–1260 (2000).

[82] Sevilla, N., McGavern, D. B., Teng, C., Kunz, S. & Oldstone, M. B. A.: Viral targeting of hematopoietic progenitors and inhibition of DC maturation as a dual strategy for immune subversion. *J Clin Invest* 113, 737–745 (2004).

[83] Wherry, E. J., Blattman, J. N., Murali-Krishna, K., van der Most, R. & Ahmed, R.: Viral persistence alters CD8 T-cell immunodominance and tissue distribution and results in distinct stages of functional impairment. *J Virol* 77, 4911–4927 (2003).

[84] Wherry, E. J. & Ahmed, R.: Memory CD8 T-cell differentiation during viral infection. *J Virol* 78, 5535–5545 (2004).

[85] Brooks, D. G., Teyton, L., Oldstone, M. B. A. & McGavern, D. B.: Intrinsic functional dysregulation of CD4 T cells occurs rapidly following persistent viral infection. *J Virol* 79, 10514–10527 (2005).

[86] Fuller, M. J., Khanolkar, A., Tebo, A. E. & Zajac, A. J.: Maintenance, loss, and resurgence of T cell responses during acute, protracted, and chronic viral infections. *J Immunol* 172, 4204–4214 (2004).

[87] Fuller, M. J. *et al.*: Cutting edge: emergence of CD127high functionally competent memory T cells is compromised by high viral loads and inadequate T cell help. *J Immunol* 174, 5926–5930 (2005).

[88] Miller, N. E., Bonczyk, J. R., Nakayama, Y. & Suresh, M.: Role of thymic output in regulating CD8 T-cell homeostasis during acute and chronic viral infection. *J Virol* 79, 9419–9429 (2005).

[89] Barber, D. L. *et al.*: Restoring function in exhausted CD8 T cells during chronic viral infection. *Nature* 439, 682–687 (2006).

[90] Pircher, H., Burki, K., Lang, R., Hengartner, H. & Zinkernagel, R. M.: Tolerance induction in double specific T-cell receptor transgenic mice varies with antigen. *Nature* 342, 559–561 (1989).

[91] Lefrancois, L.: Protection against lethal viral infection by neutralizing and nonneutralizing monoclonal antibodies: distinct mechanisms of action in vivo. *J Virol* 51, 208–214 (1984).

[92] Christian, A. Y., Barna, M., Bi, Z. & Reiss, C. S.: Host immune response to vesicular stomatitis virus infection of the central nervous system in C57BL/6 mice. *Viral Immunol* 9, 195–205 (1996).

[93] Luijkx, T. A., van Gaans-van den Brink, J. A. M., van Dijken, H. H., van den Dobbelsteen, G. P. J. M. & van Els, C. A. C. M.: Hyperproliferation of B cells specific for a weakly immunogenic PorA in a meningococcal vaccine model. *Clin Vaccine Immunol* 15, 1598–1605 (2008).

[94] Andreasen, S. O., Christensen, J. E., Marker, O. & Thomsen, A. R.: Role of CD40 ligand and CD28 in induction and maintenance of antiviral CD8+ effector T cell responses. *J Immunol* 164, 3689–3697 (2000).

[95] Masopust, D., Vezys, V., Marzo, A. L. & Lefrancois, L.: Preferential localization of effector memory cells in nonlymphoid tissue. *Science* 291, 2413–2417 (2001).

[96] Battegay, M. *et al.*: Antiviral immune responses of mice lacking MHC class II or its associated invariant chain. *Cell Immunol* 167, 115–121 (1996).

[97] Kundig, T. M. *et al.*: Duration of TCR stimulation determines costimulatory requirement of T cells. *Immunity* 5, 41–52 (1996).

[98] Thomsen, A. R. *et al.*: Cooperation of B cells and T cells is required for survival of mice infected with vesicular stomatitis virus. *Int Immunol* 9, 1757–1766 (1997).

[99] Andersen, C., Jensen, T., Nansen, A., Marker, O. & Thomsen, A. R.: CD4(+) T cell-mediated protection against a lethal outcome of systemic infection with vesicular stomatitis virus requires CD40 ligand expression, but not IFN-gamma or IL-4. *Int Immunol* 11, 2035–2042 (1999).

[100] Maloy, K. J. *et al.*: CD4(+) T cell subsets during virus infection. Protective capacity depends on effector cytokine secretion and on migratory capability. *J Exp Med* 191, 2159–2170 (2000).

[101] Gellin, B. G. & Broome, C. V.: Listeriosis. *JAMA* 261, 1313–1320 (1989).

[102] Kaufmann, S. H., Hug, E. & De Libero, G.: Listeria monocytogenes-reactive T lymphocyte clones with cytolytic activity against infected target cells. *J Exp Med* 164, 363–368 (1986).

[103] Bishop, D. K. & Hinrichs, D. J.: Adoptive transfer of immunity to Listeria monocytogenes. The influence of in vitro stimulation on lymphocyte subset requirements. *J Immunol* 139, 2005–2009 (1987).

[104] Harty, J. T., Schreiber, R. D. & Bevan, M. J.: CD8 T cells can protect against an intracellular bacterium in an interferon gamma-independent fashion. *Proc Natl Acad Sci U S A* 89, 11612–11616 (1992).

[105] Busch, D. H., Pilip, I. M., Vijh, S. & Pamer, E. G.: Coordinate regulation of complex T cell populations responding to bacterial infection. *Immunity* 8, 353–362 (1998).

[106] Ladel, C. H., Flesch, I. E., Arnoldi, J. & Kaufmann, S. H.: Studies with MHC-deficient knock-out mice reveal impact of both MHC I- and MHC II-dependent T cell responses on Listeria monocytogenes infection. *J Immunol* 153, 3116–3122 (1994).

[107] Geginat, G., Schenk, S., Skoberne, M., Goebel, W. & Hof, H.: A novel approach of direct ex vivo epitope mapping identifies dominant and subdominant CD4 and CD8 T cell epitopes from Listeria monocytogenes. *J Immunol* 166, 1877–1884 (2001).

[108] Skoberne, M., Schenk, S., Hof, H. & Geginat, G.: Cross-presentation of Listeria monocytogenes-derived CD4 T cell epitopes. *J Immunol* 169, 1410–1418 (2002).

[109] Schiemann, M., Busch, V., Linkemann, K., Huster, K. M. & Busch, D. H.: Differences in maintenance of CD8+ and CD4+ bacteria-specific effector-memory T cell populations. *Eur J Immunol* 33, 2875–2885 (2003).

[110] Pope, C. *et al.*: Organ-specific regulation of the CD8 T cell response to Listeria monocytogenes infection. *J Immunol* 166, 3402–3409 (2001).

[111] Shen, H. *et al.*: Recombinant Listeria monocytogenes as a live vaccine vehicle for the induction of protective anti-viral cell-mediated immunity. *Proc Natl Acad Sci U S A* 92, 3987–3991 (1995).

[112] Weber, S. E. *et al.*: Adaptive islet-specific regulatory CD4 T cells control autoimmune diabetes and mediate the disappearance of pathogenic Th1 cells in vivo. *J Immunol* 176, 4730–4739 (2006).

[113] Cantor, J. & Haskins, K.: Recruitment and activation of macrophages by pathogenic CD4 T cells in type 1 diabetes: evidence for involvement of CCR8 and CCL1. *J Immunol* 179, 5760–5767 (2007).

[114] Dorner, B. G. *et al.*: Coordinate expression of cytokines and chemokines by NK cells during murine cytomegalovirus infection. *J Immunol* 172, 3119–3131 (2004).

[115] Faunce, D. E. & Stein-Streilein, J.: NKT cell-derived RANTES recruits APCs and CD8+ T cells to the spleen during the generation of regulatory T cells in tolerance. *J Immunol* 169, 31–38 (2002).

[116] Matloubian, M., David, A., Engel, S., Ryan, J. E. & Cyster, J. G.: A transmembrane CXC chemokine is a ligand for HIV-coreceptor Bonzo. *Nat Immunol* 1, 298–304 (2000).

[117] Beaty, S. R., Rose, C. E. J. & Sung, S.-S. J.: Diverse and potent chemokine production by lung CD11bhigh dendritic cells in homeostasis and in allergic lung inflammation. *J Immunol* 178, 1882–1895 (2007).

[118] Matzer, S. P., Rodel, F., Strieter, R. M., Rollinghoff, M. & Beuscher, H. U.: Constitutive expression of CXCL2/MIP-2 is restricted to a Gr-1high, CD11b+, CD62Lhigh subset of bone marrow derived granulocytes. *Int Immunol* 16, 1675–1683 (2004).

[119] Friedman, R. S., Jacobelli, J. & Krummel, M. F.: Surface-bound chemokines capture and prime T cells for synapse formation. *Nat Immunol* 7, 1101–1108 (2006).

[120] Lore, K., Sonnerborg, A., Spetz, A. L., Andersson, U. & Andersson, J.: Immunocytochemical detection of cytokines and chemokines in Langerhans cells and in vitro derived dendritic cells. *J Immunol Methods* 214, 97–111 (1998).

[121] Homann, D. *et al.*: Mapping and restriction of a dominant viral CD4+ T cell core epitope by both MHC class I and MHC class II. *Virology* 363, 113–123 (2007).

[122] Heckman, K. L. & Pease, L. R.: Gene splicing and mutagenesis by PCR-driven overlap extension. *Nat Protoc* 2, 924–932 (2007).

[123] Tsou, C.-L. *et al.*: Critical roles for CCR2 and MCP-3 in monocyte mobilization from bone marrow and recruitment to inflammatory sites. *J Clin Invest* 117, 902–909 (2007).

[124] Aslanian, A. M. & Charo, I. F.: Targeted disruption of the scavenger receptor and chemokine CXCL16 accelerates atherosclerosis. *Circulation* 114, 583–590 (2006).

[125] Eslin, D. E. *et al.*: Transgenic mice studies demonstrate a role for platelet factor 4 in thrombosis: dissociation between anticoagulant and antithrombotic effect of heparin. *Blood* 104, 3173–3180 (2004).

[126] Park, M. K. *et al.*: The CXC chemokine murine monokine induced by IFN-gamma (CXC chemokine ligand 9) is made by APCs, targets lymphocytes including activated B cells, and supports antibody responses to a bacterial pathogen in vivo. *J Immunol* 169, 1433–1443 (2002).

[127] Homann, D. *et al.*: Evidence for an underlying CD4 helper and CD8 T-cell defect in B-cell-deficient mice: failure to clear persistent virus infection after adoptive immunotherapy with virus-specific memory cells from muMT/muMT mice. *J Virol* 72, 9208–9216 (1998).

[128] Humann, J., Bjordahl, R., Andreasen, K. & Lenz, L. L.: Expression of the p60 autolysin enhances NK cell activation and is required for listeria monocytogenes expansion in IFN-gamma-responsive mice. *J Immunol* 178, 2407–2414 (2007).

[129] Davis, M. ApE: A Plasmid Editor. http://www.biology.utah.edu/jorgensen/wayned/ape/ (2009).

[130] Munro, S. & Pelham, H. R.: A C-terminal signal prevents secretion of luminal ER proteins. *Cell* 48, 899–907 (1987).

[131] Swift, S., Lorens, J., Achacoso, P. & Nolan, G. P.: Rapid production of retroviruses for efficient gene delivery to mammalian cells using 293T cell-based systems. *Curr Protoc Immunol* Chapter 10, Unit 10.17C (2001).

[132] Peterson, F. C., Thorpe, J. A., Harder, A. G., Volkman, B. F. & Schwarze, S. R.: Structural determinants involved in the regulation of CXCL14/BRAK expression by the 26 S proteasome. *J Mol Biol* 363, 813–822 (2006).

[133] Christensen, J. E., Andreasen, S. O., Christensen, J. P. & Thomsen, A. R.: CD11b expression as a marker to distinguish between recently activated effector CD8(+) T cells and memory cells. *Int Immunol* 13, 593–600 (2001).

[134] Lin, Y., Roberts, T. J., Sriram, V., Cho, S. & Brutkiewicz, R. R.: Myeloid marker expression on antiviral CD8+ T cells following an acute virus infection. *Eur J Immunol* 33, 2736–2743 (2003).

[135] Ghosn, E. E. B., Yang, Y., Tung, J., Herzenberg, L. A. & Herzenberg, L. A.: CD11b expression distinguishes sequential stages of peritoneal B-1 development. *Proc Natl Acad Sci U S A* 105, 5195–5200 (2008).

[136] Lanier, L. L., Phillips, J. H., Hackett, J. J., Tutt, M. & Kumar, V.: Natural killer cells: definition of a cell type rather than a function. *J Immunol* 137, 2735–2739 (1986).

[137] Gordon, S. & Taylor, P. R.: Monocyte and macrophage heterogeneity. *Nat Rev Immunol* 5, 953–964 (2005).

[138] Vremec, D. *et al.*: Production of interferons by dendritic cells, plasmacytoid cells, natural killer cells, and interferon-producing killer dendritic cells. *Blood* 109, 1165–1173 (2007).

[139] Poltorak, A. N. *et al.*: MIP-1 gamma: molecular cloning, expression, and biological activities of a novel CC chemokine that is constitutively secreted in vivo. *J Inflamm* 45, 207–219 (1995).

[140] Coelho, A. L. *et al.*: The chemokine CCL6 promotes innate immunity via immune cell activation and recruitment. *J Immunol* 179, 5474–5482 (2007).

[141] Link, A. *et al.*: Fibroblastic reticular cells in lymph nodes regulate the homeostasis of naive T cells. *Nat Immunol* 8, 1255–1265 (2007).

[142] Alferink, J. *et al.*: Compartmentalized production of CCL17 in vivo: strong inducibility in peripheral dendritic cells contrasts selective absence from the spleen. *J Exp Med* 197, 585–599 (2003).

[143] Britschgi, M. R., Link, A., Lissandrin, T. K. A. & Luther, S. A.: Dynamic modulation of CCR7 expression and function on naive T lymphocytes in vivo. *J Immunol* 181, 7681–7688 (2008).

[144] Mueller, S. N. *et al.*: Regulation of homeostatic chemokine expression and cell trafficking during immune responses. *Science* 317, 670–674 (2007).

[145] Unsoeld, H. *et al.*: Abrogation of CCL21 chemokine function by transgenic over-expression impairs T cell immunity to local infections. *Int Immunol* 19, 1281–1289 (2007).

[146] Stenstad, H., Svensson, M., Cucak, H., Kotarsky, K. & Agace, W. W.: Differential homing mechanisms regulate regionalized effector CD8alphabeta+ T cell accumulation within the small intestine. *Proc Natl Acad Sci U S A* 104, 10122–10127 (2007).

[147] Homey, B. *et al.*: CCL27-CCR10 interactions regulate T cell-mediated skin inflammation. *Nat Med* 8, 157–165 (2002).

[148] Huang, V. *et al.*: Cutting edge: rapid accumulation of epidermal CCL27 in skin-draining lymph nodes following topical application of a contact sensitizer recruits CCR10-expressing T cells. *J Immunol* 180, 6462–6466 (2008).

[149] Schaffner, A., Rhyn, P., Schoedon, G. & Schaer, D. J.: Regulated expression of platelet factor 4 in human monocytes–role of PARs as a quantitatively important monocyte activation pathway. *J Leukoc Biol* 78, 202–209 (2005).

[150] El-Gedaily, A., Schoedon, G., Schneemann, M. & Schaffner, A.: Constitutive and regulated expression of platelet basic protein in human monocytes. *J Leukoc Biol* 75, 495–503 (2004).

[151] Piqueras, B., Connolly, J., Freitas, H., Palucka, A. K. & Banchereau, J.: Upon viral exposure, myeloid and plasmacytoid dendritic cells produce 3 waves of distinct chemokines to recruit immune effectors. *Blood* 107, 2613–2618 (2006).

[152] von Hundelshausen, P., Petersen, F. & Brandt, E.: Platelet-derived chemokines in vascular biology. *Thromb Haemost* 97, 704–713 (2007).

[153] Mueller, A. *et al.*: CXCL4-induced migration of activated T lymphocytes is mediated by the chemokine receptor CXCR3. *J Leukoc Biol* 83, 875–882 (2008).

[154] Lasagni, L. *et al.*: An alternatively spliced variant of CXCR3 mediates the inhibition of endothelial cell growth induced by IP-10, Mig, and I-TAC, and acts as functional receptor for platelet factor 4. *J Exp Med* 197, 1537–1549 (2003).

[155] Farber, J. M.: Mig and IP-10: CXC chemokines that target lymphocytes. *J Leukoc Biol* 61, 246–257 (1997).

[156] Sierro, F. *et al.*: Disrupted cardiac development but normal hematopoiesis in mice deficient in the second CXCL12/SDF-1 receptor, CXCR7. *Proc Natl Acad Sci U S A* 104, 14759–14764 (2007).

[157] Fehniger, T. A. *et al.*: Acquisition of murine NK cell cytotoxicity requires the translation of a pre-existing pool of granzyme B and perforin mRNAs. *Immunity* 26, 798–811 (2007).

[158] Harris, D. P. *et al.*: Reciprocal regulation of polarized cytokine production by effector B and T cells. *Nat Immunol* 1, 475–482 (2000).

[159] Bystry, R. S., Aluvihare, V., Welch, K. A., Kallikourdis, M. & Betz, A. G.: B cells and professional APCs recruit regulatory T cells via CCL4. *Nat Immunol* 2, 1126–1132 (2001).

[160] Zhu, X. *et al.*: Analysis of the major patterns of B cell gene expression changes in response to short-term stimulation with 33 single ligands. *J Immunol* 173, 7141–7149 (2004).

[161] Hijikata, A. *et al.*: Construction of an open-access database that integrates cross-reference information from the transcriptome and proteome of immune cells. *Bioinformatics* 23, 2934–2941 (2007).

[162] Robertson, M. J.: Role of chemokines in the biology of natural killer cells. *J Leukoc Biol* 71, 173–183 (2002).

[163] Kaech, S. M., Hemby, S., Kersh, E. & Ahmed, R.: Molecular and functional profiling of memory CD8 T cell differentiation. *Cell* 111, 837–851 (2002).

[164] Wherry, E. J. *et al.*: Molecular signature of CD8+ T cell exhaustion during chronic viral infection. *Immunity* 27, 670–684 (2007).

[165] Blattman, J. N. *et al.*: Estimating the precursor frequency of naive antigen-specific CD8 T cells. *J Exp Med* 195, 657–664 (2002).

[166] Badovinac, V. P., Haring, J. S. & Harty, J. T.: Initial T cell receptor transgenic cell precursor frequency dictates critical aspects of the CD8(+) T cell response to infection. *Immunity* 26, 827–841 (2007).

[167] Slifka, M. K., Rodriguez, F. & Whitton, J. L.: Rapid on/off cycling of cytokine production by virus-specific CD8+ T cells. *Nature* 401, 76–79 (1999).

[168] Wherry, E. J. *et al.*: Lineage relationship and protective immunity of memory CD8 T cell subsets. *Nat Immunol* 4, 225–234 (2003).

[169] Martin, P. *et al.*: Quiescent and activated mouse granulocytes do not express granzyme A and B or perforin: similarities or differences with human polymorphonuclear leukocytes? *Blood* 106, 2871–2878 (2005).

[170] Rose, J. & Whitt, M. *Rhabdoviridae: The Viruses and their Replication, Field's Virology* (Lippincott Williams and Wilkins, 2001), 4th edn.

[171] Murali-Krishna, K. *et al.*: Counting antigen-specific CD8 T cells: a reevaluation of bystander activation during viral infection. *Immunity* 8, 177–187 (1998).

[172] Marzo, A. L., Vezys, V., Williams, K., Tough, D. F. & Lefrancois, L.: Tissue-level regulation of Th1 and Th2 primary and memory CD4 T cells in response to Listeria infection. *J Immunol* 168, 4504–4510 (2002).

[173] Whitmire, J. K., Asano, M. S., Murali-Krishna, K., Suresh, M. & Ahmed, R.: Long-term CD4 Th1 and Th2 memory following acute lymphocytic choriomeningitis virus infection. *J Virol* 72, 8281–8288 (1998).

[174] Varga, S. M. & Welsh, R. M.: High frequency of virus-specific interleukin-2-producing CD4(+) T cells and Th1 dominance during lymphocytic choriomeningitis virus infection. *J Virol* 74, 4429–4432 (2000).

[175] Jabbari, A. & Harty, J. T.: Secondary memory CD8+ T cells are more protective but slower to acquire a central-memory phenotype. *J Exp Med* 203, 919–932 (2006).

[176] Masopust, D., Ha, S.-J., Vezys, V. & Ahmed, R.: Stimulation history dictates memory CD8 T cell phenotype: implications for prime-boost vaccination. *J Immunol* 177, 831–839 (2006).

[177] Wolint, P., Betts, M. R., Koup, R. A. & Oxenius, A.: Immediate cytotoxicity but not degranulation distinguishes effector and memory subsets of CD8+ T cells. *J Exp Med* 199, 925–936 (2004).

[178] Pardo, J. *et al.*: Apoptotic pathways are selectively activated by granzyme A and/or granzyme B in CTL-mediated target cell lysis. *J Cell Biol* 167, 457–468 (2004).

[179] Harrington, L. E., Galvan, M., Baum, L. G., Altman, J. D. & Ahmed, R.: Differentiating between memory and effector CD8 T cells by altered expression of cell surface O-glycans. *J Exp Med* 191, 1241–1246 (2000).

[180] Seder, R. A., Darrah, P. A. & Roederer, M.: T-cell quality in memory and protection: implications for vaccine design. *Nat Rev Immunol* 8, 247–258 (2008).

[181] De Rosa, S. C. *et al.*: Vaccination in humans generates broad T cell cytokine responses. *J Immunol* 173, 5372–5380 (2004).

[182] Pantaleo, G. & Koup, R. A.: Correlates of immune protection in HIV-1 infection: what we know, what we don't know, what we should know. *Nat Med* 10, 806–810 (2004).

[183] Darrah, P. A. *et al.*: Multifunctional TH1 cells define a correlate of vaccine-mediated protection against Leishmania major. *Nat Med* 13, 843–850 (2007).

[184] Guan, E., Wang, J. & Norcross, M. A.: Identification of human macrophage inflammatory proteins 1alpha and 1beta as a native secreted heterodimer. *J Biol Chem* 276, 12404–12409 (2001).

[185] Allen, S. J., Crown, S. E. & Handel, T. M.: Chemokine: receptor structure, interactions, and antagonism. *Annu Rev Immunol* 25, 787–820 (2007).

[186] Comerford, I. & Nibbs, R. J. B.: Post-translational control of chemokines: a role for decoy receptors? *Immunol Lett* 96, 163–174 (2005).

[187] Hao, S. & Baltimore, D.: The stability of mRNA influences the temporal order of the induction of genes encoding inflammatory molecules. *Nat Immunol* 10, 281–288 (2009).

[188] Slifka, M. K. & Whitton, J. L.: Functional avidity maturation of CD8(+) T cells without selection of higher affinity TCR. *Nat Immunol* 2, 711–717 (2001).

[189] Fischer, F. R., Luo, Y., Luo, M., Santambrogio, L. & Dorf, M. E.: RANTES-induced chemokine cascade in dendritic cells. *J Immunol* 167, 1637–1643 (2001).

[190] Germain, R. N. *et al.*: Making friends in out-of-the-way places: how cells of the immune system get together and how they conduct their business as revealed by intravital imaging. *Immunol Rev* 221, 163–181 (2008).

10 Acknowledgments

This dissertation would not have been possible without the support of numerous individuals. Foremost, my debt of gratitude goes to Prof. Dirk Homann who not only enabled me to perform my research in his laboratory but also provided excellent discussions, advice, and most importantly, encouragement throughout the years. His ability to recall papers down to figure numbers have been quite useful and amusing at the same time. Not only became I to appreciate Prof. Homann's vast scientific knowledge and skills, but also his passion for interests beyond science. He patiently provided the vision, encouragement and mentoring necessary for me to complete my dissertation.

Prof. Dr. Habré deAngelis and Prof. Dr. Dirk Busch deserve a special thanks as my thesis committee members and advisors as well as Prof. Dr. Klingenspor for chairing the thesis committee.

My fellow lab members made the Barbara Davis Center a convival place to work. In particular, I would like to thank Tom Nguyen for his excellent technical assistance and 'after-hour bailouts' throughout the years; Francisco 'Cisco' Ramirez for his repeated, yet failed attempts to have me straighten out my mouse colonies and fellow Ph.D. student Bennett Davenport for helpful discussions, entertainment and for being himself, a cheerful person who brightens up the lab.

A thanks to the flow cytometry core manager and naturalist Philip Pratt duty-fully answered calls on weekends and after-hours to solve the one or other cytometer-related issue. The work on human chemokine profiles would not have been possible without the help of the laboratory of Hugo Rosen and Lucy Golden-Mason who not only provided valuable advice but also human samples, antibody reagents and flow time. I would like to thank Prof. Dr. John Hutton and his lab, especially Dr. Leah Sheridan who taught me some of the basics of confocal microscopy and provided valuable help with the image processing and data analysis. Dr. Suparna Sarka, Dr. Howard Davidson, Seija Hackle, Jay Walters, Champa Patel, Anita Hohenstein, Dr. Pierre Pirot and Dr. Janet Wenzlau deserve credit for all their support, reagents, advice and camaraderie over the years. The molecular core, spearheaded by Randy Wong, provided excellent technical support over the years and squeezed in last-minute sequencing requests without much fuss. Learning the basics of MHC-II tetramer production from Francis Crawford of the Kappler-Marrack lab National Jewish Hospital was a real treat and I am thankful for advice and reagents from Dr. Tomasz Sosinowski and Dr. Eric Clambey as well. I am

grateful for reagents and protocols received from the laboratories of Drs. George Eisenbarth, Tom Lane and Laurel Lenz. My apologies go to the numerous colleagues, family members and friends who I cannot continue listing who have supported me in one way or another over the past years.

Finally, I would like to acknowledge my family and especially my parents, my wife Lisa and my children Ford and Stella, who offered unconditional love and support throughout. Without the forgiveness and encouragement of my immediate family, who had to tolerate last minute changes to the family schedule more than once, this thesis would not have been possible.